Chemical and electrical modification of polypropylene surfaces

Stephen James Ebbens

CHEMICAL AND ELECTRICAL MODIFICATION OF POLYPROPYLENE SURFACES

Stephen James Ebbens

Ph.D. Thesis

Department of Chemistry

University of Durham

September 2000

For Mum and Dad

STATEMENT OF COPYRIGHT

DECLARATION

The work described in this thesis was carried out in the Department of Chemistry at the University of Durham between October 1997 and September 2000. It is the original work of the author except where otherwise acknowledged, and has not been previously submitted for a degree in this or any other university.

Imaging SIMS was performed by Ian Fletcher at ICI Wilton, England

LIST OF PUBLICATIONS

Work in this thesis has been published or will be submitted for publication as follows:

"Surface Enrichment of Fluorochemical Doped Polypropylene Films", Ebbens, S. J.; Badyal, J. P. S., in preparation.

"The Effect of Polymer Molecular Weight on Surface Enrichment in Fluorochemical Doped Polypropylene Films", Ebbens, S. J.; Badyal, J. P. S., in preparation.

"Fluorochemical Enrichment Of Polypropylene Surfaces: The Role Of Additive Structure", Ebbens, S. J.; Badyal, J. P. S., in preparation.

"Spatially Confined Charge Deposition Onto Polymer Surfaces Using A Scanning Probe Microscope", Ebbens, S. J.; Badyal, J. P. S., in preparation.

"Mapping Charge on Fluorochemical Doped Polypropylene Film Surfaces", Ebbens, S. J.; Badyal, J. P. S., in preparation.

"Localised Attachment of Polystyrene Beads to Polypropylene Surfaces Using EFM" Ebbens, S. J.; Badyal, J. P. S., in preparation.

ACKNOWLEDGEMENTS

I would like to thank my supervisor, Professor Jas Pal Badyal for his assistance and encouragement throughout my Ph.D. I also acknowledge my industrial sponsors at 3M both in Newton Aycliffe, England and St. Paul, America for their advice and useful discussions.

Thanks to George, Barry and Kelvin in the electrical workshop and Jim and Neil in the mechanical workshop for their technical assistance.

I would like to also mention all my family and friends who have provided support and welcome distractions over the last three years. Finally thanks to all the members of Lab 98 past and present; you have provided much advice and laughter.

ABSTRACT

Although many multi-component polymer systems are well characterised, the surface properties of polymers mixed with low surface energy additives have received little attention. In addition, the new branches of scanning probe microscopy that enable high resolution mapping and modification of surface charge distributions have been infrequently applied to polymer surfaces.

The surface segregation of a fluorochemical additive directly from a polypropylene host matrix has been investigated by AFM and other surface analysis techniques. The level of surface enrichment was found to be governed by the temperature and duration of annealing. Further investigation revealed that the speed and extent of surface enrichment of the additive increases with polymer molecular weight. The effect of additive structure on surface segregation has also reported.

A method of depositing charge onto polypropylene substrates from a high potential scanning AFM tip was developed. The relation between AFM tip-voltage and the level of charge deposited on the substrate suggested that a localised corona discharge was generated. AFM scanning parameters were found to effect the deposition of charge.

The charging behavior of fluorochemical doped polypropylene surfaces was investigated on macroscopic scales using a scanning electrometer probe, and on microscopic scales using EFM. Fluorochemical domains at the surface have been found to preferentially accumulate both positive and negative charge. Surface charge distributions were found to become more uniform during annealing.

Sub-micron particle capture by charged surfaces was investigated using EFM. In addition, spatially confined amine beads were deposited onto a patch of localised charge and subsequently functionalised to produce a metallic gold coating.

QUOTATIONS

"If god made the solids, then the devil made their surfaces"

WOLFGANG PAULI

"The larger the searchlight, the larger the circumference of the unknown"

DICK TAYLOR

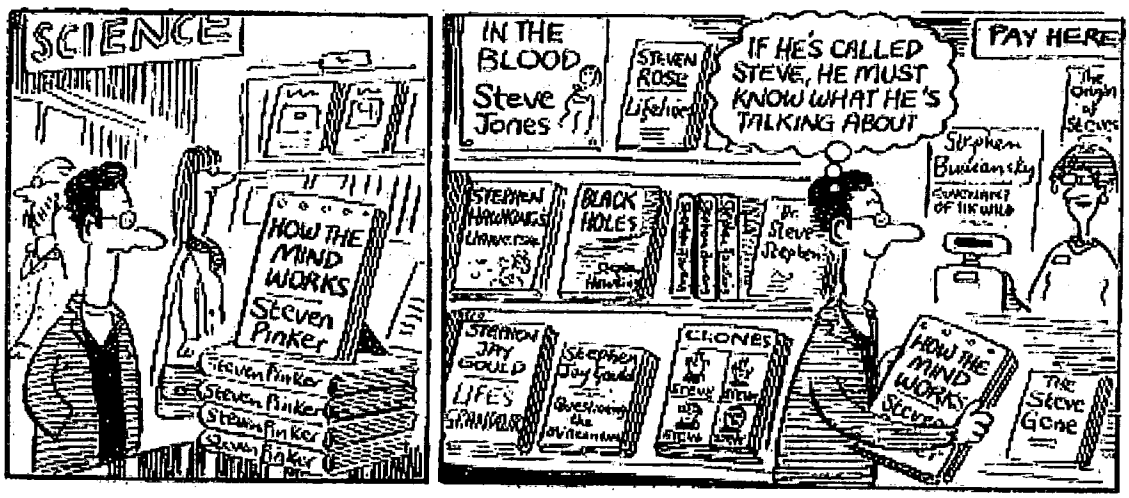

(Kipper Williams in "The Times" Newspaper, 8th February 1998)

TABLE OF CONTENTS

CHAPTER 2: FLUOROCHEMICAL DOPED POLYPROPYLENE SURFACES

CHAPTER 4: CHARGED FLUOROCHEMICAL DOPED POLYPROPYLENE FILM SURFACES

ABBREVIATIONS

AFM:	Atomic Force Microscopy
EFM:	Electric Force Microscopy
XPS:	X-ray Photoelectron Spectroscopy
SIMS:	Secondary Ion Mass Spectrometry
TSC:	Thermally Stimulated Current
iPP:	Isotactic Polypropylene
PTFE:	Poly(tetrafluoroethylene)
APS:	Poly(amino-propyl) siloxane
FEP:	Poly(tetrafluoroethylene-co-hexafluoropropylene)

CHAPTER 1

INTRODUCTION TO POLYPROPYLENE, POLYMER SURFACE MODIFICATION AND SURFACE ANALYSIS TECHNIQUES

1.1. Overview

This Chapter aims to introduce some structural features of polypropylene; provide a background to relevant methods for chemical and electrical surface modification; and describe the surface analysis techniques used.

1.2. Polypropylene

1.2.1. Chemical Structure and Stereochemistry

The chemical repeat unit of polypropylene is

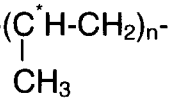

where C^* is a chiral centre. Polymers with this chemical structure are subdivided according to their stereochemistry. Atactic polypropylene has no stereospecificty at the chiral centres along the polymer chain, syndiotactic polypropylene has alternate r and s chiral centres, and isotactic polypropylene has the same chirality at each centre. Isotactic polypropylene (iPP) substrates have been used extensively in this work, consequently the remainder of this section focuses on polymer chains with this stereochemistry.

1.2.2. Crystallinity

Solidified isotactic polypropylene exhibits a high degree of crystallinity and is well known to produce complex structures on the molecular and the supermolecular scale.[1,2] The crystallization of iPP is of particular interest due to its ability to crystallize in four modifications[1] and the unusual phenomena of "cross-hatching" in its crystalline structure. The α-form of iPP is the most commercially useful phase.[3]

1.2.3. Polymer Chain Conformations

Although there are an infinite number of conformations that a polymer chain can adopt, in practice crystalline chain conformation is uniquely determined by

an interplay of energetics and kinetics.[4] For iPP, all of the crystal forms involve the packing of just one helical conformation. This is a three-fold helix consisting of a regular sequence of TGTGTGTG... internal rotations with a 6.5 Å chain axis repeat distance.[1] This helical configuration arises from the need to avoid methyl-methyl steric hindrance. Both left-handed and right-handed helices are possible.

1.2.4. Isotactic Polypropylene Crystal Structures

1.2.4.1. α-Phase

The crystal structure of the α-phase was solved by Natta and Corridini in 1960.[5] The overall geometry of the crystal cell is monoclinic, Figure 1.1. Helical packing proceeds so that any helix interacts mostly with helices of opposite chirality. This produces an alternation in the b axis direction of layers parallel to the ac plane made of only left-handed, or right-handed helices. Various representations of the crystal structure and the space group symmetry have been published.[1,4] In addition, a helix may either point up, or down depending on the orientation of its methyl groups relative to the helix axis. The unit cell allows for statistical occupation of up or down helices, however prolonged annealing produces an ordered arrangement.[6]

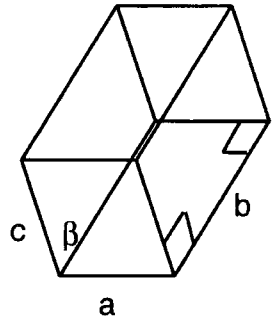

Cell parameters:

a = 6.65 Å;
b = 20.96 Å;
c = 6.5 Å;
β = 99°80

Figure 1.1 The crystal cell of α-polypropylene.

1.2.4.2. β, γ and Smetic Modifications

The β-phase of iPP has a hexagonal unit-cell,[7,8] while γ-iPP is triclinic.[9] There is still debate over the structure of the fourth "smetic" phase. X-ray diffraction suggests a degree of order somewhere between crystalline and amorphous.

1.2.5. Factors Influencing Crystal Structure

Crystallization of polypropylene at low to moderate undercooling exclusively produces the α-modification. As the crystallization temperature (T_c) reduces (equivalent to a higher cooling rate for non-isothermal crystallization) increasing amounts of the β-form are included.[2,10] However, the β-modification rarely exceeds 15 % of the total crystallized material.[10] The temperature at which the β-modification is introduced depends on the polymer grade; however in general at temperatures above 132 °C, only the α-phase is present.[10] A maximum temperature for β-phase inclusion has been predicted by theory (140-141 °C) and a suggested lower temperature limit (100 °C)[12] has been confirmed by experiment.[11]

It is possible to produce higher amounts of β-modification by using a "temperature gradient" approach, or by the addition of β-nucleating agents. Use of a selective β-phase nucleator and careful control of thermal conditions can produce pure β-iPP.[12] The γ-phase is produced from low molecular weight iPP, and during high pressure crystallization.[13,14] Smectic iPP results from quenching of the melt. Quenching rates of up to 10,000 K min^{-1} fail to produce a totally amorphous sample.

1.2.6. Macroscopic Polymer Structures: Spherulites

1.2.6.1. Polymer Spherulites[2]

Polymers in a quiescent melt mainly crystallize into spherulitic structures. "Spherulite" refers to an accumulation of crystallites having a spherical shape or symmetry that have formed by uniform growth in all directions from a central nucleus. When thin films are observed during isothermal crystallisation with transmission polarization microscopy, spherulites appear as birefringent disc-like formations seeded on random crystal nuclei, growing radially at a constant rate. On contacting, the growth fronts produce a multitude of polygonal formations bounded by straight or curved lines.

Space filling in spherulites is thought to result from branching and subsequent splaying of growing lamellae at small non-crystallographic angles. Originally the

origin of splaying was attributed to the accumulation of non-crystallising components at the growth front.[15] This interpretation has been disputed by Basset who has found evidence that suggests segregation of contaminants does not effect spherulitic morphology. Instead factors such as cilia pressure (loose loops on the fold surface of lamellae) are invoked to explain branching and splaying.[16,17]

1.2.6.2. Spherulite Types

A rich variety of spherulite structures can be generated during the crystallization of iPP. These are usually identified according to their appearance in polarizing optical microscopy. For example, spherulites may be either radial or ringed. In radial spherulites, growth proceeds in a linear fashion from the nucleus. Whereas in ringed spherulites helical growth occurs, producing concentric dark rings in polarizing micrographs.

Spherulites are often classified according to their birefringence. The birefringence of a spherulite, Δn, is defined as the difference in the refractive indices along the spherulites' radial and tangential directions, Equation 1.1.[18]

$$\Delta n = n_r - n_t \qquad \textbf{Equation 1.1}$$

A spherulite is classified optically positive if n_r is greater than n_t. The origin of birefringence in polymeric material results from the interaction of incident radiation with the helical chain structure.[19]

A multitude of spherulite types have been identified optically.[20] The original work of Padden and Keith identified five types of spherulites.[21] They observed that α-phase spherulites changed their birefringence continuously from negative to positive with increasing supercooling. While, β-phase spherulites were reported to occur sporadically at crystallization temperatures less than 132 °C. Observations have also shown that spherulites with positive birefringence form at high crystallization temperatures.[22] β-modification hedrites have also been reported. Hedrites are about 1 μm in size and are thought to derive from the spiral growth of lamellae around a screw dislocation.

1.2.7. Internal Spherulite Structures

1.2.7.1. The Origin of Positive Birefringence in α-iPP Spherulites

The existence of optically positive α-spherulites is unexpected. Both theoretical optical anisotropy calculations,[23] and birefringence measurements on stretched polypropylene fibres[23] show that the refractive index of polypropylene chains is larger parallel to their helical axis than perpendicular to it. The classical view of spherulites consisting of radial or nearly radial lamellae (R-lamellae) would suggest that the helical axis of the chain is mainly orientated tangentially. This would imply that all spherulites are negatively birefringent, Figure 1.2.

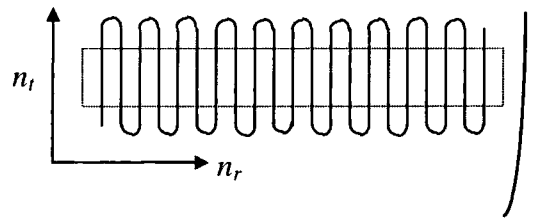

Figure 1.2 Radial lamellae place the polymer chains' helix axis in the tangential direction.

In fact, positive birefringence is possible in α-spherulites because of a second set of parallel lamellae in the tangential direction (T-lamellae). Such lamellae are formed by large angle branching from R-lamellae, producing a texture known as "cross-hatching". T-lamellae have been observed by optical microscopy, transmission electron microscopy (TEM) and scanning electron microscopy.[3,10,17,18,24] T-lamellae are observed to make a constant angle with R-lamellae (80° or 100°). The proportions of T- (positive contribution to birefringence) and R- (negative contribution to birefringence) lamellae in a spherulite can be calculated from birefringence measurements.[18] Positive birefringence occurs when the R-lamellae fraction, f_r is less than 0.665 while spherulites are negatively birefringent if f_r is greater than 0.665.[21]

1.2.7.2. Effect of Crystallization Temperature on Cross-Hatching in α-iPP

Decreasing the crystallization temperature of α-iPP produces a gradual transition from optically negative to positive spherulites.[20] This reflects a decrease in the fraction of R-lamellae with decreasing crystallization temperature. Micrographs of spherulite structure with lamellae resolution have

indeed revealed such a correlation.[10,17,24] At T_c=160 °C spherulites are composed of radially growing dominant lamellae with the space between filled by nearly parallel lamellae. The onset of cross-hatching is observed when T_c is between 155 °C and 150 °C. In this temperature range cross-hatching starts to fill in some of space between lamellae, however the generation of parallel lamellae still determines local morphology.[17] At T_c=140 °C, T-lamellae are obvious in TEM micrographs and are well developed. At 130 °C T-lamellae are poorly developed and the cross-hatching density is high.

At low temperatures the cross-hatched lamellae develop at the same time as the leading radial lamellae, and so T and R lamellae have similar thickness. Whereas at high temperatures T lamellae grow after radial lamellae, have less annealing time and are thinner.[24]

1.2.7.3. Molecular Explanation of Cross-Hatching in α-iPP

In 1968 it was suggested that T-lamellae are generated by epitaxial growth on the ac face of R-lamellae to allow favourable interdigitation of methyl groups.[18] This turned out to be correct, and this idea has now been refined to include the effect of polymer helix chirality.[1,25] In fact, T-lamellae are nucleated when the pattern of alternating sheets of oppositely handed helices along the b axis is broken by the deposition of a helix of the same hand as those in the neighbouring row, Figure 1.3. In this case, interdigitation of methyl groups is maintained by rotating the helical axis through the monoclinic angle, resulting in a branching nucleus, Figure 1.3.

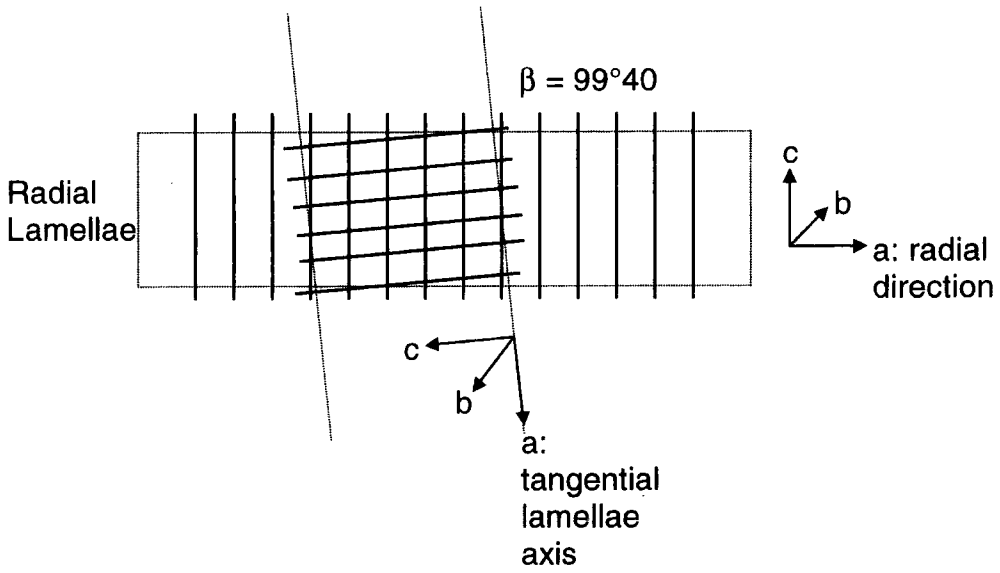

Figure 1.3 Accidental deposition of a ac layer of the same helical chirality as the previous row initiates the formation of T-lamellae. Note that the fastest growth rate is along the a axis of the monoclinic cell.

This interpretation explains the temperature dependence of cross-hatching. At high crystallization temperatures the diffusion rate is high, and deposition occurs at a low rate; reducing the possibility of branching. Whereas, at lower temperatures the rate of chain deposition is large and nucleation on growth faces is important.[25]

1.2.8. The Size and Shape of iPP Spherulites

As the crystallization temperature decreases the average spherulite size decreases due to an increase in the average density of nuclei. The thermodynamic barrier for nucleation is proportional to ΔT^{-2} (where $\Delta T = T_m - T_c$, and T_m is the melting temperature) whereas the barrier to growth is proportional to ΔT^{-1}. Therefore as the crystallization temperature decreases, the rate of nucleation increases to a considerably greater extent than the spherulite growth rate from the nuclei.[2]

The combination of nucleation behaviour and spherulite growth rate accounts for the shape of spherulite boundaries. In a single phase system, the growth rates of all nuclei are the same, and so the boundary surface is determined by the formation of crystalline nuclei. Under isothermal conditions, nucleation may proceed simultaneously (athermal nucleation) or at different moments (thermal

nucleation).[2] Models of spherulite boundaries show that if neighbouring spherulites nucleate at the same time and grow at the same rate then the boundary between them will be a straight line (planar in 3-dimenisons).[26] However, if nucleation is staggered then the boundary will be hyperbolic (a hyperboloid in 3-dimensions). If another phase is present, then the spherulite growth rates will differ, allowing spherical and cardioid boundaries to form. Continuous cooling in a single phase system gives the same interspherulitic boundary geometry as in the isothermal case.[26] The situation for continuously cooled multi-phase systems is more complex and has not been solved.

1.3. Polymer Surface Modification Methods

1.3.1. Chemical Surface Modification

1.3.1.1. Introduction

Surface chemistry (and morphology) determines the way in which polymeric materials interact with their environment. The modern world is replete with examples of materials that rely on tailored surface properties resulting from careful control of the chemical functionalities present in their outermost regions. Water repellent garments, non-stick surfaces, anti-fog lenses, adhesives and many more all rely on surface modification.

Methods of altering polymer surface chemistry include, plasma treatment (with gases[27] or polymerisable monomers[28]), wet chemical treatment,[29] surface grafting,[29] UV irradiation,[28] and flame treatment.[29] Another strategy exploits the fact that in some polymer systems mixing in a low concentration of a polymer or small molecular additive can enrich the surface with a desired functionality. The remainder of this section outlines the factors that determine the surface composition in these binary systems.

1.3.1.2. Binary Polymer Systems

Three types of two-component polymer systems are commonly identified: polymer-polymer blends, polymer-additive systems and co-polymers. In polymer blends two or more different polymers are present, in polymer-additive systems a polymer is mixed with a small molecule, whilst in co-polymer systems blocks of differing types of monomer are linked together by chemical bonds.[30]

1.3.1.3. Polymer Blends

Polymer blends are divided into two types according to the degree of mixing of their components: miscible and immiscible.[31]

(a) Immiscible Blends

In immiscible blends containing two different polymers, the surface is generally enriched by the lower surface energy component.[32] As an example, polystyrene/poly(ethyleneoxide) blend surfaces are enriched in the lower surface energy polystyrene component for all bulk compositions.[33] As fluoropolymers are renowned for their low surface energy, they often exhibit surface segregation. For example, a poly(perfluoromethylmethacrylate) and poly(methylmethacrylate) blend with only 0.01% fluorinated component by weight, contains 24% fluorine in its outermost region.[34]

Bulk thermodynamics favours complete de-mixing of immiscible blends, which would result in a surface completely covered by the lower surface energy component. In practice, equilibrium is not usually obtained, and other factors govern surface composition. These can be intrinsic such as relative wettabilities and the degree of phase separation, or extrinsic such as sample preparation and blend morphology.[4]

Annealing allows equilibrium to be more closely approached. At elevated temperatures, polymer molecules are able to relax, migrate and then reorganise into a more thermodynamically favourable state.[35] One example is that a layer of polystyrene can diffuse through a covering layer of poly(ethyleneoxide) during heating, to further lower surface energy.[33]

Although surface energy differences are the main driving force for surface enrichment, other factors can alter a blends surface composition. Increasing the side chain length of a higher surface energy blend component, provides steric hindrance to the surface migration of a low surface energy polymer.[34] Chain stiffness is also an important factor. Single-chain mean field theory simulations suggest that for stiff/flexible mixtures, stiff chains segregate to the surface to achieve more efficient packing.[36] The crystallinity of each blend component can also determine the extent of segregation. In a polyolefin blend consisting of an amorphous and a crystalline component, the amorphous component significantly enriched the surface.[37]

(b) Miscible Polymer Blends

As well as the factors discussed above, miscible polymer blends also undergo temperature and concentration dependent phase transitions that may influence surface segregation.[38] The correspondence between surface energy differences and surface excess is well illustrated for a miscible polystyrene/poly(vinylmethyl ether) blend where polystyrene preferentially segregates to the surface.[32] In this case, the extent of surface enrichment increases with the molecular weight of the polystyrene component. This effect was rationalised by the known decrease of surface energy with increasing polymer molecular weight. A good correlation between the mathematical relation describing the change in surface energy with molecular weight and the observed surface compositions was obtained.

1.3.1.4. Polymer Additives

Polymer additives are larger than common solvent molecules, but much smaller than polymer chains. Many polymer additives are designed to stabilise bulk polymers, by acting as antioxidants. For these applications, the accumulation of additive at the polymer-air interface is undesirable as it will lead to leaching and an uneven distribution of additive molecules throughout the polymer.[39] However, low-surface energy additives can be used to modify surface chemistry.[40,41] As for the polymer blend systems, surface energy differences between the additive and host polymer drive surface segregation.[41] Additive molecules are normally considered to diffuse to the surface through the amorphous phase of semi-crystalline host polymers.[39] Consequently the

structural features of the host polymer play a large part in determining the behaviour of the additive at the surface. For example in one study additive molecules were found to appear at a polypropylene surface in the amorphous boundaries between spherulites, and then spread across the surface by diffusion along spherulite radii.[42] Quantitative relationships have been established between polymer amorphous free volumes and additive diffusion rates.[43]

An additive's size and shape also effects its ability to diffuse through a host matrix to achieve surface enrichment.[44] This trend has been quantitatively related to the specific free volume of the additive.

The compatibility of an additive with the host polymer will also effect its distribution.[39] Factors such as the physical state of the additive and its interactions with the polymer, itself and other additives determine compatibility.[39]

1.3.2. Electrical Surface Modification

1.3.2.1. Introduction

Surfaces that retain a permanent electric field following charging, are called electrets.[45] They find applications in a wide range of technologies (e.g. microphones and xerography). One class of electrets that have found particular use are thin polymer films, whose electric field results from charge implanted from external sources. A range of polymers, including polyolefins and fluorocarbon polymers display excellent charge storage properties.[46] This arises from the low electrical conductivity of these polymers and the existence of localised traps for charge carriers caused by impurities, structural defects in monomer units and imperfections in crystalline order.[45]

Three main processes exist for the generation of polymer electrets: irradiation by low energy electrons, contact with liquids, and corona discharge. These are now briefly introduced.

1.3.2.2. Electret Formation by Low-Energy Electrons

The exposure of a polymer electret to a beam of mono-energetic electrons produces a controlled density of charge carriers with known polarity at a depth precisely determined by the penetration of the electrons.[45] This method has little commercial use (it is technologically complex and requires vacuum apparatus), but due to the high degree of control it has been used to study the physical properties of electret materials.[47]

1.3.2.3. Electret Formation by Contact with Liquid

When a dielectric surface is exposed to a conducting liquid, charge transfer occurs onto the surface. This surface charge can then be introduced into the bulk by ageing, resulting in the formation of stable electrets with high surface charge density.[45]

1.3.2.4. Electret Formation by Corona Discharge

Exposure of polymer electrets to corona discharge is a commercially useful method of charging, and can achieve charge life-times comparable to those of films charged with an electron beam.[45] Corona discharge is defined as a self-sustainable, non-disruptive, electrical discharge which occurs when a sufficiently high potential difference exists between asymmetric electrodes such as a fine wire and a plate.[48] The polarity of a corona discharge is determined by the high field electrode. Corona discharges are further sub-divided according to the corona voltage. With increasing voltage the positive corona becomes a continuous glow discharge, while negative discharges enter the Trichel pulses regime before also becoming continuous glows.[49] During corona discharge, ionization occurs in the region close to the tip where the field strengths are greatest. Following generation, the ions drift to the grounded plate (samples undergoing modification are placed on this) under the influence of the electric field. More control over the level of surface charge can be achieved by placing a biased grid between the tip and the sample (corona triode).[48] The ions responsible for charging depend on corona polarity, discharge gas and humidity. The species present in air corona discharges are detailed in Table 1.1.

% HUMIDITY	POSITIVE CORONA	NEGATIVE CORONA
0	$(H_2O)_nNO^+$,	CO_3^-
↓	$(H_2O)_n(NO_2)^+$,	↓
	$(H_2O)_nH^+$	
	↓	10% become hydrated
100	n increases	$(H_2O)_nCO_3^-$

Table 1.1 Species responsible for corona charging.

As well as implanting charge, corona discharges can cause chemical and morphological transformations to polymer surfaces.[50]

1.4. Characterisation Techniques

1.4.1. Scanning Probe Microscopy

1.4.1.1. Introduction

Since the development of contact mode atomic force microscopy (AFM) in 1986,[51] many new variations have sprung into use. Scanning probe microscopies can now measure surface mechanical properties,[52] perform localised thermal analysis,[53] obtain information about the electromagnetic properties of surfaces without wavelength limiting resolution,[53] and map magnetic and electrical fields[54] with unrivalled lateral resolution. This section focuses on two advances: the use of an intermittent contact mode to allow mapping of heterogeneous systems (Tapping Mode AFM) and the development of techniques to map electric fields (Electric Force Microscopy).

1.4.1.2. Basic Principles

Atomic Force Microscopes consist of a sharp probe tip (typical radius of curvature = 13 nm[55]) mounted on an ultra-light cantilever which is suspended in a fixed position above a xyz piezoelectric scanner. The probe is most

commonly made by masking and etching a silicon surface.[56] Recording an image involves the scanner executing a raster scan underneath the tip in the xy plane. As the tip moves across the surface one of its physical properties reflecting the magnitude of the tip-surface interaction is monitored. For example in contact mode AFM the deflection of the cantilever is recorded using a beam bounce method (cantilever deflection reflects the tip-sample force). A feedback circuit is then used to adjust the z-scanners position so as to maintain a constant tip-surface interaction. The movements executed in the z-direction form a topographic image of the surface (in this case recorded at constant force).

The high resolution of atomic force microscopy arises from a combination of the features of the instrumental design. Sharp tips provide good sensitivity to surface topography and enable images of cusps to be recorded (objects with aspect ratios higher than the tips' profile will be broadened or not fully tracked). The low mass of the cantilever, together with the optical detection method allows response to incredibly low forces (10^{-9} N).[56] Excellent xy resolution is achieved by high precision, accurately calibrated scanners.

1.4.1.3. Tapping Mode Atomic Force Microscopy

The drawback of using contact mode AFM to examine soft surfaces (e.g. polymers), is that damage to the tip and sample may occur. This is because of the dragging motion of the tip across the surface.[57] In Tapping Mode, lateral forces are reduced by causing the tip to oscillate at or near its resonance frequency (70 kHz - 350 kHz depending on the probe type).[58] Under these conditions, the tip is picked up and moved, rather than being dragged across the surface. Tapping Mode operates by monitoring the amplitude of tip oscillation at its resonance frequency (using optical interferometery). As a freely vibrating probe approaches a surface it will experience a loss in energy as it starts to make intermittent contact with the surface (in fact, the resonance peak shifts to higher frequencies, so that the frequency being monitored is moved further from resonance).[59] This energy loss will cause a reduction in the oscillation amplitude at the monitoring frequency. A feedback loop is used to maintain a constant oscillation amplitude while scanning, and the adjustments necessary form a Tapping Mode height image. The important variables in

Tapping Mode imaging are the probe's free amplitude (i.e how hard it is driven before contacting the surface) and the amplitude during tapping (the set-point).[59] A derived quantity; the set-point : free amplitude ratio is often used to summarise the imaging mode; low values signify hard tapping, while higher values signify softer tip-sample interactions. Insufficient free-amplitudes (<20 nm) prevent the tip from leaving the contamination layer.[60] These parameters can effect height contrast.[60]

In addition to monitoring the amplitude of the tip oscillation, the phase shift between the exciting frequency and the tip's response can also be recorded. The resulting phase images are valuable tools in mapping heterogeneous surfaces.[60] Although spectacular image contrast is often obtained, the interpretation of phase shifts is difficult, and they correlate with the Tapping Mode parameters mentioned above. Contrast in published phase images has been attributed to factors including, elasticity,[59] hydrophobicity,[61,62] adhesion,[63] and energy dissipation.[60]

1.4.1.4. Electric Force Microscopy (EFM)

EFM was initially developed as a variation of non-contact AFM. In non-contact AFM, the same oscillation amplitude feedback described for Tapping Mode is used, however instead of intermittently touching the surface, the tip is raised a short distance above the surface (0.1 - 10 nm).[64] Under these conditions, Van-der Waals forces are responsible for changes in the tips' oscillation amplitude. However, for charged surfaces additional electrostatic forces are also present at the surface, and will contribute to changes in oscillation amplitude. From this prototype EFM, many variations have emerged, Table 1.2.

In this work a commercial method that combines Tapping Mode and non-contact mode has been used: lift-mode EFM.[65] Lift-mode EFM entails initially recording a Tapping Mode height scan line. This height data is then used to ensure that the tip is held a fixed distance above the surface during a second non-contact "lifted" scan along the same scan line. The lift-height is defined by the user (normally 5-50 nm). During the lift-mode scan line the tip continues oscillating, and changes in its vibrational characteristics will reflect the long range forces above the sample. However in contrast to other non-contact EFM

methods, the tips' phase shift rather than its amplitude is used to detect the electric field gradient above the surface. Phase shifts are highly sensitive to long-range forces. Another advantage of lift-mode is that Tapping Mode phase data can be simultaneously collected. It is also possible to apply a small d.c. voltage to the tip while scanning, to assist the determination of surface polarity.

Ref.	Description of Technique	Applications
66.	This method employs a non-contact approach. By applying a d.c. voltage to an oscillating tip and grounding the sample an extra force reflecting the capacitative gradient between tip and sample is introduced and measured.	Images of variations in tip-sample capacitance across surfaces.
66.	A non-contact method, where a.c. voltage is applied to the tip. This generates an additional oscillation that is detected using a lock-in amplifier.	Obtained simultaneous images of the capacitance and topography of surfaces.
64, 67.	A grounded tip follows a constant force contour above the sample, as described in the text. This is normal non-contact mode AFM.	Employed to image regions of charge deposited by pulsed discharge from a EFM tip, and used to image ferroelectric domain walls in the ferroelectric-ferroelastic material $Gd_2(MoO_4)_3$.
64, 68.	Standard non-contact AFM with a d.c. bias voltage applied to the sample.	Determined the sign of charge deposited during corona discharge from a EFM tip.
69.	Having initially recorded a contact mode scan line, the tip is raised between 50-100 nm above the surface and made to follow the surface topography. During this fixed lift-height scan the deflection of the probe is measured. This deflection signal corresponds to the electrostatic forces.	Imaging domain inverted gratings.
70, 71, 54, 72.	An a.c. bias current is applied between the tip and the sample in non-contact mode. Detection electronics allow the sign and level of surface charge to be determined simultaneously with topography.	Demonstrated single charge carrier sensitivity, imaged ferroelectric domain walls and compared the effect of corona discharge with contact charging.
73.	A contact mode method, using a conducting tip to measure the tip-sample capacitance as a function of lateral position.	Imaged "bits" of deposited charge on a semi-conductor surface.

Table 1.2 Summary of EFM experiments reported in the literature.

1.4.2. X-ray Photoelectron Spectroscopy (XPS)

XPS uses soft x-rays to photoeject[74] core level electrons from atoms in the uppermost region of the sample (1-5 nm).[75] These photoelectrons pass through an electron analyser prior to detection, resulting in a spectrum of electron intensity as a function of kinetic energy (KE). According to energy conservation the binding energy (BE) of the electrons is given by Equation 1.2:

$$KE = h\nu - BE - \phi \qquad \textbf{Equation 1.2}$$

where $h\nu$ is the energy of the incident photons and ϕ is the spectrometer work function.

Ultra-high vacuum is necessary to ensure that the photoelectrons reach the electron analyser without colliding with background gas molecules.[76] Suitable x-ray sources must have line widths sufficiently narrow so as not to limit energy resolution, and a characteristic energy high enough to eject a wide range of core level electrons. Mg Kα ($h\nu$ = 1253.6 eV; line width = 0.7 eV) and Al Kα ($h\nu$ = 1486.6 eV; line width = 0.85 eV) satisfy these conditions.

Each elements' core level electrons have a characteristic binding energy (although H and He cannot be photoionized by usual X-ray sources), and so XPS spectra provide elemental analysis. If suitable reference compounds are available, then the intensity of XPS signals can be quantified to give surface elemental abundances. Binding energies show small variations according to the atoms' chemical environment. For example, the attachment of groups that withdraw electron density from the atom (e.g. fluorination), will cause an increase in core level electron binding energies as a result of their decreased nuclear screening. Greater electron withdrawal results in a greater increase in binding energy.[77]

The surface sensitivity of XPS is a result of the inelastic mean free path length, λ, of the photoelectrons. λ is a statistical quantity reflecting the average distance an emitted electron can travel within the solid before being involved in

an inelastic collision. Once such collisions occur, the electron will no longer appear in the XPS peak. Inelastic path lengths depend on the energy of the electron, and so vary for different elements, Figure 1.4. However, most elements contained in polymers emit photoelectrons with energies in the range of 100 eV - 1000 eV. Such electrons can only escape from within a few monolayers of the sample surface, Figure 1.4.

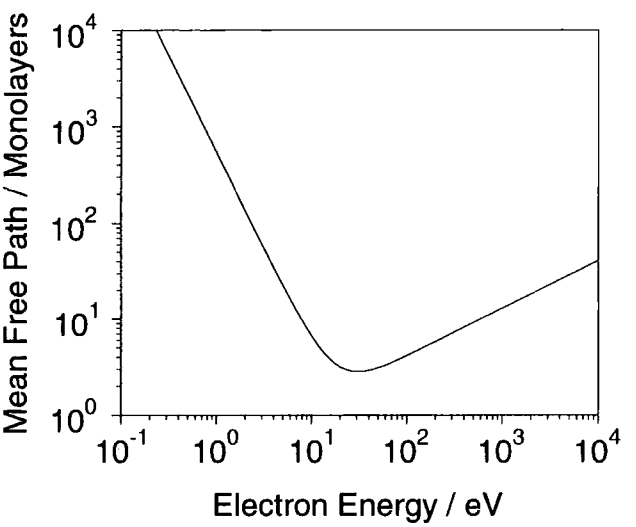

Figure 1.4 The dependence of inelastic mean free path length, λ on the emitted electron energy for elements.

When electrons are detected normal to the sample surface, 95 % of electrons at a given energy emerge from within 3λ of the sample surface (the escape depth). However by changing the angle at which electrons are detected (the take-off angle, θ) the escape depth is scaled to 3λsinθ, Figure 1.5.[76]

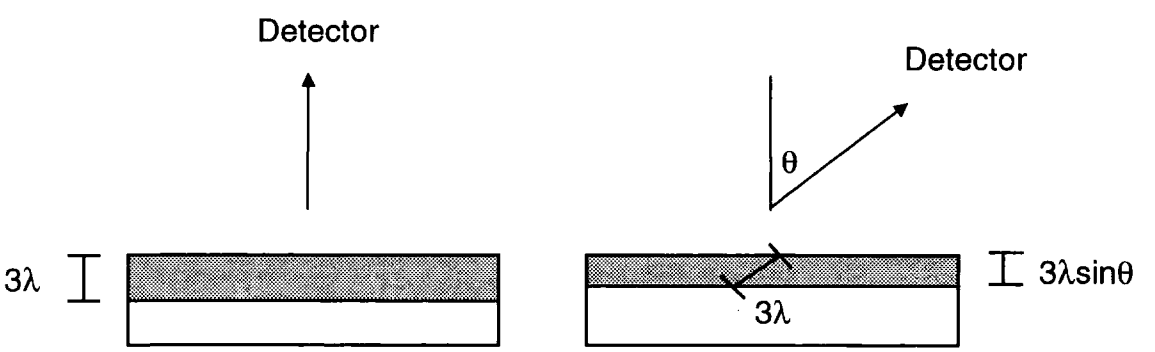

Figure 1.5 Angle resolved XPS.

The instrumental design of XPS apparatus has been described in detail elsewhere.[76]

1.4.2.1. Secondary Ion Mass Spectroscopy (SIMS)

In SIMS an ion beam (commonly O^-, Cs^+, Xe^+, Ar^+, Ga^+, O_2^+) of energy 0.5-20 keV is used to erode the sample surface and generate secondary elemental or cluster ions that are subsequently extracted from the surface by an electric field and detected in a quadrupole or time-of-flight (TOF) mass spectrometer.[78] These secondary ions usually come from the top monolayer of the exposed surface. Results can be presented as a function of mass, location or depth. Static SIMS records the mass distribution of ions using a low flux of incident ions to prevent erosion of the sample. In contrast, a high ion flux is used in dynamic SIMS to erode the surface as well as generating secondary ions. Imaging is possible either by rastering the ion beam across the sample (secondary ion microprobe) or by using ion optics to obtain a stigmatic image of the sample (secondary ion microscope).[79]

1.4.3. Contact Angle Measurements

1.4.3.1. Introduction

Contact angle analysis is an extremely surface sensitive technique (top 5-10 Å).[80] The behaviour of a droplet of liquid on the surface of a solid is determined by the surface tensions of both the droplet and the solid surface. On a smooth surface the equilibrium contact angle arises from a balance of forces and can be expressed in terms of surface tensions, Figure 1.6 and Equation 1.3 (Young's equation[81]). Contact angles reflect the degree of repellency of a surface to a given probe liquid, higher angles indicating greater repellency.

Instrumentally, static contact angles are most accurately determined using a video contact angle apparatus. This allows the deposition of a known volume of probe liquid onto the surface of interest. A CCD camera focused on the droplet as it rests on the substrate allows the capture of a static image. Software is then used to calculate the contact angle from the image.

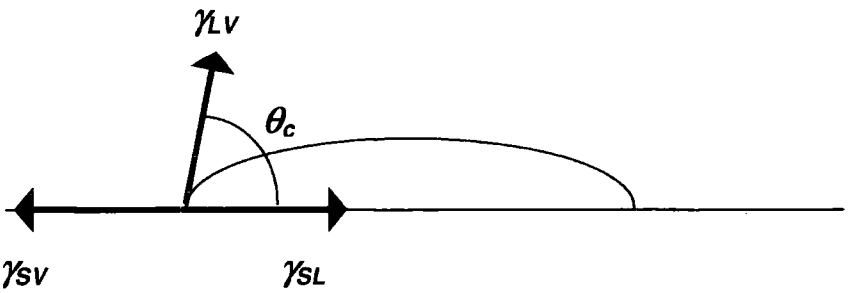

Figure 1.6 The contact angle experiment: the contact angle is the angle between the marked tangent and the liquid/solid interface, θ_c. The forces are: a force tending to decrease droplet size to minimise liquid/gas interface area, γ_{LV}; a force tending to minimise the solid/liquid interface area, γ_{SL}, and a force tending to minimise the solid/gas interface area, γ_{SV}. Resolving the forces leads to an expression for the contact angle, Equation 1.3.[82]

$$\cos(\theta_c) = \frac{\gamma_{SV} - \gamma_{SL}}{\gamma_{LV}}$$ **Equation 1.3**

1.4.3.2. Surface Energy Determination

If two or more contact angles are recorded with liquids of known surface tensions, then estimates of the surface energy of the solid may be obtained. The two methods used in this work are detailed below.

(a) Owen and Wendt Method

This method allows surface energy to be estimated from contact angle measurements using two different liquids.[83] The method derives from Young's equation (rearranged as Equation 1.4) and Fowke's idea that surface tensions could be split into dispersive and polar components, Equation 1.5

$$\gamma_{SV} = \gamma_{SL} + \gamma_{LV}\cos\theta_c$$ **Equation 1.4**

$$\gamma = \gamma^d + \gamma^p$$ **Equation 1.5**

Superscripts are d; dispersive and p; polar.

Owen and Wendt proposed that the solid-liquid surface tension could be written as the geometric mean of the solid-vapour and liquid-vapour surface tensions, Equation 1.6. Combining this with Youngs' equation gives Equation 1.7.

$$\gamma_{SL} = \gamma_S + \gamma_L - 2(\gamma_S^d \gamma_L^d)^{1/2} - 2(\gamma_S^p \gamma_L^p)^{1/2}$$ **Equation 1.6**

$$\gamma_{LV}(1+\cos\theta_c) = 2(\gamma_{SV}^d \gamma_{LV}^d)^{1/2} + 2(\gamma_{SV}^p \gamma_{LV}^p)^{1/2}$$ **Equation 1.7**

By measuring the contact angles of two high boiling point liquids, for which the dispersive and polar parameters (γ^p_{LV} and γ^d_{LV}) are known, Equation 1.7 can be solved to give the dispersive and polar contributions of the surface's energy (γ^p_{SV} and γ^d_{SV}).

(b) Zisman Plots

A Zisman plot is constructed by choosing a set of liquids from the same homologous series and measuring their contact angles with the surface of interest. A plot of the cosine of the contact angles versus the liquids' surface tensions approximates to a linear relationship.[84] By extrapolating the line of best fit to cosθ = 1, the critical surface tension is obtained. Any liquid with a surface tension smaller than this value will spread out when contacted with the surface.

1.4.4. Electrometer

Electrometers comprise a metallic probe suspended above the surface of interest. They are able to record the surface potential of the region immediately below the probe, using a null potential method. An a.c. voltage of magnitude V_{ac} and frequency ω is applied to the probe, resulting in a force, F, which depends on the potential between probe and sample, V_{dc}, the probe/sample capacitance gradient, $\frac{dC}{dz}$, and time, t, Equation 1.8. This force will cause the tip to oscillate.

$$F = \frac{dC}{dz} V_{dc} V_{ac} \cos\omega t$$ **Equation 1.8**

The instrument's electronics alter the probe voltage until the oscillation ceases (i.e. there is no force), at this point the voltage on the probe is the same as the surface potential, and a measurement is recorded.

1.5. References

[1] Lotz, B.; Wittmann, J. C.; Lovinger, A. J. *Polymer* **1996**, *37*, 4979.

[2] Varga, J. *J. Mater. Sci.* **1992**, *27*, 2557.

[3] Yamada, K.; Matsumoto, S.; Tagashira, K.; Hikosaka, M. *Polymer* **1998**, *39*, 5327.

[4] *Concise Encyclopaedia of Polymer Science and Engineering*; Kroschwitz, J. I. Ed.; Wiley: New York, p 221.

[5] Natta, G.; Corridini, P. *Nuovo Cimento Suppl.* **1960**, *15*, 40.

[6] Brükner, S.; Meille, S. V.; Petraccone, V.; Pirozzi, B. *Prog. Polym. Sci.* **1991**, *16*, 361.

[7] Meille, S. V.; Ferro, D. R.; Brükner, S.; Lovinger, A. J.; Padden, F. J. *Macromolecules* **1994**, *27*, 2615.

[8] Lotz, B.; Kopp, S.; Dorset, D. C. R. *Acad. Sci. Paris.* **1994**, *319*, Ser. IIb, 187.

[9] Brükner, S.; Meille, S. V. *Nature* **1989**, *340*, 455.

[10] Al-Raheil, I. A.; Qudah. A. M.; Al-Share, M. *J. Appl. Polym. Sci.* **1998**, *67*, 1259.

[11] Lotz, B.; Fillon, B.; Therry, A.; Wittmann, J. C. *Polym. Bull.* **1991**, *25*, 101.

[12] Varga, J. *J. Thermal Anal.* **1986**, *31*, 165.

[13] Awaya, H. *J. Polym. Sci. Polym. Lett. Ed.* **1966**, *4*, 127.

[14] Turner-Jones, A. *Polymer* **1971**, *12*, 487.

[15] Keith, H. D.; Padden, F. J. *J. Appl. Phys.* **1963**, *34*, 2409.

[16] White, H. M.; Bassett, D. C. *Polymer* **1997**, *38*, 5515.

[17] Olley, R. H.; Bassett, D. C. *Polymer* **1989**, *30*, 399.

[18] Binsbergen, F. L.; De Lange, B. G. M. *Polymer* **1968**, *9*, 23.

[19] Atkins, P. W. *Physical Chemistry*, 5th ed.; Oxford University Press: Oxford, p 762.

[20] Padden, F. J.; Keith, H. D. *J. Appl. Phys.* **1959**, *30*, 1479.

[21] Awaya, H. *Polymer* **1988**, *29*, 591.

[22] Bassett, D. C.; Olley, R. H. *Polymer* **1984**, *25*, 935.

[23] Keedy, D. A.; Powers, J.; Stein, R. S. *J. Appl. Phys.* **1960**, *31*, 1911.

[24] Janimark, J. J.; Cheng, S. Z. D.; Giusti, P. A.; Hsieh, E. T. *Macromolecules* **1991**, *24*, 2253.

[25] Lotz, B.; Wittmann, J. C. *J. Polym. Sci., Part B: Polym. Phys.* **1986**, *24*, 1541.

[26] Stachurski, Z. H.; Macniol, J. *Polymer* **1998**, *23*, 5717.

[27] Yasuda, T.; Yoshida, K.; Okuno, T. *J. Polym. Sci., Part B: Polym. Phys.* **1988**, *26*, 2061.

[28] Chan, C.-M.; Ko, T.-M.; Hiraoka, H. *Surf. Sci. Rep.* **1996**, *24*,1.

[29] Garbassi, F.; Morra, M.; Occhiello, E. *Polymer Surfaces: From Physics to Technology*; Wiley: New York, 1994; Chapter 7.

[30] Schmitt, R. L.; Gardella, J. A.; Magill, J. H.; Salvat, I. L.; Chin, R. L *Macromolecules* **1985**, *18*, 2675.

[31] *Polymer Handbook*, 2nd ed.; Brandrup, J., Immergut, E. H.; Eds.; Wiley: New York, 1975, p 211.

[32] Bhatia, Q. S.; Pan, D. H.; Koberstein J. T. *Macromolecules* **1988**, *21*, 2166.

[33] Thomas, H. R.; O`Malley, J. J. *Macromolecules* **1981**, *14*, 1316.

[34] Park, I. J; Lee, S. B.; Choi, C. K. *J. Appl. Poly. Sci.* **1994**, *54*, 1449.

[35] Kassis, C. M.; Steehler, J. K.; Bates, D. E.; Guan, Z.; Romack, T. J.; DeSimone, J. M; Linton, R. W. *Macromolecules* **1996**, *29*, 3247.

[36] Carignano, M. A.; Szleifer, I. *Europhys. Lett.* **1995**, *30*, 525.

[37] Brant, P.; Karim, A.; Douglas, J. F.; Bates, F. S. *Macromolecules* **1996**, *29*, 5628.

[38] Cowie, J. M. G. *Polymers: Chemistry and Physics of Modern Materials*, 2nd ed.; Blackie Academic and Professional: London, 1991, p 177.

[39] Földes, E. *Angew. Makromol. Chem.* **1998**, *261*, 65.

[40] Sargent, R. R.; Alexander, J. R. U. S. Patent 5,560,992, 1996.

[41] Champagne, F.; Li, J. -F.; Schreiber, H. P.; Dipola-Baranyi, G. *J. Appl. Polym. Sci.* **1994**, *54*, 743.

[42] Billingham, N. C.; Calvert, P. D.; Uzuner, A. *Eur. Polym. J.* **1989**, *25*, 839.

[43] Földes, E *J. Appl. Polym. Sci.* **1993**, *48*, 1905.

[44] Földes, E *Polym. Degrad. Stab.* **1995**, *49*, 57.

[45] Hilczer, B; Malecki, J. *Electrets*; Elsevier: New York, 1986.

[46] Kressmann, R.; Sessler, G. M.; Günther, P. *IEEE Trans. Dielect. Elect. Insul.* **1996**, *3*, 607.

[47] Watson, P. K. *IEEE Trans. Dielect. Elect. Insul* **1995**, *2*, 915.

[48] Giacometti, J. A; Oliveria, O. O. *IEEE Trans. Elect. Insul.* **1992**, *27*, 924.

[49] Loeb, L. B. *Electrical Coronas*; University of California Press: Berkeley, 1965; p 326.

[50] Sapieha, S.; Cerny, J.; Klemberg-Sapieha, J. E.; Martinu, L. *J. Adhesion* **1993**, *42*, 91.

[51] Binnig, G.; Quate, C. F. *Phys. Rev. Lett.* **1986**, *57*, 930.

[52] Burnham, N. A.; Colton, R. J. *J. Vac. Sci. Technol. A* **1989**, *7*, 2906.

[53] Pylkki, R. J.; Moyer, P. J.; West, P. E. *Jpn. J. Appl. Phys.* **1994**, *33*, 3785.

[54] Saurenbach, F.; Terris, B. D. *Appl. Phys. Lett.* **1990**, *56*, 1703.

[55] Ramirez-Aguilar, K. A. *Langmuir* **1998**, *14*, 2562.

[56] Quate, C. F. *Surf. Sci.* **1994**, *299-300*, 980.

[57] Digital Instruments Application Notes. http://www.di.com/Appnote/TapMode/tapmodeMain.html (accessed September 2000).

[58] Zhong, Q.; Innis, D.; Kjoller, K. K.; Elings, V. B. *Surf. Sci. Lett.* **1993**, *290*, L688.

[59] Brandsch, R.; Bar, G. *Langmuir* **1997**, *13*, 6349.

[60] Bar, G.; Thomann, Y.; Brandsch, R.; Cantow, H. J.; Whangbo, M. -H *Langmuir* **1997**, *13*, 3807.

[61] Refier, D.; Windeit, R.; Kumpf. R. J.; Karbach, A.; Fuchs, H. *Thin Solid Films* **1995,** *264,* 148.

[62] Chen, X.; Davies, M. C.; Roberts, C. J.; Tendler, S. J. B; Williams, P. M.; Davies, J.; Dawkes, A. C.; Edwards, J. C. *Ultramicroscopy* **1998**, *75*, 171.

[63] Finot, M. O.; McDermott, M. T. *J. Am. Chem. Soc.* **1997**, *119*, 8564.

[64] Stern, J.E.; Terris, B.D.; Mamin, H.J.; Rugar, D. *Appl. Phys. Lett.* **1988**, *53*, 2717.

[65] Digital Instruments *Electric Force Microscopy* ; Support Note No. 231, Rev A, 1996.

[66] Martin, Y.; Abraham, D.W.; Wickramsinghe, H.K. *Appl. Phys. Lett.* **1988**, *52*, 1103.

[67] Luthi, R.; Haefke, H.; Meyer, K.P.; Meyer, E.; Howald, L.; Guntherodt, H. J. *J. Appl. Phys.* **1993**, *74*, 7461.

[68] Morita, S.; Fukano, Y.; Uchiashi, T.; Okusako, T.; Sugawara, Y.; Yamanishi, Y.; Oasa, T. *Jpn. J. Appl. Phys.* **1993** *32*, L1701.

[69] Bluhm, H.; Wadas, A.; Weisendanger, R.; Roshko, A.; Aust, J.A.; Nam, D. *Appl. Phys. Lett.* **1997**, *71*, 146.

[70] Terris, B.D.; Stern, J.E.; Rugar, D.; Mamin, H. J. *Phys. Rev. Lett.* **1989**, *63*, 2669.

[71] Schönenberger, C.; Alvarado, S.F. *Phys. Rev. Lett.* **1990**, *65*, 3162.

[72] Schönenberger, C. *Phys. Rev. B.* **1992**, *45*, 3861.

[73] Barrett, R.C.; Quate, C.F. *J. Appl. Phys.* **1991**, *70*, 2725.

[74] Sherwood, P. M. A. In *Spectroscopy*, Straughan, B. P., Walker, S., Eds.; Chapman and Hall: London, 1976.

[75] Seah, M. P.; Deanch, W. A. *Surf. Interface Anal.* **1979**, *1*, 2.

[76] *Practical Surface Analysis*, 2nd ed. ;Briggs, D., Seah, M. P. Eds.; Wiley: New York, 1990; Vol. 1.

[77] Beamson, G.; Briggs D. *High Resolution XPS of Organic Polymer. The Scienta ESCA300 Database*; Wiley: New York, 1992.

[78] MacDonald, R. J.; King; B. V. Chapter 5. In *Surface Analysis Methods in Materials Science*; O`Conner, D. J., Sexton, B. A., Smart, R. St. C., Eds.; Springer and Verlang: Berlin, 1992.

[79] *Practical Surface Analysis*, 2nd ed. ;Briggs, D., Seah, M. P. Eds.; Wiley: New York, 1992; Vol. 2.

[80] Langmuir, I. *Phys. Rev.* **1929**, *33*, 954.

[81] Young, T. *Philos. Trans. R. Soc. London* **1805**, *95*, 65.

[82] Atkins, P. W. *Physical Chemistry*, 4th ed.; Oxford University Press: Oxford, p150.

[83] Owens, D. K.; Wendt, R. C. *J. Appl. Polym. Sci.* **1969**, *13*, 1741.

[84] Shafrin, E. G.; Zisman, W. A. *J. Phys. Chem.* **1960**, *64*, 1292.

CHAPTER 2

FLUOROCHEMICAL DOPED POLYPROPYLENE SURFACES

2.1. Introduction

Fluorinated surfaces are renowned for their oil and water repellency,[1] chemical inertness, low coefficient of friction, and low dielectric constant.[2] These properties are exploited in protective clothing,[3] stain-proof textiles,[4] medical implants,[5] marine coatings,[6] etc. Conventional methods employed for generating fluorinated surfaces include: direct reaction with F_2,[7] plasma treatment using fluorine containing gases,[8] plasma polymerisation of fluoromonomers,[9] VUV assisted fluorination,[10] sputter deposition of fluorocarbon layers from a polytetrafluorethylene (PTFE) target,[11] and chemical derivatisation.[12] All of these methods are applied to a pre-formed substrate.

An alternative approach is to mix in a small amount of fluorine containing material during polymer processing,[4,13-15] which preferentially segregates to the surface as a result of its low surface energy.[16-18] Annealing the formed polymer can then be used to increase the extent of segregation.[19] Previous examples of surface enrichment include fluoropolymer/polyolefin blends,[18] fluorinated blocks within copolymer systems,[16] fluorocarbon groups located at the end of polymer chains,[17] and fluorochemical additives.[20,21] Studies of the latter category are limited to spun cast systems: examples include a PTFE – polyurethane – PTFE additive mixed into polyether sulfone[20] and fluorinated esters doped into alkyd resin.[21]

The factors affecting the segregation of fluorinated additives are poorly understood compared to other multi-component systems. For example, the segregation of fluoropolymers has been widely studied in the past,[19,22] and shown to be dependent upon crystallinity,[23] blend composition,[24] polymer molecular structure[22] and thermal history of the sample.[19,24] Whereas surface enrichment phenomena employing fluorine containing additives has received very little attention.[20,21] Some "diffusion-in" experiments addressing the migration of non-fluorinated additives have been previously carried out,[25] however the role played by polymer molecular weight has not been addressed.

The segregation behaviour in multi-phase fluorine containing systems is also known to depend on the molecular structure of the fluorochemical dopant. For

example, in the case of polymer blend systems comprising polystyrene and perfluorohexane double end capped polystyrene, the number of styrene units contained between the perfluorinated end groups in the polymeric additive governs the extent of surface enrichment.[26] However, the effect of fluorochemical additive structure on segregation behaviour has not been investigated.

This chapter studies the surface segregation behaviour of extruded fluorochemical doped polymer films. The effect of annealing (Section 2.2), polymer molecular weight (Section 2.3) and additive structure (Section 2.4) are investigated.

2.2. Surface Enrichment of Fluorochemical Doped Polypropylene Films

2.2.1. Introduction

In this section the surface segregation of a fluorochemical additive directly from a polymer melt is described. The system comprises polypropylene and a bis-perfluorinated additive: 1-octanesulfonamide,N,N'-[1,6-hexanediylbis[(2-oxo-3,5-oxazolidinediyl)methylene]]bis[1,1,2,2,3,3,4,4,5,5,6,6,7,7,8,8,8-heptadecafluoro-N-methyl],[27] Structure 2.1. XPS, optical microscopy, Tapping Mode AFM, imaging SIMS, and contact angle analysis have been used to characterise the surface of these polymer films.

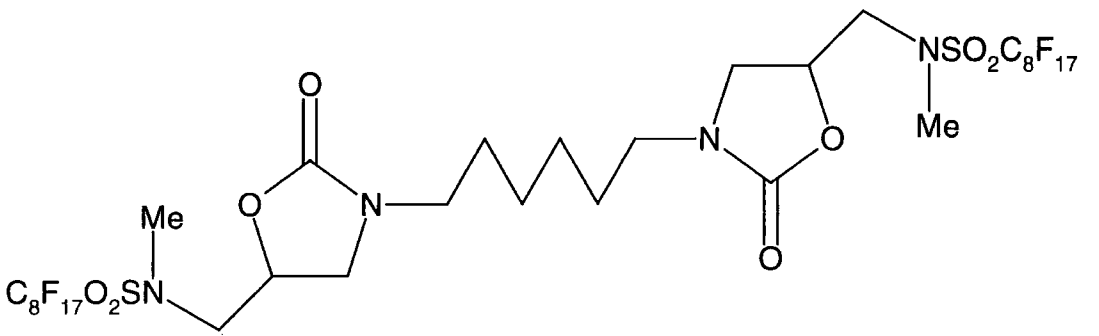

Structure 2.1 Bis-perfluorinated additive.

2.2.2. Experimental

The following two films were prepared by melt blowing: a reference substrate comprising isotactic polypropylene (Exxon 3505; melt flow index 400); and the same grade polypropylene mixed with 1% wt. of the fluorochemical additive. Subsequent annealing studies were carried out in a temperature controlled oven, where a piece of film was laid flat onto a clean metal plate. The surface exposed to air was then analysed for physiochemical changes.

XPS spectra were recorded on a VG Escalab MkII spectrometer equipped with an unmonochromatised Mg K_α X-ray source (1253.6 eV), and a hemispherical analyser. Photoemitted core level electrons were collected at a fixed take-off angle (75° away from the sample surface, except for angle resolved experiments) with electron detection in constant analyser energy (CAE) mode

with 20 eV pass energy. Data was acquired on an interfaced computer. Instrument calibration was performed using the gold $4f_{7/2}$ reference peak at 83.8 eV with a full-width-at-half-maximum (fwhm) of 1.2 eV. No radiation damage was observed during the time scale taken for data accumulation. Sensitivity factors determined using calibration compounds were taken as C(1s) : F(1s) : O(1s) : N(1s) : S(2p) equals 1.00 : 0.24 : 0.39 : 0.65 : 0.49.

Optical micrographs were obtained using an Olympus BX40 microscope with top lighting (x 50 objective).

AFM micrographs were acquired with a Digital Instruments Nanoscope III. Damage to the tip or sample was minimised by using Tapping Mode AFM.[28] In addition to height images, phase images reflecting the mechanical properties of the surface were obtained by choosing a setpoint : free amplitude ratio of 0.5 (setpoint = 50 nm; free amplitude = 100 nm).[29] Image analysis was performed using Scion Image beta release 3b software.

TOF-SIMS analysis was carried out with a Physical Electronics 7200 instrument which has been described previously.[30] A liquid metal ion gun was used for imaging (25 keV Ga^+) with a sub-micron spot size (~0.5 μm). The total ion-flux was kept well under 10^{13} ions cm^{-2} (static conditions).

Sessile drop contact angle measurements were carried out at 20 °C using a video capture apparatus (A.S.T. Products VCA2500XE). The chosen probe liquids were: high purity water (B.S. 3978 Grade 1), hexadecane (Aldrich, 99% purity) and methylene iodide (Aldrich, 99% purity).

2.2.3. Results

2.2.3.1. Surface Analysis of Pure and Fluorochemical Doped Polypropylene Films

XPS was used to measure the C, F, O, N and S elemental abundances within the top 2-5 nm of each sample,[31] Table 2.1. Only carbon spectral features corresponding to $\underline{C}_xH_y$ were observed for the pure polypropylene film (since XPS is not sensitive to hydrogen). In the case of the fluorochemical doped polyolefin film, the ratio of F : O : N : S at the surface was found to be consistent with the molecular formula of the additive (40% C, 42.5% F, 10% O, 5% N and 2.5% S; again H is excluded). The overall fluorochemical coverage at the surface was calculated to be 21.2 ± 0.6% (based on percentage F detected by XPS). Hence, there is a considerable surface excess compared to the 1% fluorochemical additive loading in the bulk.

Sample	Percentage Elemental composition				
	C(1s)	F(1s)	O(1s)	N(1s)	S(2p)
Pure polypropylene	100.0	0.0	0.0	0.0	0.0
Fluorochemical + polypropylene	86.8 ± 0.2	9.0 ± 0.3	2.1 ± 0.3	1.6 ± 0.4	0.5 ± 0.2

Table 2.1 XPS analysis.

Optical microscopy showed that both films crystallise to form spherulites, which impinge to produce mainly polygonal boundaries, Figure 2.1. The spherulite diameters were measured along their widest axis, Table 2.2; and it was found that spherulites in the fluorochemical doped film are slightly larger compared to those associated with the pure polypropylene substrate.

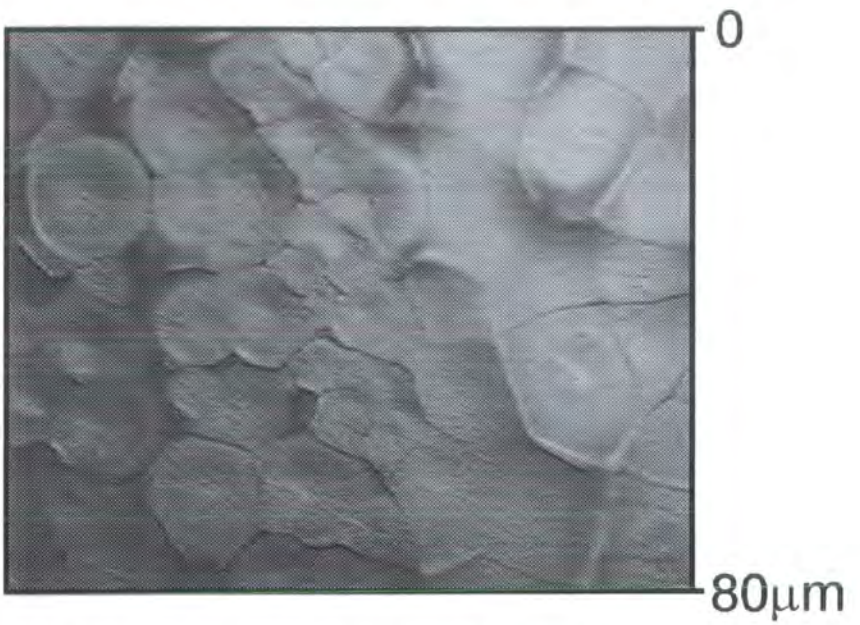

Figure 2.1a Optical micrograph of pure polypropylene.

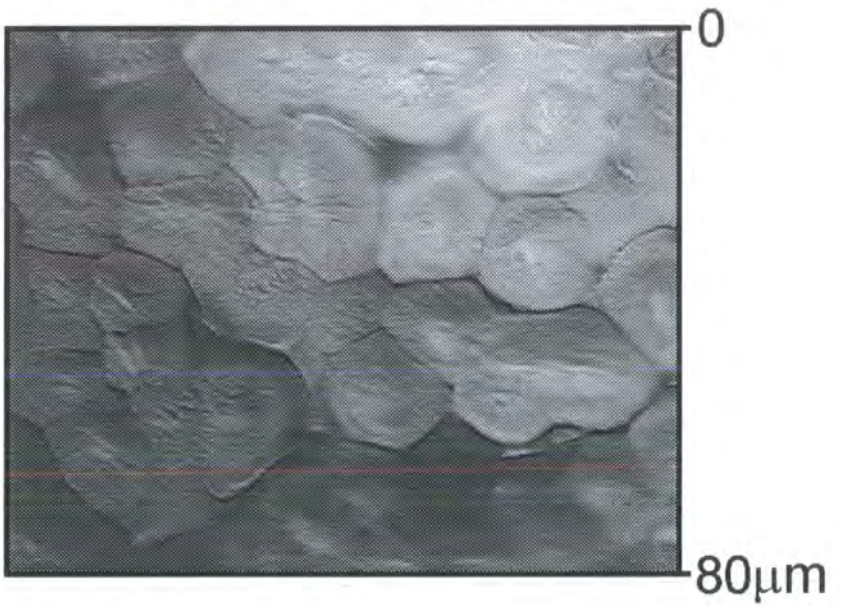

Figure 2.1b Optical micrograph of fluorochemical doped polypropylene.

Sample	Mean diameter / μm	Standard deviation / μm
Pure polypropylene	14.9	± 4.5
Fluorochemical + polypropylene	15.3	± 4.9

Table 2.2 Spherulite sizes determined by optical microscopy.

Low resolution height and phase Tapping Mode AFM images of pure polypropylene film also display spherulitic morphology, with mostly polygonal edges, Figure 2.2a. Organisation of lamellae within each spherulite is evident at higher resolution, Figure 2.2b. For the chosen set of AFM phase imaging parameters, the highly crystalline lamellae appear brighter than the amorphous surround due to their higher density.[32] Rows of lamellae appear arranged both tangentially to, and along, the radial direction of the spherulite, Figure 2.2c. Spherulitic morphology is also evident in the Tapping Mode AFM micrograph of the doped fluorochemical sample, Figure 2.3a. However, the phase image reveals additional bright dots and patches not seen in the case of the pure film, Figure 2.2, or the corresponding optical micrograph, Figure 2.1b. These regions of high phase shift are randomly distributed across the surface and do not correlate with topographical features, Figures 2.3b and c. Image analysis shows that these high phase shift fluorochemical regions cover 28 ± 1% of the surface. This is slightly more coverage than that measured by XPS, and the difference can be attributed to the greater surface sensitivity of the AFM technique, in conjunction with a concentration gradient at the surface (Tapping Mode AFM is only sensitive to the outermost surface, whereas XPS probes 2-5 nm into the sample[31]). Small underlying polypropylene crystallites can be identified at high resolution, however these have no specific orientation in contrast to the pure polypropylene sample, Figure 2.3c.

Prior to annealing, the F^- TOF-SIMS image of the doped film surface displayed bright striations corresponding to patches of fluorochemical additive at the polymer surface, Figure 2.4a. The total ion image reflects sample topography, Figure 2.4b.

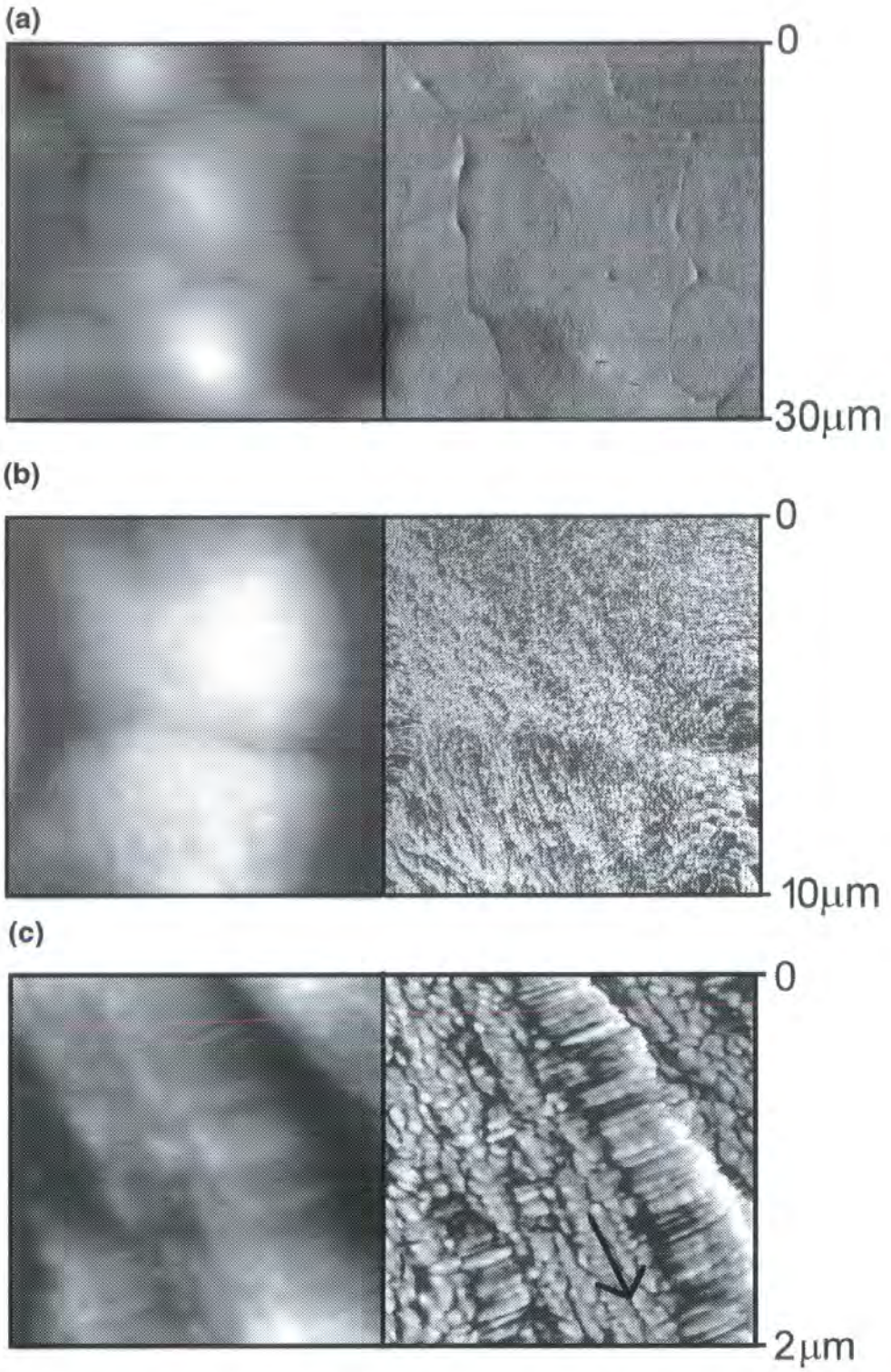

Figure 2.2 Tapping Mode AFM micrographs of pure polypropylene (LHS: height; RHS: phase): (a) 30 μm x 30 μm; (b) 10 μm x 10 μm; and (c) 2 μm x 2 μm (the radial direction of the spherulite is indicated by an arrow).

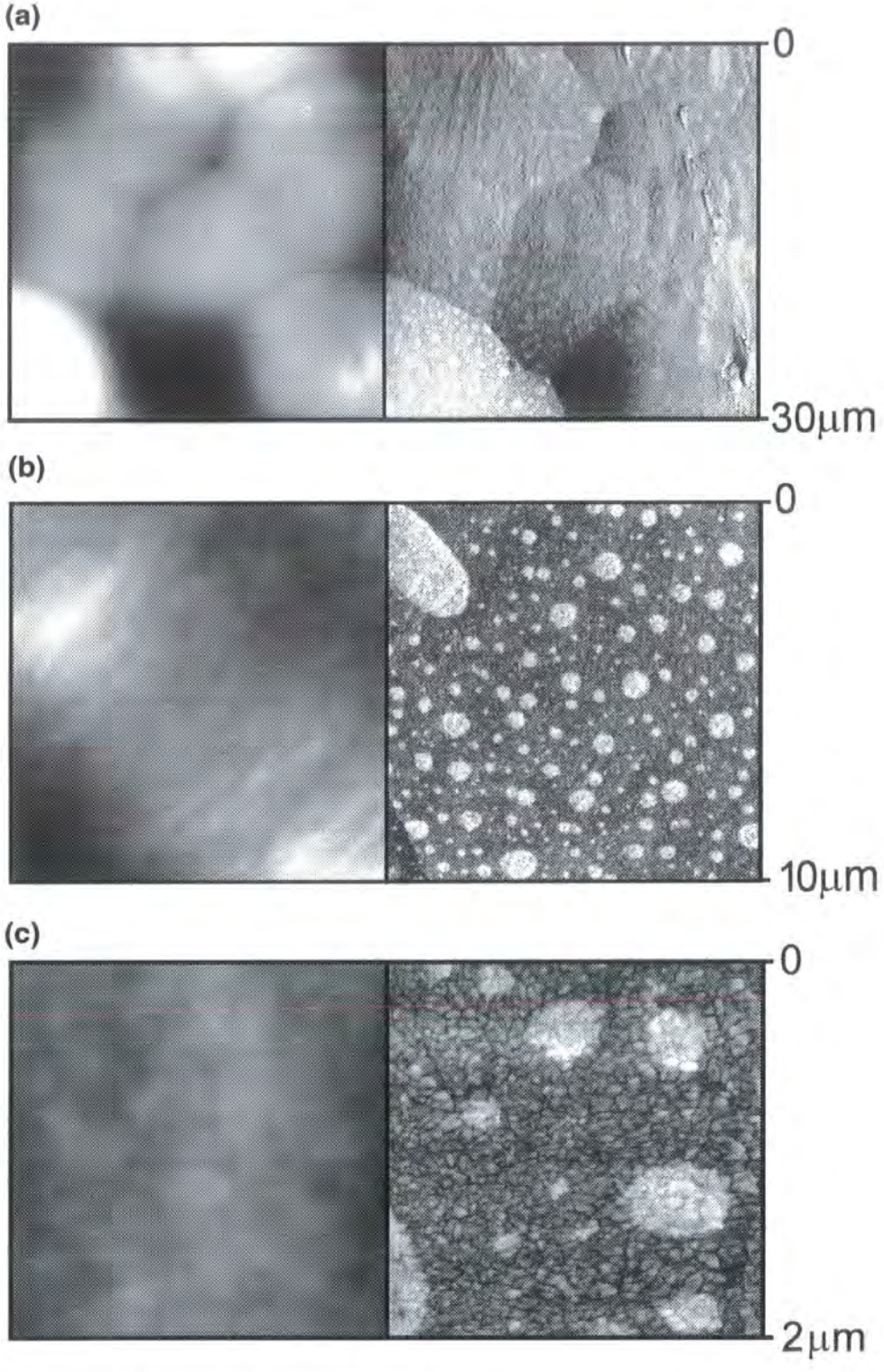

Figure 2.3 Tapping Mode AFM micrographs of fluorochemical doped polypropylene (LHS: height; RHS: phase): (a) 30 μm x 30 μm; (b) 10 μm x 10 μm; and (c) 2 μm x 2 μm.

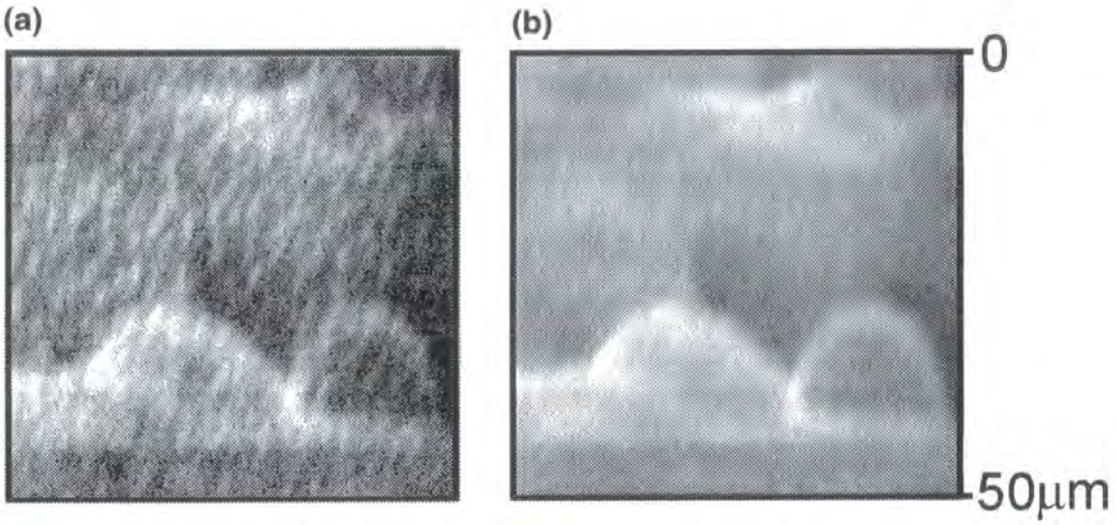

Figure 2.4 50 μm × 50 μm SIMS images of doped polypropylene: (a) F^- ion image; and (b) total ion image.

2.2.3.2.The Effect of Annealing

Annealing at 80 °C and 130 °C did not alter the XPS surface composition of the pure polypropylene film. Whereas in the case of the fluorochemical doped material, the rate of additive build-up at the surface slowed with lengthening annealing period, until eventually a limiting coverage was reached, Figure 2.5. A maximum fluorochemical coverage of about 34% was measured after annealing at 80 °C for 64 hours, Figure 2.5a. At the higher temperature of 130 °C, the maximum coverage was greater, corresponding to approximately 80% coverage after just 15 minutes, Figure 2.5b.

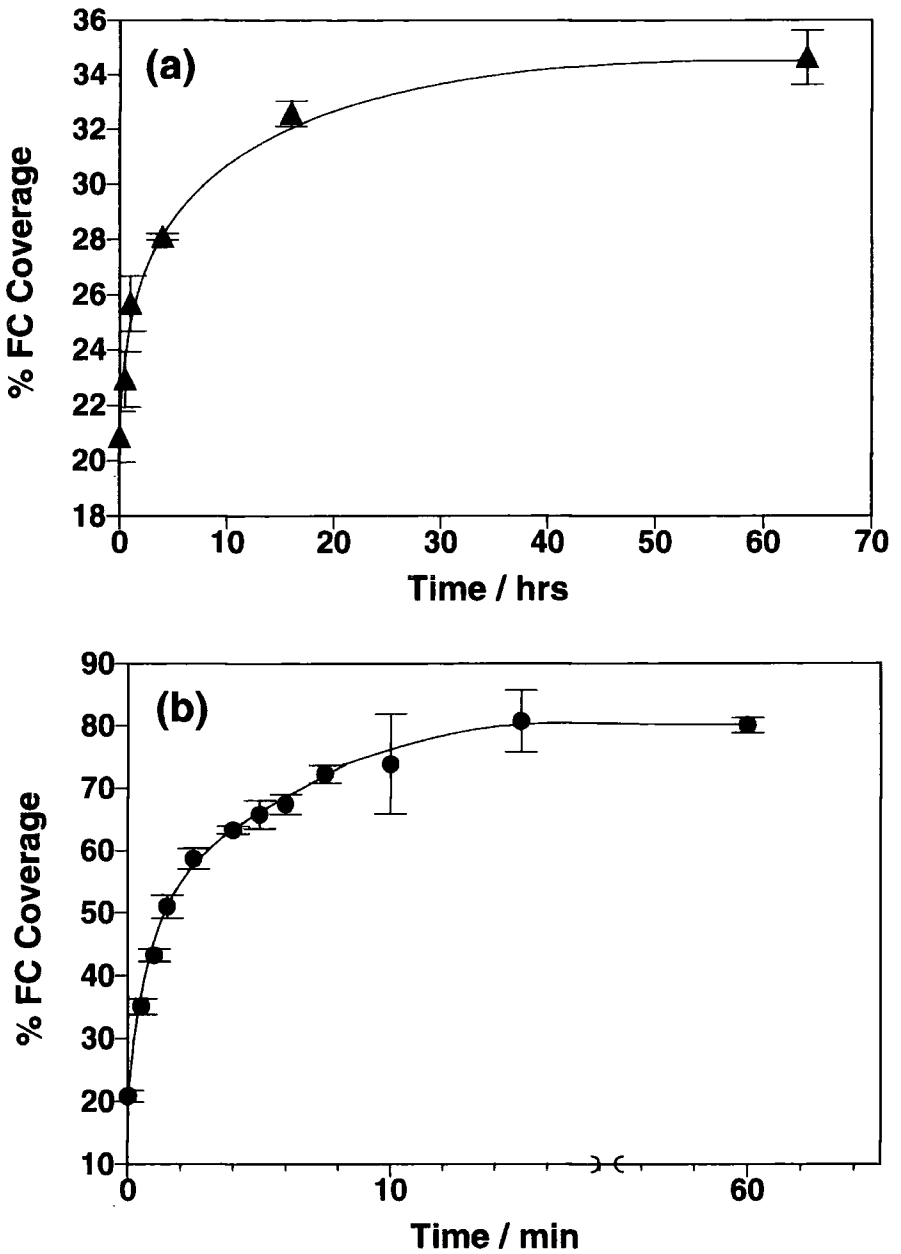

Figure 2.5 XPS additive coverage as a function of annealing time: (a) 80 °C; (b) 130 °C.

On this premise, a series of surfaces with varying fluorochemical coverage were prepared by annealing the doped film at 130 °C for increasing periods of time. These were then characterised by XPS, contact angle measurements, phase imaging AFM, and TOF-SIMS. For each set of annealing conditions, the pure polypropylene sample was employed as a fluorochemical-free reference substrate.

Water (surface energy: polar component = 50.7 mN m^{-1} and dispersive component = 22.1 mN m^{-1})[33] and hexadecane (surface energy: dispersive

component only = 27.5 mN m^{-1})[33] contact angles were measured as a function of the amount of fluorochemical present at the surface, Figure 2.6. Water and hexadecane contact angles exhibit a fairly linear rise versus additive coverage. As expected on the basis of surface energetics, hexadecane wets pure polypropylene (surface energy: = 38 m Nm^{-1}).[33]

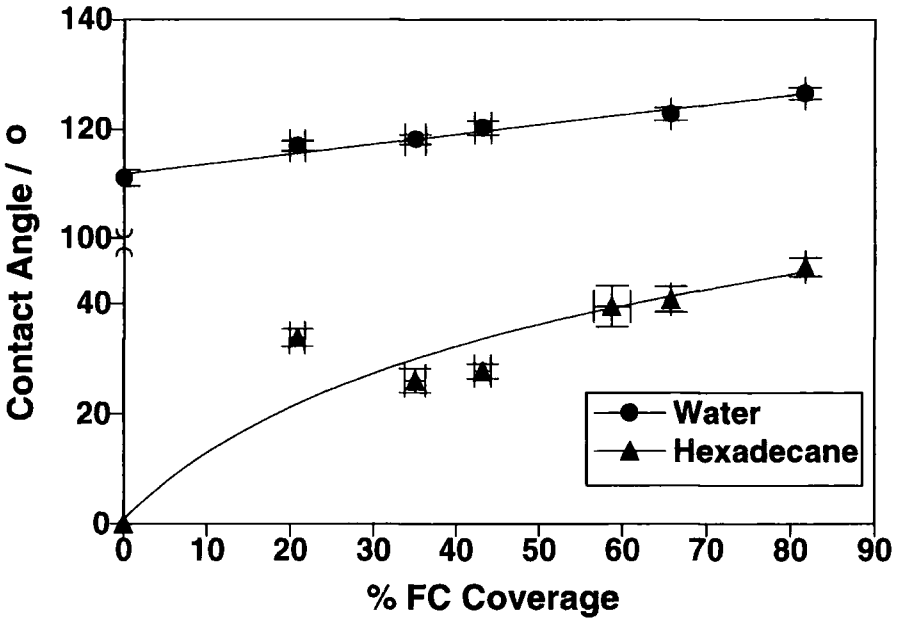

Figure 2.6 Water and hexadecane contact angles as a function of fluorochemical coverage (determined by XPS).

Tapping mode AFM phase images showed that the surface distribution of fluorochemical additive changes from discrete dots and patches, to a connected network with increasing surface coverage, Figure 2.7. The surface concentration determined by XPS was found to be in good agreement with the data obtained from AFM image analysis. As indicated previously, Tapping Mode AFM images portray slightly greater coverage compared to XPS due to the higher surface sensitivity of AFM.

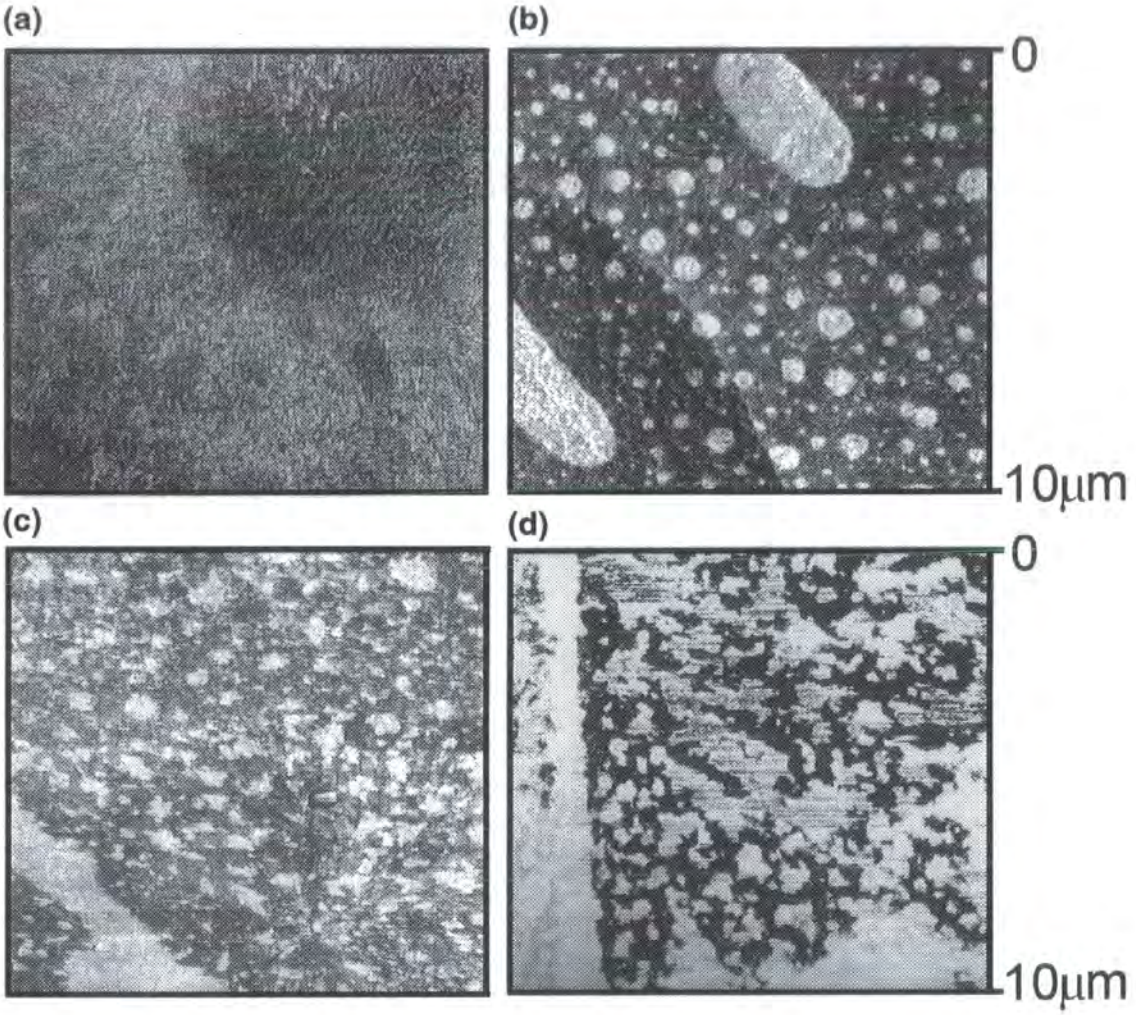

Figure 2.7 Tapping Mode AFM phase images at the surface (all images are 10 μm × 10 μm): (a) pure polypropylene; (b) 21% fluorochemical coverage by XPS, 27.7% in image; (c) 32% fluorochemical coverage by XPS, 38.8 % in image; (d) 61% fluorochemical coverage by XPS, 65.7 % in image.

Imaging SIMS confirmed the effect of annealing on the distribution of fluorochemical additive at the surface, by showing an uniform F^- signal across the polymer film, Figure 2.8a. Again, the total ion image reflects the sample morphology, Figure 2.8b.

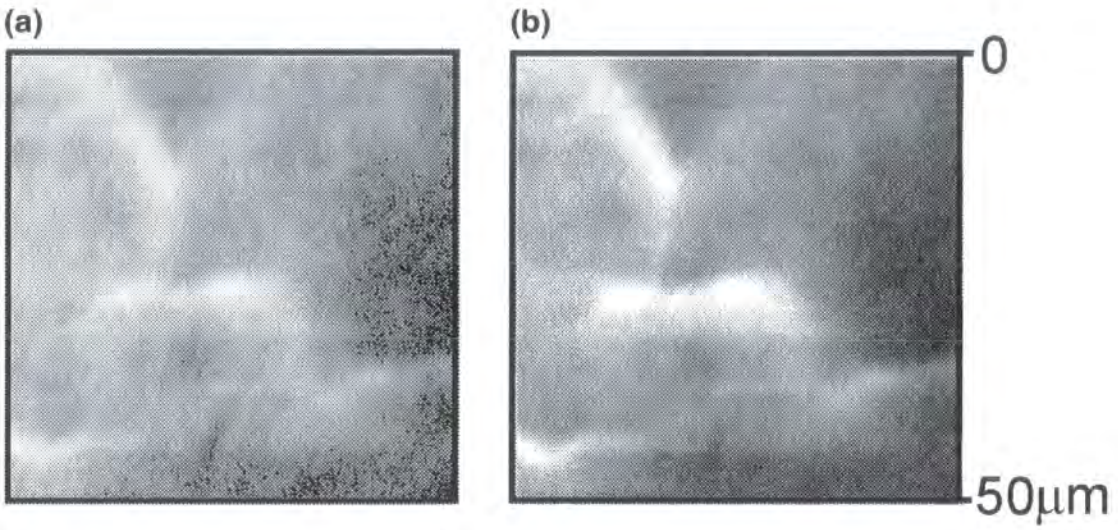

Figure 2.8 50 μm × 50 μm SIMS images of doped polypropylene annealed at 130 °C for 15 minutes: (a) F^- ion image; and (b) total ion image.

2.2.3.3.Surface Concentration Gradient

F(1s) electrons experience a smaller mean free path compared to F(2s) electrons.[31] Consequently the F(1s)/F(2s) intensity ratio can provide an insight into the concentration gradient of fluorinated moieties at the surface. Poly(tetrafluoroethylene) (PTFE) film was used as a reference, since it contains a uniform distribution of fluorinated functionalities, yielding a F(1s)/F(2s) value of 23.1 ± 0.4. A F(1s)/F(2s) ratio of 33.0 ± 2.5 was measured for high coverage fluorochemical doped polypropylene (produced by annealing at 130 °C for 15 minutes, see Figure 2.5b). This ratio is greater than the value for PTFE, and therefore it can be concluded that a concentration gradient of additive exists within the topmost 2-5 nm of the surface (the XPS sampling depth).

Further insight into the variation of additive concentration with depth at the surface was gained by angle resolved XPS.[31] The sampling depth at a given take-off angle, θ is given by $3\lambda\sin\theta$, where λ is the mean free path of the photoelectrons in the polymer.[31] Hence, as the take-off angle is reduced, surface sensitivity is enhanced. For a given high fluorochemical coverage film (produced by annealing at 130 °C for 15 minutes), it was found that the C(1s) signal intensities of the $\underline{C}F_2$ group (292.2 eV) and the $\underline{C}F_3$ group (294.2 eV) increase relative to the hydrocarbon peak (285.0 eV) with decreasing take-off angle, Figure 2.9(a) (C(1s) spectra were fitted to five Mg $K\alpha_{1,2}$ components: $\underline{C}_xH_y$ (285 eV), $\underline{C}$-O (286.6 eV), $\underline{C}$=O / O-$\underline{C}$-O (287.8 eV), $\underline{C}F_2$ (291.2 eV) and $\underline{C}F_3$ (293.3 eV);[34] in addition Mg $K\alpha_{3,4}$ satellite peaks shifted by ~9 eV towards lower binding energy were taken into consideration). The aforementioned surface concentration gradient was confirmed by plotting the F(1s)/C(1s) ratio and the relative amounts of F, N, O and S versus relative sampling depth, Figure 2.9b and c respectively. In the latter case, it is evident that as the sampling depth decreases, the proportion of F exceeds the expected theoretical amount (based on random additive conformation in the surface region), and the concentration of O is lower. In conjunction with the observed relative increase of CF_3 versus CF_2, Figure 2.9a, this confirms that the fluorochemical segments of the additive are preferentially aligned outwards at the surface.

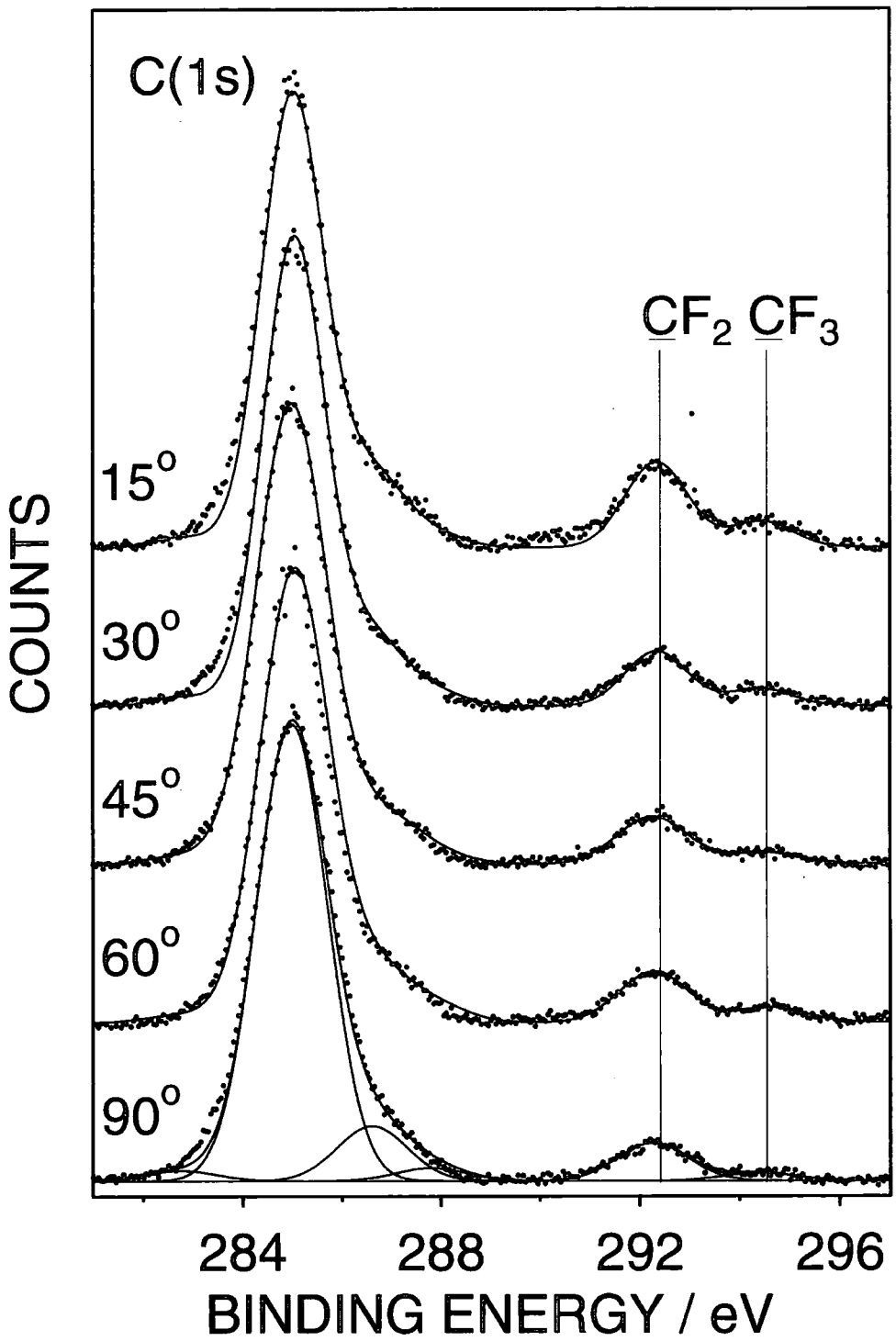

Figure 2.9a C_{1s} envelope as a function of take-off angle.

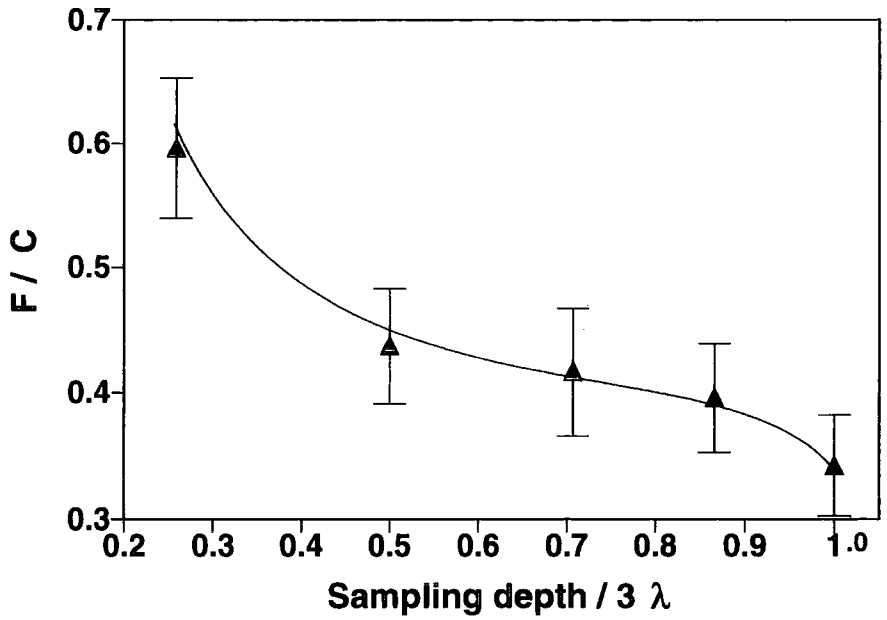

Figure 2.9b Variation of F / C ratio with sampling depth.

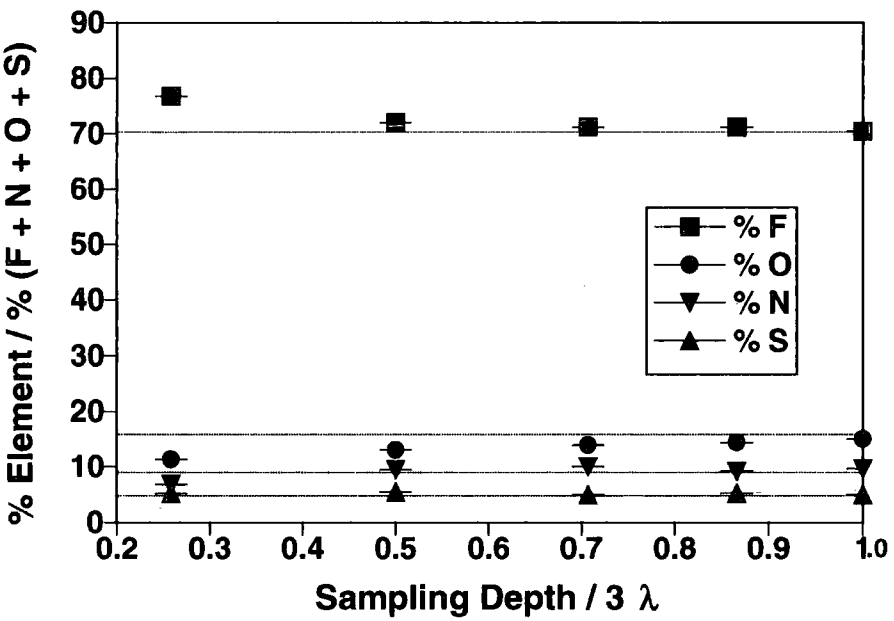

Figure 2.9c Variation in amount of F, N, O and S at the surface with sampling depth. Horizontal dashed lines show the predicted results assuming the additive is randomly orientated at the surface.

2.2.4. Discussion

The straight edged spherulite boundaries discernible in the optical and large scale Tapping Mode AFM images (Figures 2.1, 2.2a and 2.3a) are consistent with athermal (simultaneous) nucleation of a single modification of polypropylene during continuous cooling conditions.[35] X-ray diffraction studies indicated that the films consist almost exclusively of the α-polymorph.[36] The small number of rounded boundaries, such as those seen in Figure 2.2a, can be attributed to the sporadic inclusion of β-phase spherulites.[35] The cross-hatched morphology seen at higher resolution by AFM phase imaging for the pure polypropylene spherulites (Figure 2.2c) has previously been observed by polarised light microscopy,[37] scanning electron microscopy,[37] transmission electron microscopy[38,39] and Tapping Mode AFM.[40] This corresponds to lamellar growth along both the radial and tangential directions within α-spherulites during the rapid cooling of the polypropylene melt.[41,42] Incorporation of non-crystallisable constituents into the melt can alter spherulite growth rates as they are expelled from the growth front.[43] In the present study, the larger spherulite size and changes in lamellae structure noted for the fluorochemical containing sample are indicative of the additive altering the polypropylene crystallization process, Figures 2.1-2.3 and Table 2.2.

Surface energies were calculated using the Owen and Wendt method[44] for the pure polypropylene film (38 ± 3 mN m^{-1}; contact angles: water = 111° and methylene iodide = 48.6°) and the pure fluorochemical additive (12 ± 1 mN m^{-1}; contact angles: water = 109.2° and hexadecane = 78.7°) On the basis of thermodynamics, the lower surface energy fluorochemical component is enriching the polypropylene surface.[16-18] However this is not able to proceed to completion, since the melt is cooled from 154 °C to ambient temperature in approximately 1 s. Subsequent annealing enables more additive to migrate towards the polymer-air interface, thereby approaching closer to thermodynamic equilibrium. The increase in additive concentration at the surface of the doped film during annealing can be rationalised in terms of kinetic and thermodynamic factors. The former is related to the additive's diffusion coefficient within the polypropylene matrix, which will increase with

temperature;[45,46] therefore maximum coverage is reached more quickly at 130 °C compared to 80 °C. Whereas thermodynamics determines the equilibrium additive coverage achievable at a given temperature. Furthermore, XPS has shown that the two perfluorinated arms present in the additive molecule adopt a conformation which exposes the fluorinated chains at the surface, further minimising the surface energy.

The observed AFM phase image contrast can be attributed to differences in elasticity,[29] hydrophobicity,[47] adhesion,[48] and energy dissipation.[49] For the moderately hard tapping conditions employed in this study, phase contrast is most likely to be due to differences in mechanical properties between the host polypropylene matrix and the fluorochemical additive.[29,50] Of particular note is the fact that the additive can be unambiguously identified in the AFM phase image, but not the height image. Whereas a recent study of a solvent cast, alkyd resin coating containing a small amount of fluorinated ester additive, displayed additive features in both height and phase images.[21]

2.3. The Effect of Polymer Molecular Weight on Surface Enrichment in Fluorochemical Doped Polypropylene Films

2.3.1. Introduction

A new set of films containing the bis-perfluorinated additive (Structure 2.1) were extruded to elucidate the effect of polymer molecular weight on additive segregation. XPS and Tapping Mode AFM analysis have been used to monitor the surface segregation behaviour of the fluorochemical additive.

2.3.2. Experimental

Melt-blown undoped and 1% wt. fluorochemical containing polypropylene films were prepared using three different molecular weight grades of polymer: low molecular weight (Exxon 3505, melt flow index = 400), medium molecular weight (Fina 3860, melt flow index = 100), and high molecular weight (Fina 3374, melt flow index = 2.5). Melt flow index is taken as a measure of how a polymer extrudes during a fixed time period, and is therefore related to molecular weight.[51] For instance, a low melt flow index corresponds to a viscous polymer melt, and hence a high molecular weight polymer.[52]

Solvent washing studies of the polymer film surfaces comprised immersion in propan-2-ol (Fisher, 99.99 % purity) for a predetermined time, followed by air drying at room temperature. Subsequent annealing of the film was carried out in a temperature-controlled oven, where pieces of polymer were laid flat on top of a clean metal plate. The outer surface was then analysed by XPS and Tapping Mode AFM for physicochemical changes.

XPS, Tapping Mode AFM and image analysis were carried out as described in Section 2.2.2.

2.3.3. Results

2.3.3.1.The Effect of Polymer Molecular Weight on Surface Segregation

XPS was used to measure the percentage elemental concentration of C, F, O, N and S in approximately the top 2-5 nm of each film sample,[31] Table 2.3. In the case of pure polypropylene, only C(1s) spectral features corresponding to $\underline{C}_xH_y$ were observed (since XPS is not sensitive to hydrogen). The ratio of F : O : N : S at the surfaces of the fluorochemical doped polypropylene films was consistent with the molecular formula of the additive (40% C, 42.5% F, 10% O, 5% N and 2.5 %S; again H is excluded). The overall fluorochemical coverage at the surface was calculated using the percentage of elemental F detected by XPS. For all three different molecular weights of polypropylene matrix, a considerable surface excess was observed compared to the 1% fluorochemical loading in the bulk. Surface enrichment increased with polymer molecular weight, Table 2.3.

Polypropylene			% XPS Elemental Analysis (± 0.5 %)					% Additive Coverage	
Melt flow index	Extrusion temperature / °C		C	F	O	N	S	XPS	AFM
400	154	Undoped	100.0	0.0	0.0	0.0	0.0	-	-
		1 % doped	86.8	9.0	2.1	1.6	0.5	21 ± 0.6	28 ± 1
100	166	Undoped	100.0	0.0	0.0	0.0	0.0		
		1 % doped	83.6	9.7	4.3	1.9	0.5	22 ± 0.8	32 ± 1
2.5	221	Undoped	100.0	0.0	0.0	0.0	0.0		
		1 % doped	58.2	30.3	6.0	4.2	1.3	69 ± 2.1	71 ± 1
Theoretical additive XPS			**40.0**	**42.5**	**10.0**	**5.0**	**2.5**		

Table 2.3 XPS and AFM surface analysis of melt-blown films.

2.3.3.2.The Effect of Polymer Molecular Weight on the Morphology of Pure Polypropylene Films

Low resolution atomic force micrographs revealed that the surface of the pure polyolefin films consist mainly of straight edged spherulites, Figure 2.10. Spherulite size was noted to decrease with increasing polymer molecular weight. This trend was quantified by measuring the widest axis of each spherulite, Table 2.4. In the case of the highest molecular weight sample, there were also some regions which could not be resolved into distinct spherulites, Figure 2.10c.

At higher spatial resolution, it is apparent that the structure of individual spherulites is also influenced by the polyolefin molecular weight, Figure 2.11. Two sets of lamellae arranged parallel and perpendicular to the radial spherulite direction are evident in the phase image of the low molecular weight polypropylene film, Figure 2.11a. Spherulites at the surface of the medium molecular weight polymer exhibit radial symmetry, Figure 2.11b. Whereas thicker, parallel lamellae sheaf are evident in the case of the high molecular weight polypropylene surface, Figure 2.11c.

Melt flow index	Pure diameter / μm	Doped diameter / μm
400	15.3	16.9
100	14.9	21.3
2.5	2.7	ill defined

Table 2.4 Spherulite sizes measured by AFM.

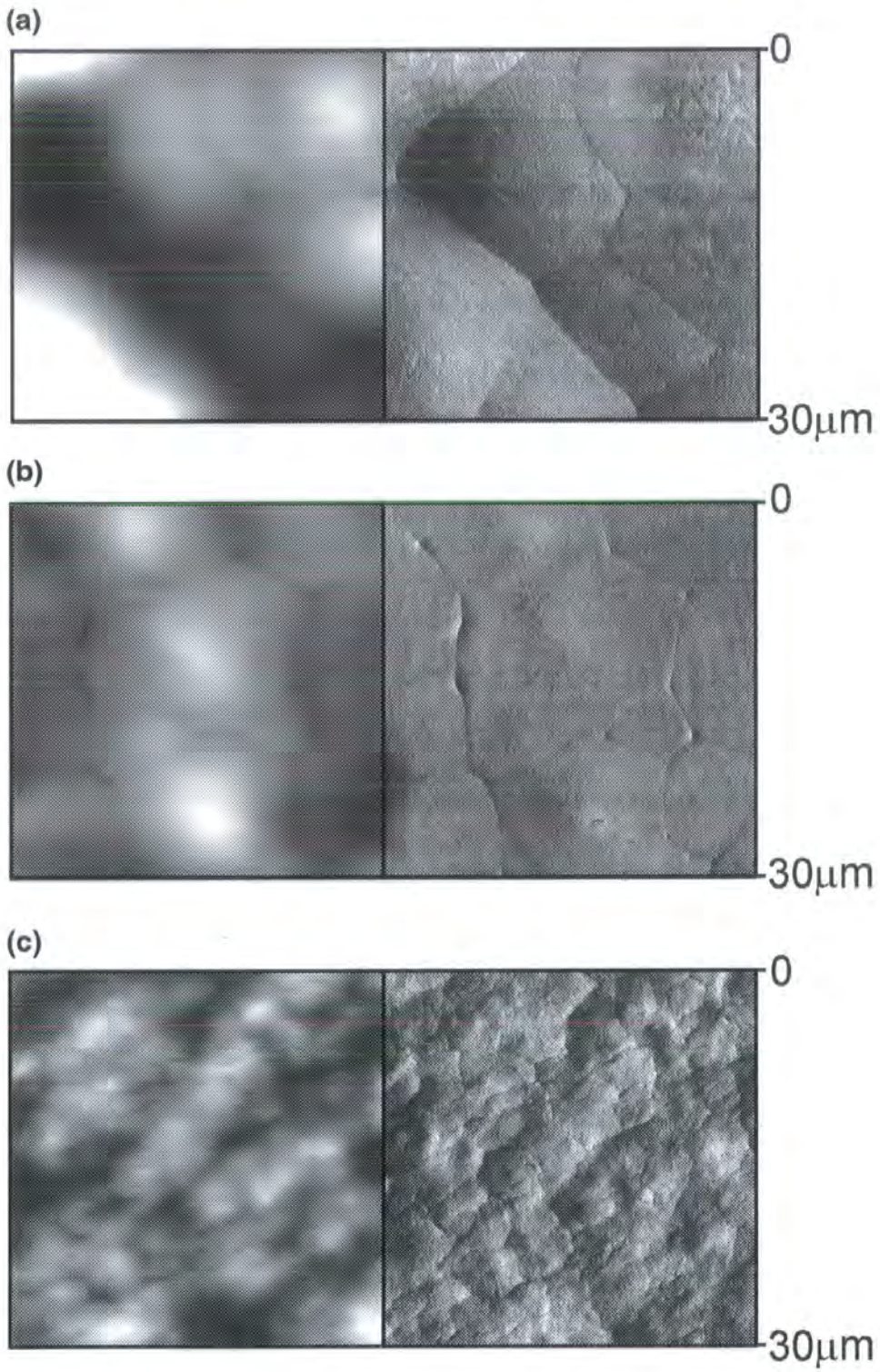

Figure 2.10 30 μm × 30 μm Tapping Mode AFM images of pure polypropylene surfaces (LHS: height; RHS: phase): (a) low molecular weight; (b) medium molecular weight; and (c) high molecular weight.

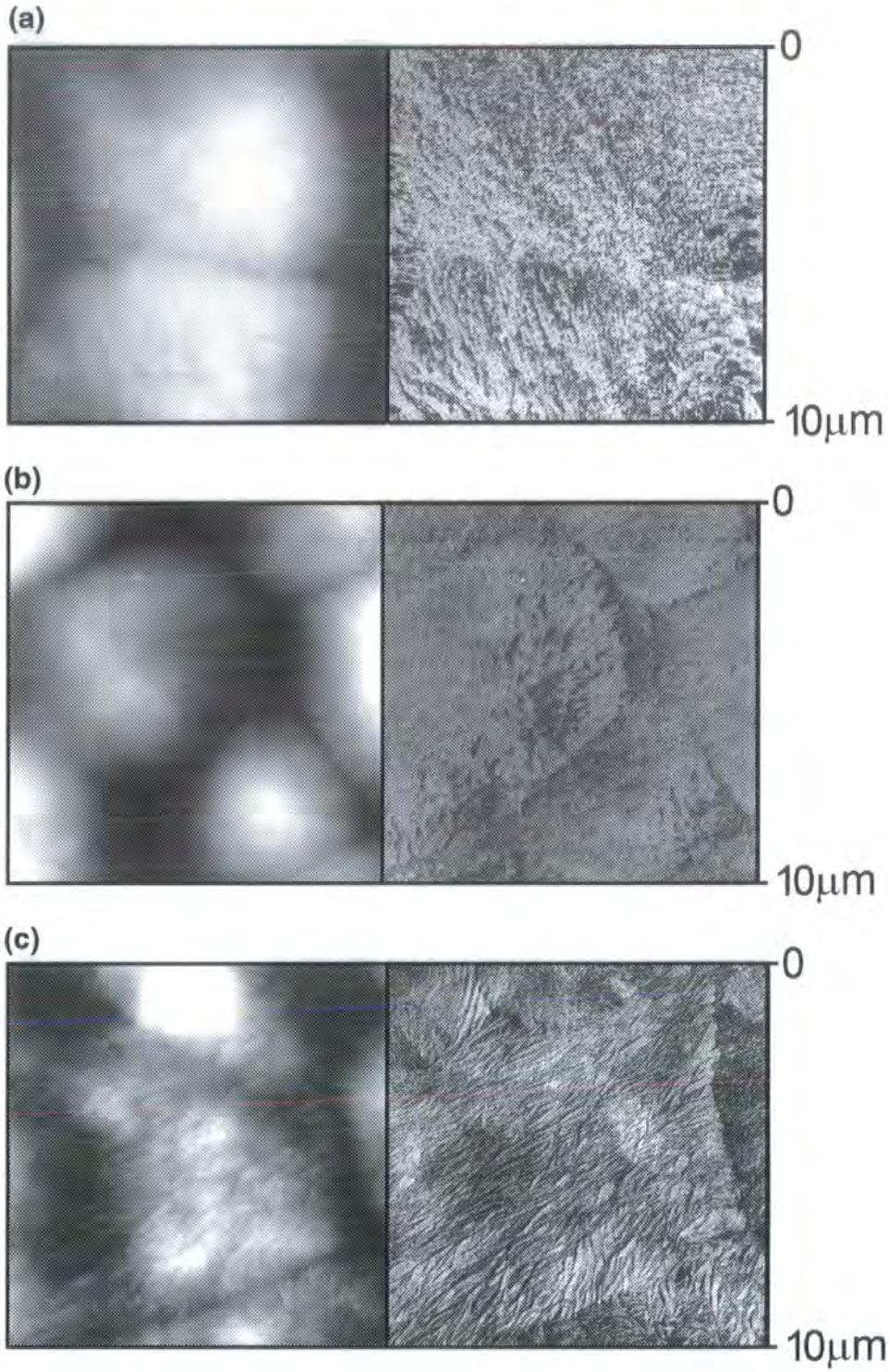

Figure 2.11 10 μm × 10 μm Tapping Mode AFM images of pure polypropylene surfaces (LHS: height; RHS: phase): (a) low molecular weight; (b) medium molecular weight; and (c) high molecular weight.

2.3.3.3.The Effect of Polymer Molecular Weight on the Surface Morphology and Additive Distribution of Fluorochemical Doped Films

The fluorochemical additive is easily identifiable in the AFM phase images of all three doped polypropylene films as regions of bright contrast, Figures 2.12 and 2.13. For the low molecular weight polymer, circular dots of fluorochemical are prominent, Figures 2.12a and 2.13a. In addition to these fluorochemical dots, elongated fluorochemical patches with a common orientation, can be seen for the medium molecular weight system, Figure 2.12b and 2.13b. Any elongation of fluorochemical patches in a common direction can be attributed to film stretching during the melt blowing process. In the case of the high molecular weight polypropylene matrix, the surface is covered with a continuous network of fluorochemical material, Figures 2.12c and 2.13c. For each of the high-resolution Tapping-mode AFM phase images, overall fluorochemical coverage (± 1%) was estimated using image analysis software, Table 2.3. Larger coverage values were measured by AFM for the low and medium molecular weight polypropylene matrices compared to corresponding XPS elemental analysis. This discrepancy can be taken as being indicative of a fluorochemical concentration gradient extending from the surface towards the bulk (Tapping Mode AFM is only sensitive to the outermost surface, whereas XPS probes 2-5 nm into the sample[31]). However, similar fluorochemical coverage was measured for the high molecular weight polypropylene matrix. This is consistent with this system experiencing the greatest surface segregation (i.e. the fluorochemical layer thickness is comparable to the XPS sampling depth).

The spherulite morphology previously seen for the pure polypropylene films was still clearly visible in the large scale atomic force micrographs of fluorochemical doped low and medium molecular weight polypropylene, Figures 2.12a and b. In fact, the mean spherulite diameters are larger compared to their pure polypropylene counterparts, Table 2.4. Again, the surface morphology of the high molecular weight sample was less well defined, Figure 2.13c.

At higher spatial resolution, the lamellae organisation previously observed for the low and medium molecular weight pure polyolefin films was absent, Figures

2.13a and b. However, thick sheaf type lamellae could still be seen for the high molecular weight polypropylene matrix.

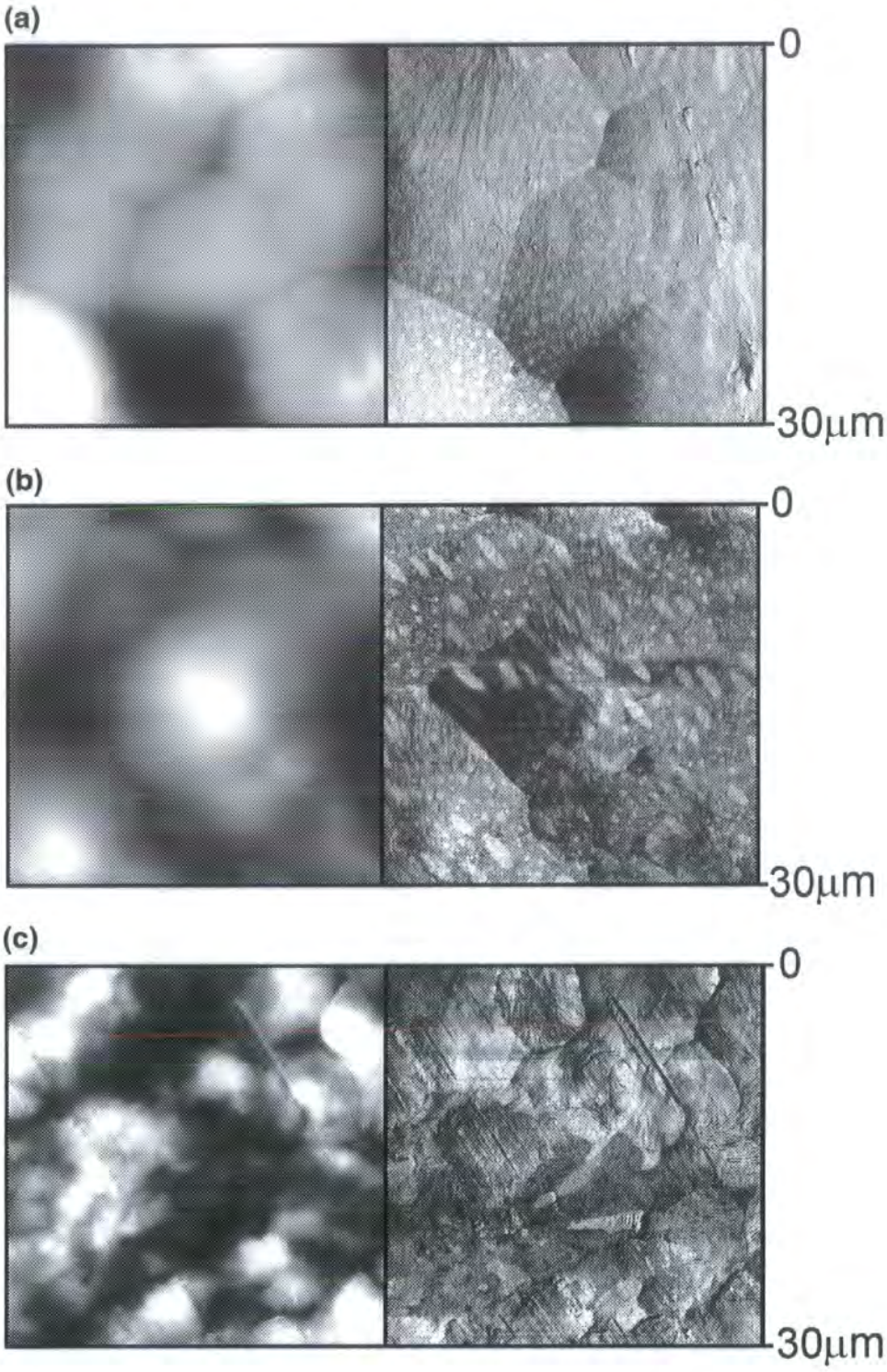

Figure 2.12 30 μm × 30 μm Tapping Mode AFM images of fluorochemical additive doped polypropylene surfaces (LHS: height; RHS: phase): (a) low molecular weight; (b) medium molecular weight; and (c) high molecular weight.

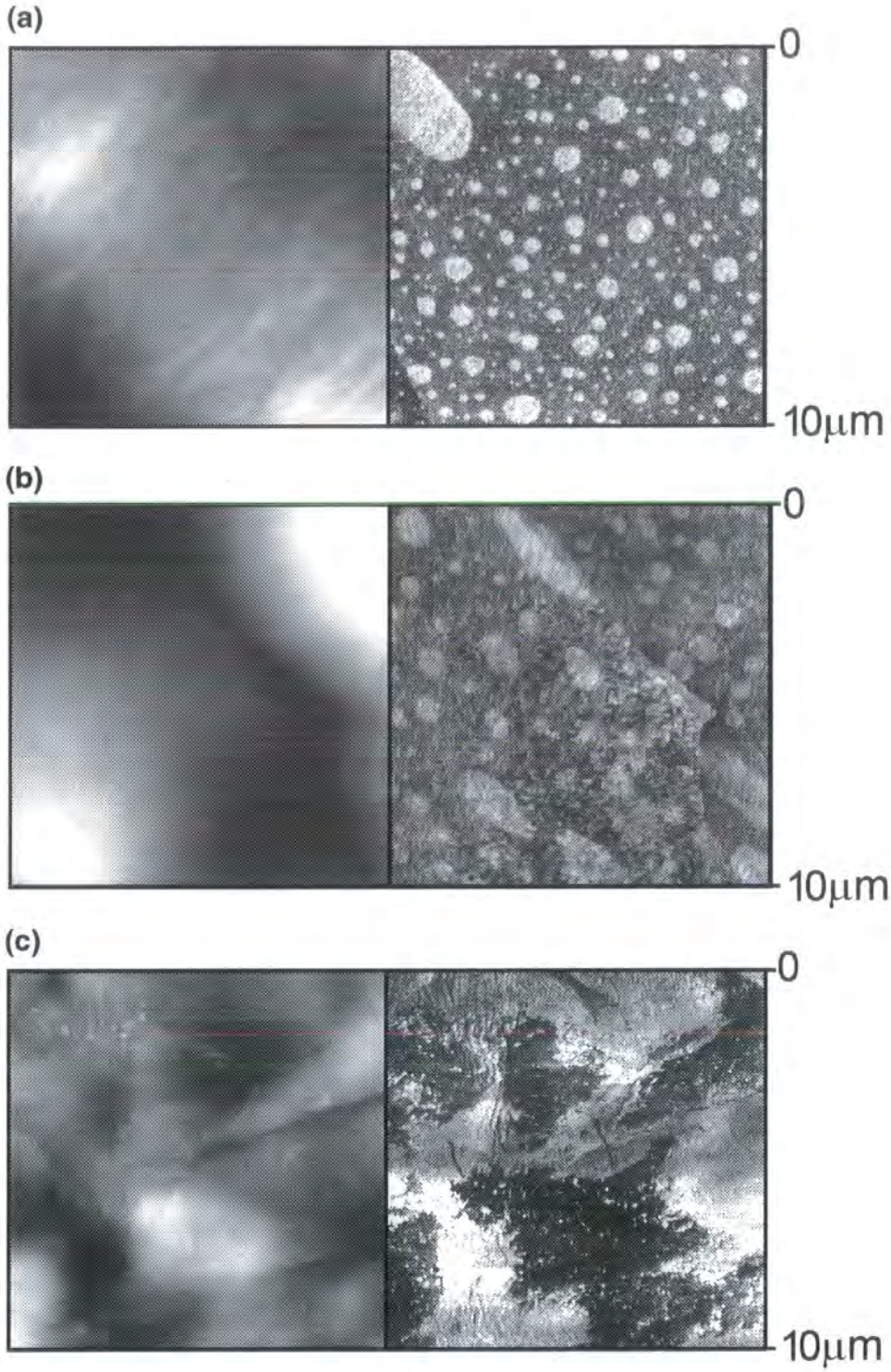

Figure 2.13 10 μm × 10 μm Tapping Mode AFM images of fluorochemical additive doped polypropylene surfaces (LHS height; RHS phase): (a) low molecular weight; (b) medium molecular weight; and (c) high molecular weight.

2.3.3.4.The Effect of Polymer Molecular Weight on the Kinetics of Fluorochemical Segregation

It has previously been shown that annealing fluorochemical containing polyolefin films can increase the extent of surface segregation (Section 2.2.3.2). Here, the rate of additive build-up at the surface during annealing was studied for all three molecular weights of polypropylene matrix. In order to compare the rate of fluorochemical migration, it was first necessary to remove additive from the outermost surface region by rinsing in propan-2-ol. This solvent was found not to dissolve the fluorochemical additive, rather it lifted fluorochemical away from the polymer surface via undercutting. In order to ensure that each sample was depleted of additive to the same extent during washing, the low and medium molecular weight samples were first annealed to obtain the same fluorochemical coverage as the high molecular weight system prior to immersion in solvent. Propan-2-ol washing was then allowed to proceed until the XPS signal from the additive molecules disappeared (1 hour exposure). This corresponded to removal of all the fluorochemical additive contained in the top 2-5 nm (XPS sampling depth).

Subsequently, each sample was annealed at 130 °C as a function of time, and the fluorochemical segregation from the bulk towards the surface was monitored by XPS. All three grades of polypropylene displayed a slowing rate of additive migration towards the surface with increasing annealing time, Figure 2.14. Eventually a point was reached where no further build-up of additive was observed, thereby indicating equilibrium had been reached. Increasing polypropylene molecular weight caused faster migration of the fluorochemical towards the surface, and also yielded greater maximum coverage (low molecular weight, additive coverage = 17%; medium molecular weight, additive coverage = 88%; and high molecular weight, additive coverage = 100%).

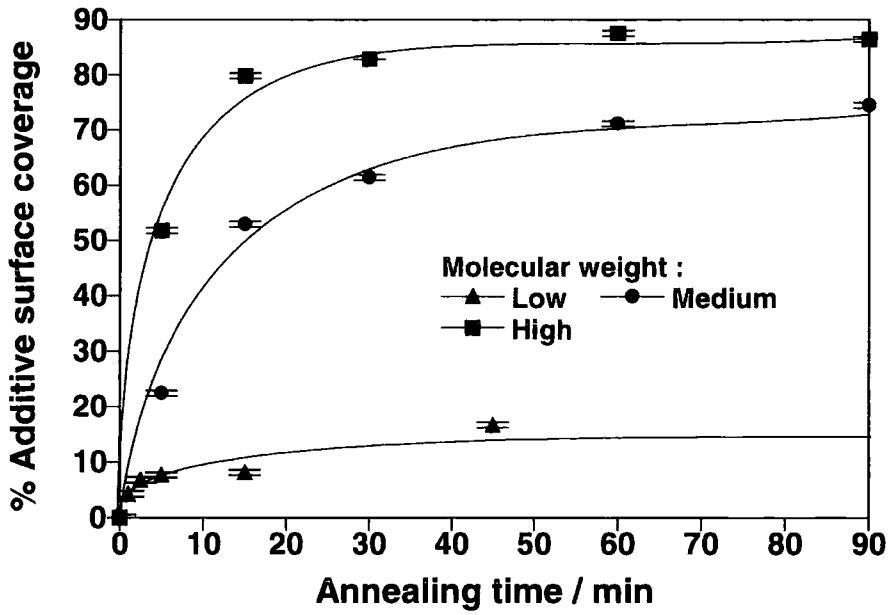

Figure 2.14 Variation in fluorochemical additive surface coverage as a function of annealing time at 130 °C.

2.3.4. Discussion

Firstly, the dependency of surface morphology upon polymer molecular weight needs to be considered for the undoped polypropylene films. It is well known that polymer spherulites tend to form as a consequence of radial crystal growth from nucleation centres, until eventually they impinge, generating spherulite boundaries. Hence, the overall spherulite size is governed by the interplay between rates of growth and nucleation. Fast growth rates accentuate spherulite diameter, whilst rapid nucleation rates restrict spherulite size due to greater impingement.[53] The drop in spherulite size seen by AFM with increasing molecular weight stems from lower polymer chain mobility reducing the growth rate,[54] combined with greater super-cooling of the melt increasing the nucleation rate,[53] Figure 2.10 and Table 2.4.

A greater restriction of polymer chain mobility with increasing polymer molecular weight can also help to explain changes seen by AFM within the individual spherulites,[55] In this case, high polymer mobility will encourage a rapid chain deposition rate onto the growing lamellae, thus promoting the probability of branching. Whereas with increasing polymer molecular weight, there is a decrease in polymer chain mobility, which makes branching events less frequent, and radial lamellae become more prominent.[55] For the highest

molecular weight polypropylene employed in the present study, sheaf devoid of radial symmetry are discernible at the centres of some spherulites, such features are characteristic of the early stage of spherulitic growth.[56] Therefore chain mobility must be so low in this case that only the initial stages of spherulite growth occur during cooling of the film from the melt.

AFM has shown that the fluorochemical additive interferes with the crystallization of polypropylene. The disruption of the surface lamellae structure seen for the lower molecular weight samples is caused by the need to expel non-crystallisable fluorochemical additive molecules from the crystal growth front,[57] Figures 2.13a and b. Less perturbation of the lamellae structure is observed for the high molecular weight polypropylene matrix, Figure 2.13c, which is most likely to be a consequence of less interpenetration between additive and polymer moieties within the melt.[17] The observed enrichment of fluorochemical additive at the surface of the doped films during the annealing studies can be attributed to a combination of faster diffusion rates at elevated temperatures[46] and surface energetics, i.e. kinetic and thermodynamic factors. Fluorochemical build-up at the air-solid interface will be favoured on the basis of its lower surface energy (surface energy of polypropylene = 38 $\pm$ 3 mN m^{-1} compared to 12 $\pm$ 1 mN m^{-1} for the fluorochemical - Section 2.2.4). The circular patches of fluorochemical seen by AFM at the surface of the doped films are consistent with a minimisation of interaction energy between the additive and the surrounding polypropylene matrix.

Since the surface energy of polypropylene is known to increase with polymer molecular weight, then there should be a corresponding increase in the energetic driving force for fluorochemical segregation.[58] This can be understood on the basis that confinement of a polymer chain to the surface region produces a decrease in conformational entropy, and so short polymer chains will be expected to lose less entropy per segment compared to longer ones.[59] Hence as the polymer molecular weight increases, there are larger entropy costs associated with retaining polypropylene chains at the surface compared to enriching the surface with the much smaller fluorochemical additive molecules. Also as the polymer chain length increases, the comparatively small additive molecule finds less space available for it to interpenetrate the polymer

matrix, thus contributing to the overall drive to expel additive towards the surface with increasing polymer molecular weight.[17] This explanation is consistent with the greater equilibrium surface coverage of fluorochemical obtained for the higher molecular weight polypropylene, Figure 2.14.

Polymer molecular weight should also have an impact upon the rate (kinetics) of fluorochemical surface segregation. Additive diffusion is known to proceed most readily through the amorphous phase of crystalline polymers such as polypropylene.[25] In fact diffusion rates tend to decrease with increasing polymer crystallinity, due to corresponding smaller volumes of available amorphous material.[46] AFM images show that surface crystallinity of the fluorochemical doped samples decreases with increasing molecular weight, Figure 2.12, (i.e. a larger fraction of amorphous crystallite boundaries is evident on the high molecular weight surface combined with a more disordered spherulite structure). Additive diffusion can occur through voids contained within the amorphous regions.[46] Such voids are more likely to arise in between larger untangled polymer molecules rather than shorter interpenetrating polymer chains. Therefore, the combination of decreasing crystallinity, a greater number of amorphous voids, and the accompanying energetic driving force for additive segregation all help to explain the faster additive diffusion rates observed during annealing as polymer molecular weight increases, Figure 2.14. The greater additive coverage with higher polymer molecular weight seen for the initial melt-blown films can also be taken as being a manifestation of these factors, Table 2.3.

2.4. Surface Enrichment of Fluorochemical Doped Polypropylene Films: the Effect of Additive Structure

2.4.1. Introduction

In this section film samples were extruded to compare the surface segregation characteristics of two structurally related fluorochemical additives introduced into a polyolefin host matrix. The bis-perfluorinated additive (Structure 2.1) is compared with a mono-perfluorinated analogue: 1-octanesulfonamide, 1,1,2,2,3,3,4,4,5,5,6,6,7,7,8,8,8 heptadecafluoro-N-methyl-N-[(3-octadecyl-2-oxo-5-oxazolindinyl)methyl], Structure 2.2.[27] Both of these molecules contain two long side arms, in one case they are both perfluorinated, whilst in the other, one is a hydrocarbon chain. The impact of this difference in terms of compatibility with the host polypropylene matrix and surface segregation behaviour has been studied using XPS, Tapping Mode AFM, and contact angle measurements.

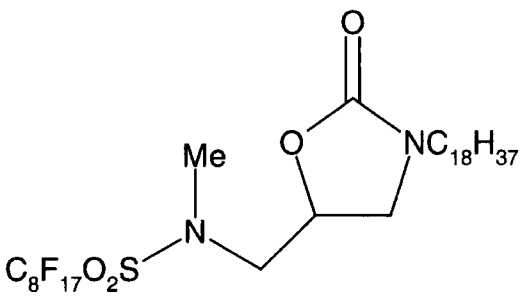

Structure 2.2: Mono-perfluorinated additive.

2.4.2. Experimental

Two melt-blown film samples were prepared using isotactic polypropylene (Fina 3860; melt flow index 100) containing 1% by weight of the mono- and bis-perfluorinated additives respectively. Surface washing experiments comprised immersion in propan-2-ol (Fisher, 99.99% purity) for a predetermined time, followed by air drying. Subsequent annealing studies were carried out in a temperature-controlled oven, where pieces of polymer film were laid flat on a clean metal plate, and the outward facing substrate surface was subsequently analysed.

XPS and Tapping Mode AFM analysis were carried out as described in Section 2.2.2.

Sessile drop contact angle measurements were carried out at 20 °C using a video capture apparatus (Instruments S.A. 2500XE). The various probe liquids (Aldrich > 99 %) used for Zisman plots and their surface tensions are listed in Table 2.5.

Liquid	**Surface Tension / m Nm^{-1} (at 20 °C)**
Hexane	18.4
Heptane	20.1
Octane	21.6
Decane	23.8
Dodecane	25.4
Tetradecane	26.6
Hexadecane	27.5

Table 2.5 Surface tension of probe liquids employed for Zisman plots.[33]

2.4.3. Results

2.4.3.1.Comparison of Surface Coverage

Both fluorochemical additives were found to preferentially accumulate at the surface during film formation in comparison to their bulk loading of 1% by weight, Table 2.6. In fact the mono-perfluorinated additive appears to completely cover the surface, whilst only partial (18%) surface enrichment of the bis-perfluorinated additive is observed. Comparison of the elemental ratios obtained from XPS for the doped films with the corresponding theoretical values for the pure additives, indicates that in the mono-perfluorinated case there is an excess of F at the surface compared to its stochiometric prediction, Table 2.6. This can be taken as being indicative of the perfluorinated arms being oriented away from the bulk polymer to minimise interfacial tension, thus accounting for the calculated surface coverages exceeding 100%. No such alignment was noted for the bis-perfluorinated system.

Additive		% Elemental analysis[a] (± 0.5 %)					% Additive coverage[b]	Critical surface energy / m Nm^{-1}
		C	F	O	N	S		
bis-	As received	88.5	7.7 (67.0)	2.4 (20.9)	1.0 (8.7)	0.4 (3.5)	18.0 (± 0.7)	-
perfluorinated	Annealed	49.3	38.0 (75.0)	7.0 (13.8)	4.0 (7.9)	1.7 (2.4)	89.4 (± 1.3)	12 (± 1)
	Theoretical	40.0	42.5 (70.8)	10.0 (16.7)	5.0 (8.3)	2.5 (4.2)	-	-
mono-	As received	54.0	36.8 (80.0)	4.7 (10.2)	2.9 (6.3)	1.6 (3.5)	119.1 (± 1.2)	14 (± 3)
perfluorinated	Theoretical	56.4	30.9 (70.9)	7.3 (16.7)	3.6 (8.3)	1.8 (4.1)	-	-

Table 2.6 XPS and surface energy characterisation of the doped polypropylene film surfaces.

[a] The numbers in brackets correspond to the non-carbon elements, which can be taken as being representative of the additive, i.e %F + %O + %N + %S = 100%.
[b] Additive surface coverage = % F by XPS / Theoretical % F.

Tapping Mode AFM height analysis showed that the surface morphology of the polypropylene film containing bis-perfluorinated additive is dominated by spherulites, Figure 2.15. The corresponding AFM phase images reveal bright phase contrast corresponding to localised regions of fluorochemical additive at the surface, overlaying the spherulites' crystalline structure (Section 2.2.3.1). The additive does not give rise to any additional contrast in the AFM height image. Whereas the height and phase images of the mono-perfluorinated doped system are very similar: the underlying spherulitic structure appears to be covered by small uniformly sized globular structures (Height ≈ 50 nm; Diameter ≈ 300 nm), Figure 2.16.

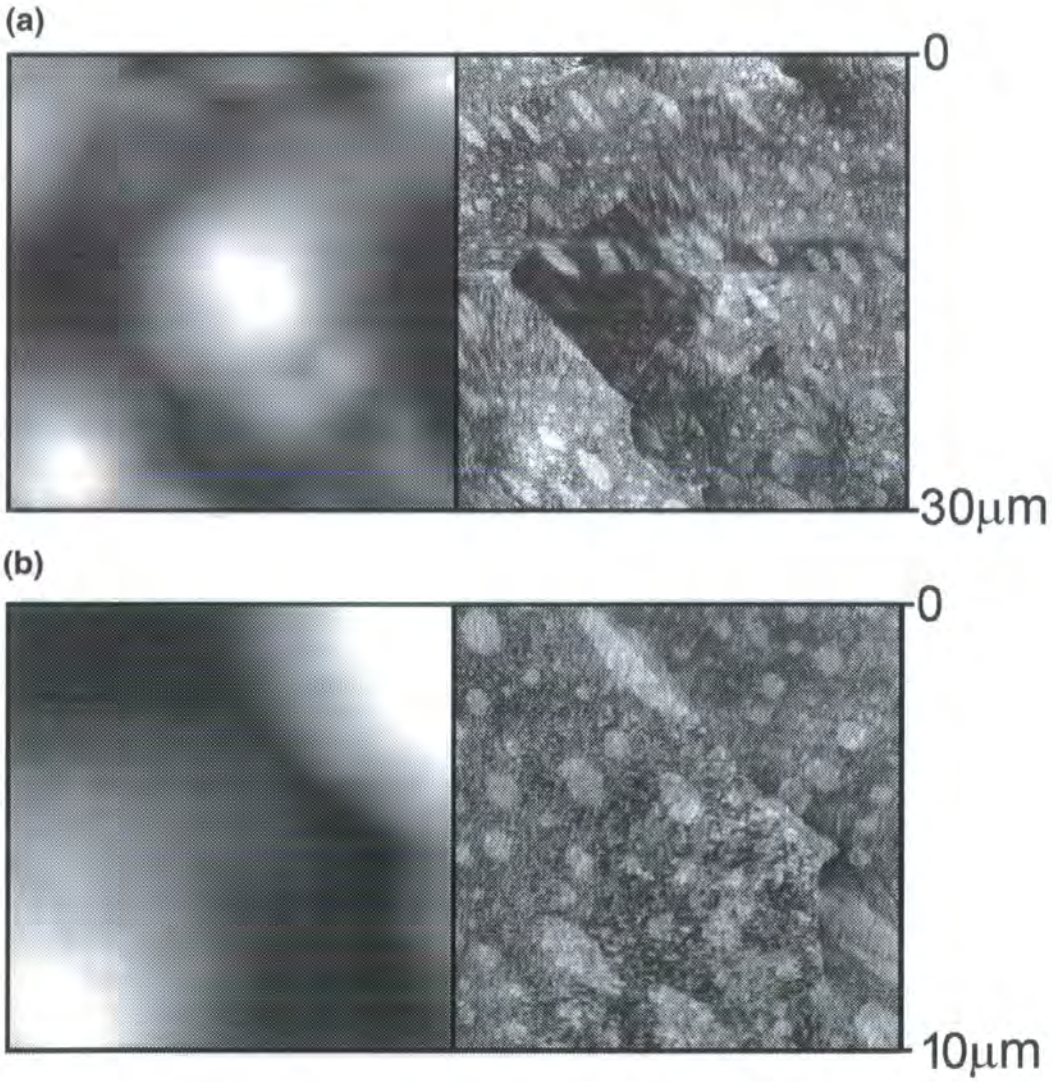

Figure 2.15 Tapping Mode AFM images of bis-perfluorinated doped polypropylene film (LHS: height ; RHS: phase): (a) 30 μm × 30 μm; and (b) 10 μm × 10 μm.

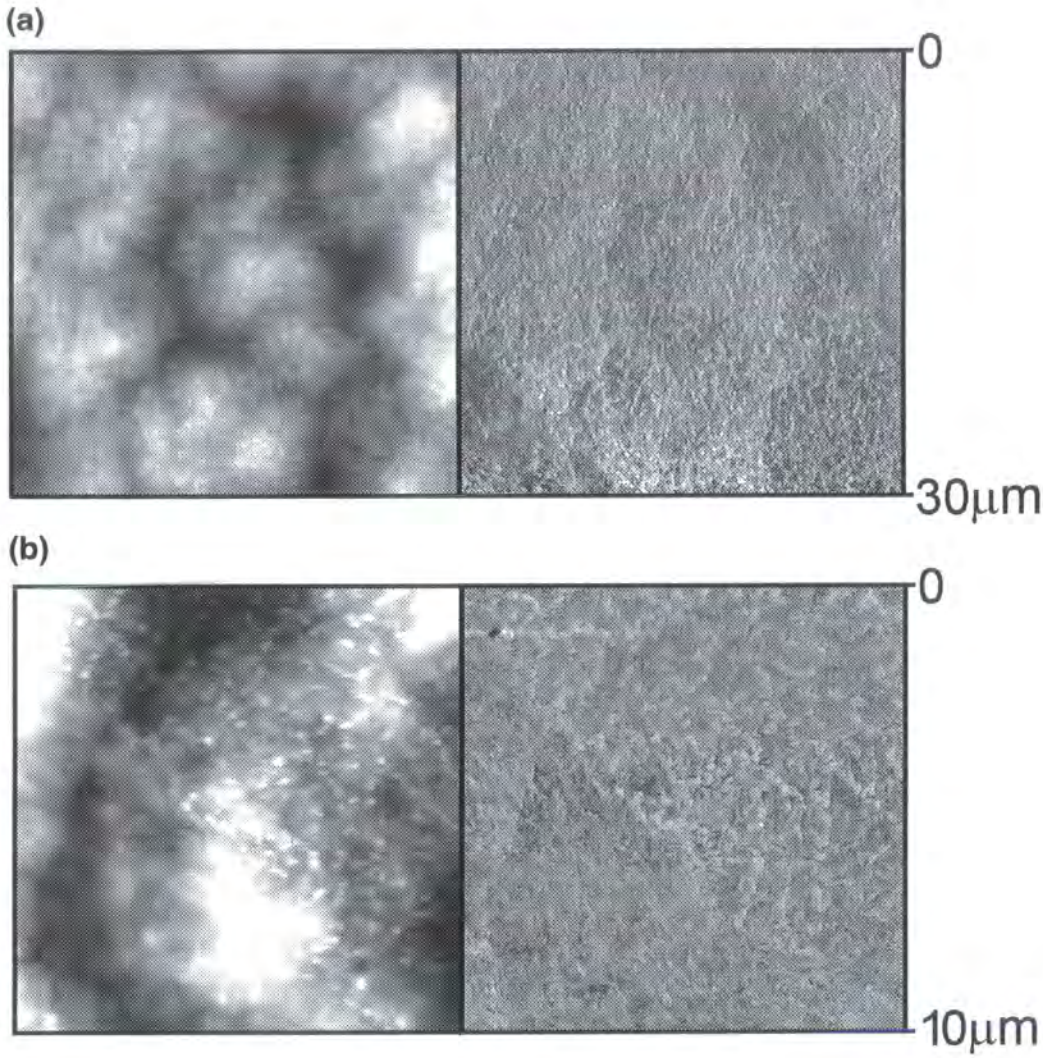

Figure 2.16 Tapping mode atomic force micrographs of mono-perfluorinated doped polypropylene films (LHS: height ; RHS: phase): (a) 30 μm × 30 μm; and (b) 10 μm × 10 μm.

Solvent washing and annealing experiments were undertaken in order to help explain the differences in behaviour between the two fluorochemical additives. As a starting point, a high coverage bis-perfluorinated doped sample was required to serve as a closer analogue to the mono-perfluorinated additive system. This was achieved by annealing the bis-perfluorinated doped sample, (150 °C, 30 min) to achieve 90 % fluorochemical surface coverage. In this case, a slight surface enrichment of F relative to the predicted elemental abundance was observed as previously noted for the mono-perfluorinated system. This corresponds to surface alignment of the perfluoroalkyl chains, Table 2.6.

Since the driving force for surface segregation is dependent upon the additive's surface energy,[16] Zisman plots were constructed in order to estimate the critical surface energy for each system.[60] This comprised plotting the cosine of contact angles obtained for a homologous series of alkane probe liquids versus their respective surface energies, Figure 2.17. Extrapolation of the best fit to $\cos(\theta) = 1$ yielded the critical surface tension. Both samples displayed a low critical surface energy value, Table 2.6. This is consistent with the aforementioned XPS and AFM analysis.

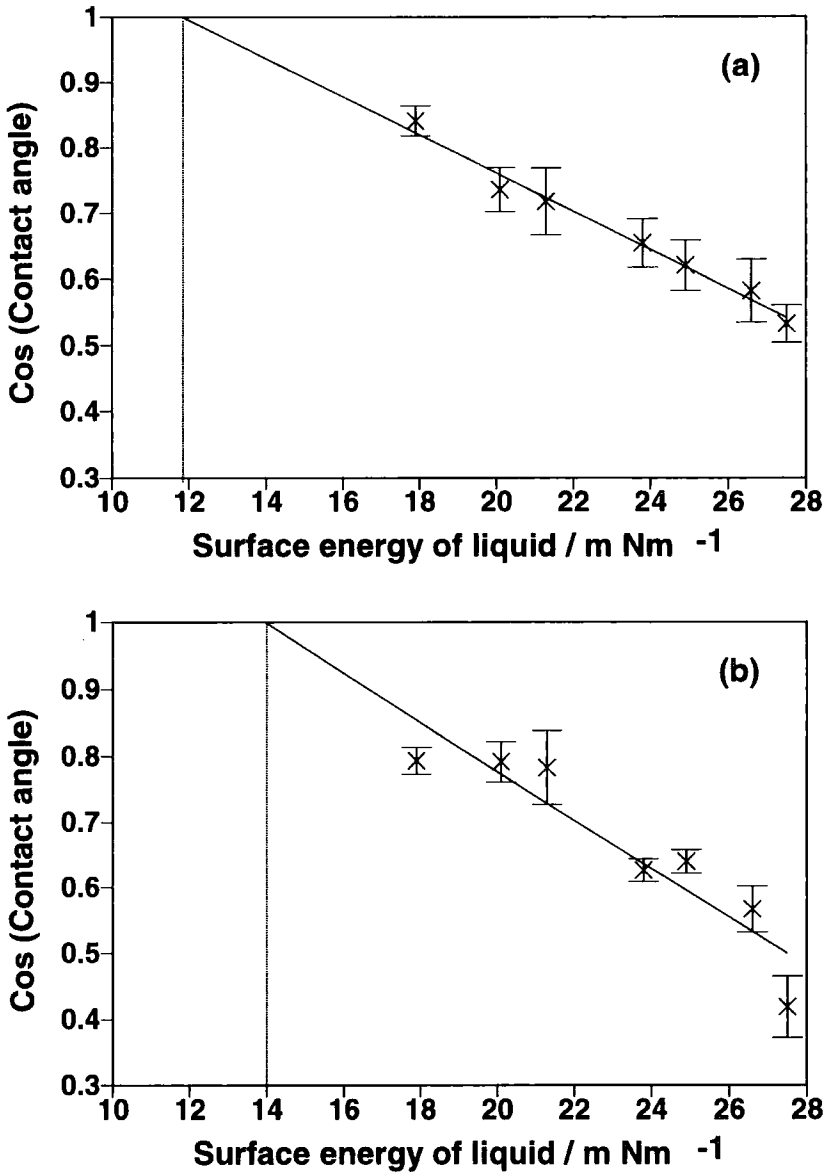

Figure 2.17 Zisman plots derived from contact angle measurements using a homologous series of linear polyolefin probe liquids: (a) high coverage bis-perfluorinated doped polypropylene (prepared by annealing at 150 °C for 30 min); and (b) mono-perfluorinated doped polypropylene.

2.4.3.2.Kinetic Studies

In order to compare the rate and extent of fluorochemical surface segregation during annealing, it was necessary to first remove all additive molecules from the surface region. This was achieved by immersing the films in propan-2-ol. High coverage bis-perfluorinated additive and equivalently annealed mono-perfluorinated additive containing polymer samples were immersed in the solvent for varying durations, and subsequently characterised by XPS, Figure 2.18. An exponential loss of both types of additive from the surface was

observed with time. The bis-perfluorinated additive disappeared at a much slower rate compared to its mono-perfluorinated equivalent: total loss of bis-perfluorinated additive from within the XPS sampling depth (2-5 nm[31]) took approximately 1 hour, whilst depletion of the mono-perfluorinated dopant was complete within 5 min.

These surface-depleted samples were then annealed at 130 °C for increasing durations and analysed by XPS, Figure 2.19. The bis-perfluorinated additive reached a maximum surface coverage of 88 % after 4 hours of annealing. In comparison, total surface coverage by the mono-perfluorinated additive took place within 15 s of annealing. In this case, the concentration of F at the surface continued to increase over the next 45 s, at which point no further compositional changes were noted, Figure 2.19.

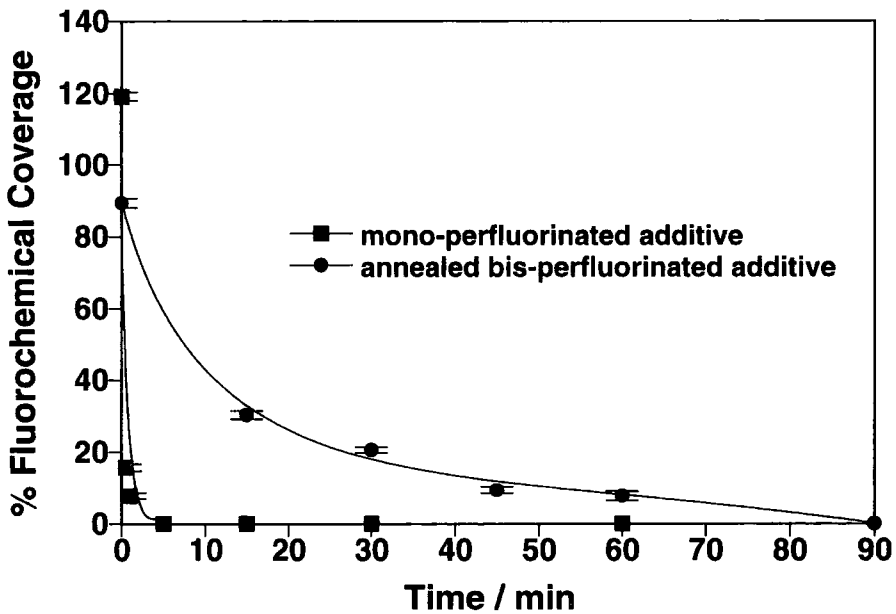

Figure 2.18 Fluorochemical additive coverage at the surface of polypropylene as a function of propan-2-ol washing time.

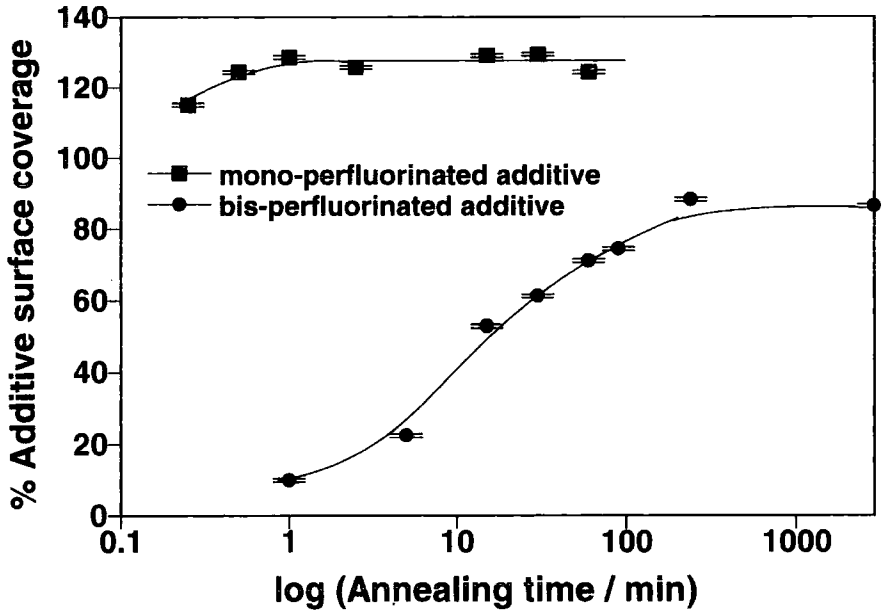

Figure 2.19 Fluorochemical additive coverage as a function of annealing time at 130 °C.

2.4.4. Discussion

Markedly different surface segregation behaviour is observed for the two additive molecules. In fact, the short period of cooling following film formation appears to be sufficient to allow the mono-perfluorinated additive to completely cover the surface and adopt conformations which maximise the amount of fluorine at the surface (thereby minimising interfacial tension). On the basis of the greater than theoretically predicted F concentration measured at the surface by XPS, the mono-substituted additive's perfluorinated arm is preferentially oriented towards the air-solid interface, whilst its higher surface energy alkane chain is directed towards the bulk, Scheme 2.1a. Such an effect has been previously observed for 1,1-dihydroperfluorooctyl acrylate - polystyrene diblock co-polymer thin films,[16] and is generally predicted for AB co-polymers (where A is high surface energy block and B is a low surface energy block).[61] In the case of the bis-perfluorinated system, this type of ordering behaviour only became apparent following annealing at elevated temperatures, Table 2.6.

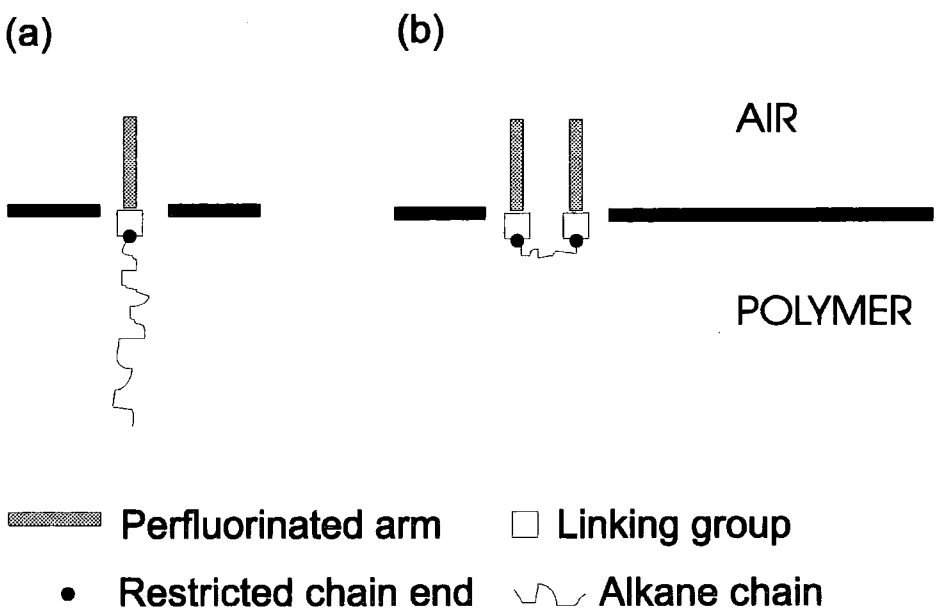

Scheme 2.1 Additive conformations: (a) Mono-perfluorinated additive (b) Bis-perfluorinated additive.

Tapping-mode AFM revealed differences in the topography of the two doped polypropylene surfaces. Height images of the bis-perfluorinated additive-containing sample depict spherulitic morphology, characteristic of crystalline polypropylene, Figure 2.15.[41] In contrast, the mono-perfluorinated doped surface contained globular features overlaying these spherulites, Figure 2.16. The corresponding AFM phase images indicate a partial coverage of bis-perfluorinated additive, whilst total surface coverage is seen for the mono-perfluorinated additive. The surface morphology for the latter can be attributed to completely segregated fluorochemical additive molecules minimising their interaction with the underlying polypropylene substrate. Large differences in surface energy between an overlayer and a substrate are known to produce globular features (these may consist of micellar structures where the perfluorinated arms point outwards from a core comprising of the higher surface energy pendant groups).[62]

Having established the differences between the as prepared films, the high coverage bis-perfluorinated doped polypropylene sample produced by annealing enabled further comparisons to be made with the mono-perfluorinated additive. Even under optimum annealing conditions, only 90% surface coverage of the bis-perfluorinated moieties could be obtained. This

segregation process was accompanied by a small degree of molecular ordering leading to a rise in F concentration at the surface. The bis-perfluorinated additive probably adopts a U-shaped conformation, with perfluorinated arms upright, enabling the higher surface energy segment to remain within the bulk polymer, Scheme 2.1b. Theory predicts such arrangements as being optimum for BAB tri-block co-polymers.[61]

A comparison between the additive removal rates during solvent washing showed that it is more difficult to remove the bis-perfluorinated additive (despite approximately similar surface coverages). The lack of any height features in the AFM images corresponding to the bis-perfluorinated additive is indicative of it being embedded within the polymer. Thus, relatively long exposure to solvent was needed to lift it away from the polypropylene surface. In contrast, the rapid removal of the mono-perfluorinated additive can be attributed to easy dislodgement of the discrete globular structures clearly visible in the AFM height images. The hydrocarbon chain in this molecule is also likely to make it more soluble in propan-2-ol.[63]

A combination of diffusion rates (kinetic) and the overall drive for segregation (thermodynamics) can help to explain the observed annealing behaviour of the two systems. Previous "diffusion in" experiments for non-fluorinated additives have indicated that, molecular weight, size and shape along with chemical composition effect their mobility and solubility within a polymer matrix.[25,46] In the present study both additives have linear structures, and so shape considerations should be similar. However, the molecular weight of the bis-perfluorinated additive is higher than the mono-perfluorinated molecule, and it has been shown that additive mobility decreases with molecular weight.[25,46] The bis-perfluorinated additive also has a second fluorinated arm which will increase the specific volume of the bis-perfluorinated additive and therefore slow its migration.[46] Both of these kinetic factors should contribute to the slower segregation of bis-perfluorinated additive at the polypropylene film surface.

Thermodynamic differences also need to be considered. The perfluoroalkyl chains contained in each additive have a significantly lower surface energy

compared to the host polypropylene matrix. Segregation of fluorochemical additive to the surface occurs as a consequence of the driving force for minimisation of surface energy.[16] On this basis, the lower surface energy bis-perfluorinated additive would be expected to segregate to a greater extent than the mono-perfluorinated molecule, however the contrary is observed, thereby suggesting other factors are responsible. In fact the relative surface compositions are consistent with theoretical calculations made for block co-polymer melts.[61] The mono-perfluorinated molecule can be regarded as being analogous to a AB di-block co-polymer (A = pendant group; B = perfluorinated chain) while the bis-perfluorinated structure can be equated to a BAB tri-block structure (A = linkage group; B = perfluorinated chain). The reported simulations predicted that AB di-block co-polymers undergo higher degrees of low energy component segregation and more tendency to phase separate than BAB tri-block equivalents, this supports our findings. A molecular-level explanation for this behaviour needs to consider the differing degrees of freedom of the two additives at the surface. Placing the fluorinated arm of the mono-perfluorinated additive at the air-solid interface constrains one end of the molecule, while the rest of the alkane chain is free to adopt any conformation. However, for both the fluorinated functionalities of the bis-perfluorinated additive to reach the interface, the linking group becomes restricted in position and conformation, Scheme 2.1. On the basis of these entropic factors, the mono-perfluorinated additive should achieve complete surface coverage more readily and phase-separate to form an energetically optimised surface morphology (as seen by AFM), whilst the more constrained bis-perfluorinated doped molecule cannot fully segregate, and can only minimise interfacial tension by forming circular domains embedded within the polymer matrix.

2.5. Conclusions

Tapping Mode AFM has been used in combination with XPS, optical microscopy, imaging SIMS, and contact angle analysis to investigate various aspects of the surface enrichment of fluorochemical doped polypropylene films. In Section 2.2 the migration of fluorochemical additive towards the surface of polypropylene film during annealing was studied. The lateral distribution of additive at the surface was found to spread outwards from isolated circular domains and patches into a continuous layer, with a corresponding drop in surface energy. Section 2.3 demonstrated that the speed and extent of surface enrichment for fluorochemical containing polypropylene films increases with polymer molecular weight. Whilst in Section 2.4 a comparison between polypropylene films containing mono- and bis-perfluorinated additive molecules has shown that the former tend to segregate to the surface much more readily. These observations have been explained by considering additive diffusion rates and surface energetics.

2.6. References

[1] Kissa, E. In *Handbook of Fibre Science and Technology*, Vol II, Part B, Lewin, M., Sello, S. B., Eds.; Marcel Dekker Inc: New York, 1984.

[2] Brady, R. F. Jr. In *Encyclopaedia of Polymer Science and Technology*, Mark, H., Bikales, N. M., Overberger, C. G., Menges, G., Eds.; Wiley: New York, 1986.

[3] DeMarco, C. G.; Mc Quade, A. J.; Kennedy, S. J. *Modern Textiles Magazine* **1960,** *Part 2*, 50.

[4] Sargent, R. R.; Alexander, J. R. U.S. Patent 5,560,992, 1996.

[5] Anderson, M. H.; Lyons, C. S.; Wigness, B. D. U.S. Patent 4,536,179,1985.

[6] Honeychuck, R. V.; Ho, T.; Wynne, K. J.; Nissan, R. A. *Chem. Mater.* **1993**, *5*, 113.

[7] Clark, D. T. ; Feast, W. J.; Musgrove, W. K. R.; Ritchie, I. *J. Polym. Sci., Part A: Polym. Chem.* **1975**, *13*, 857.

[8] Yasuda, T.; Yoshida, K.; Okuno, T. *J. Polym. Sci, Part B: Polym. Phys.* **1988**, *26*, 2061.

[9] Wang, J. H.; Chen, J. J.; Timmons, R. B. *Chem. Mater.* **1996**, *8*, 2212.

[10] Wheale, S. H. Physicochemical Phenomena at the Plasma - Polymer Interface. Ph.D. Thesis, Durham University, 1997.

[11] Ryan, M. E.; Fonseca, J. L. C.; Tasker, S.; Badyal, J. P. S. *J. Phys. Chem.* **1995**, *99*, 4261.

[12] Popat, R. H.; Sutherland, I.; Shang, E. -S. *J. Mater. Chem.* **1995**, *5*, 713.

[13] Fitzgerald, P. H.; Raiford, K. G.; Greenwood, E. J. U.S. Patent 5,798,402, 1998.

[14] Raiford, K. G.; Liss, T. A.; Greenwood, E. U.S. Patent 5,898,046,1997.

[15] Smith, R. S. U.S. Patent 5,672,651, 1997.

[16] Kassis, C. M.; Steehler, J. K.; Betts, D. E.; Guan, Z. B.; Romack, T. J.; Desimone, J.M.; Linton, R. W. *Macromolecules* **1996**, *29*, 3247.

[17] Schaub, T. F.; Kellogg, G. J.; Mayes, A. M. *Macromolecules* **1996**, *29*, 3982.

[18] Champagne, F.; Li, J. F.; Schreiber, H. P.; Dipaloa-Baranyi, G. *J. Appl. Polym. Sci.* **1994**, *54*, 743.

[19] Thomas, H. R.; O'Malley, J. J. *Macromolecules* **1981**, *14*, 1316.

[20] Hamza, A.; Pham, V. A.; Matsuura, T.; Santerre, J. P. *J. Membr. Sci.* **1997**, *131*, 217.

[21] Sauer, B. B.; McLean, R. S.; Thomas, R. R. *Langmuir* **1998**, *14*, 3045.

[22] Park, I. J.; Lee, S. B.; Choii, C. K. *J. Appl. Polym. Sci.* **1994**, *54*, 1449.

[23] Brant, P.; Karim, A.; Douglas, J. F.; Bates, F. S. *Macromolecules* **1996**, *29*, 5628.

[24] Bhatia, Q. S.; Pan, D. H.; Koberstein, J. T. *Macromolecules* **1988**, *21*, 2166.

[25] Földes, E. *Polym. Degrad. Stab.* **1995**, *49*, 57.

[26] Affrossman, S.; Betrand, P.; Hartshorne, M.; Kiff, T.; Leonard, D.; Pethrick, R. A.; Richards, R. W. *Macromolecules* **1996**, *29*, 5432.

[27] Jones, M. E.; Rousseau, A. D U.S. Patent 5,411,576, 1995.

[28] Zhong, Q.; Innis, D.;Kjoller, K. Elings, V.B. *Surf. Sci.* **1993**, *14*, 3045.

[29] Magonov, S. N.; Elings, V. B.; Whangbo, M. H. *Surf. Sci.* **1997**, *375*, L385.

[30] Boyd, R.D.; Kenwright, A.M.; Briggs, D.; Badyal J.P.S. *Macromolecules* **1997**, *30*, 5429.

[31] *Practical Surface Analysis*; 2nd ed. ;Briggs, D., Seah, M. P. Eds.; Wiley: New York, 1990; Vol. 2.

[32] Magonov, S. N. *Scanning* **1997**, *19*, 163.

[33] Jasper, J. J. *J. Phys. Chem. Ref. Data* **1972**, *1*, 841.

[34] Clark, D. T.; Shuttleworth, D. *J. Polym. Sci., Chem. Ed.* **1980**, *18*, 27.

[35] Stachurski, Z. H.; Macniol, J. *Polymer* **1998**, *23*, 5717.

[36] Work carried out by 3M, St, Paul, MN

[37] Al-Raheil, I. A.; Qudah, A. M. *J. Appl. Polym. Sci.* **1998**, *67*, 1259.

[38] Yamada, K.; Matsumoto, S.; Tagashira, K.; Hikosaka, M. *Polymer* **1998**, *39*, 5327.

[39] White, H. M.; Bassett, D. C. *Polymer* **1997**, *38*, 5515.

[40] Schonherr, H.; Snetivy, D.; Vancso, G. J. *Polym. Bull.* **1993**, *30*, 567.

[41] Varga, J. *J. Mater. Sci.* **1992**, *27*, 2557.

[42] Awaya, H. *Polymer*, **1998**, *29*, 591.

[43] Yan, C; Mao, X. *Acta. Polym.* **1998**, *6*, 671.

[44] Owens, D. K.; Wendt, R. C. *J. Appl. Polym. Sci.* **1969**, *13*, 1741.

[45] Billingham, N. C In *Oxidative Inhibition of Organic Materials* Vol. II Pospisil, J.; Klemchuk, P. P., Eds., CRC Press, Boca Raton Florida, 1989.

[46] Földes, E. *Angew. Makromol. Chem.* **1998**, *261*, 65.

[47] Refier, D.; Windeit, R.; Kumpf. R. J.; Karbach, A.; Fuchs, H. *Thin Solid Films* **1995**, *264*, 148.

[48] Finot, M. O.; McDermott, M. T. *J. Am. Chem. Soc.* **1997**, *119*, 8564.

[49] Cleveland, J. P.; Ancykowski, B.; Schnid, A. E.; Elings, V. B. *Appl. Phys. Lett.* **1998**, *72*, 2613.

[50] Bar, G.; Thomann, Y.; Brandsch, R.; Cantow, H. J. *Langmuir* **1997**, *13*, 3807.

[51] Alger, M. *Polymer Science Dictionary*, 2nd ed.; Chapman and Hall: London, 1997.

[52] Malkan, S. R.; Wadsworth, L. C. *INB Nonwovens* **1991**, *2*, 46.

[53] Chen, H.-L.; Li, L.-J.; Ou-Yeng, W.-C.; Hwang, J. C.; Wong, W.-Y. *Macromolecules* **1997**, *30*, 1718.

[54] Hoffman, J. D. *Polymer* **1982**, *23*, 656.

[55] Lotz, B.; Wittmann, J. C. *J. Polym. Sci; Part B: Polym. Phys.* **1986**, *24*, 1541.

[56] Olley, R. H.; Bassett, D. C. *Polymer* **1989**, *30*, 399.

[57] Quijada-Garrido, I.; Baeeales-Rienda, J. M.; Pereña, J. M.; Frutos, G *Polymer* **1997**, *38*, 5125.

[58] Wu, S. *Polymer Interface and Adhesion*; Dekker: New York, 1982.

[59] Hariharan, A.; Kumar, S. K.; Russell, T. P. *J. Chem. Phys.* **1993**, *99*, 4041.

[60] Shafrin. E. G.; Zisman, W. A. *J. Phys. Chem.* **1960**, *64*, 519.

[61] Hariharan, A.; Harris, J. G. *J. Phys. Chem.* **1995**, *99*, 2788.

[62] Boyd, R. D.; Greenwood, O. D.; Hopkins, J.; Badyal, J. P. S. *J. Adhes. Sci. Technol.* **1995**, *9*, 311.

[63] Jones, M. E. 3M company, St. Paul, MN. Personal Communication, 2000.

CHAPTER 3

SPATIALLY CONFINED CHARGE DEPOSITION ONTO POLYMER SURFACES USING A SCANNING PROBE MICROSCOPE

3.1. Introduction

Charged surfaces find many uses: electrostatic filter media,[1] device manufacture (such as microphones),[2] microbe resistant packaging,[3] optical display devices,[4] and biomedical applications.[5] In addition to these large scale uses, the deposition of localised charge regions onto insulating surfaces is of interest for memory storage devices.[6]

In the past, measurement of the variation in charge density across a surface has been limited to mm scales using electrostatic probes.[7] The advent of electric force microscopy (EFM) now enables charge distributions to be mapped at much higher spatial resolution,[8-11] and also provides a means for depositing localised regions of charge.[9] Initial attempts using this technique comprised applying high voltage pulses to a static AFM tip positioned above the surface.[8,9] This produced point-like charge distributions (minimum diameter = 70 nm) with controlled polarity. Deposition of such point charges has also been achieved by contacting the microscope tip with the surface.[6] Both methods produce small point charges, which are of potential interest for memory storage. For high resolution patterning applications, control of the size and shape of the deposited charge is an important criterion. One example is the localised poling of thin ferroelectric films, which can be achieved by applying a voltage to a scanning EFM tip.[12] In addition, localised surface potential modification of Langmuir-Blodgett films has recently been demonstrated using near-field irradiation from a scanning Kelvin microscope tip.[13]

In this chapter, a localised high voltage discharge extending from an EFM tip is used to deposit well-defined regions of charge onto polymer surfaces. These modified substrates could be potentially useful for fabricating structures on the sub-micron scale.

3.2. Theory

3.2.1. The Effect of Force Gradients on the Phase Shift of a Freely Oscillating AFM Cantilever

The phase lag of an oscillating cantilever, ϕ is defined as the difference in phase between the actual frequency of oscillation and the driving source. Phase lags are normally expressed as angles. In the case of Tapping Mode atomic force microscopy, the acquired phase shift images actually represent the difference between the phase lag of the freely vibrating cantilever and the phase lag of the cantilever interacting with an underlying substrate, Equation 3.1.[14,15]

$$\Delta\phi = \phi_{free} - \phi_{interacting} \qquad \textbf{Equation 3.1}$$

Where $\Delta\phi$ is the displayed AFM phase shift, ϕ_{free} is the phase lag of the freely vibrating cantilever, and $\phi_{interacting}$ is the phase lag of the interacting cantilever. The driving frequency of the freely vibrating cantilever is normally chosen to be close to its resonance frequency. According to the theory of driven oscillators, the phase lag of a vibrating cantilever at its maximum amplitude (resonance) is equal to 90°.[16] Hence the phase lag of the freely vibrating cantilever, ϕ_{free} is 90°, Figure 3.1a.

However when tip-substrate interactions are present, the frequency at which maximum amplitude occurs will shift away from the driving frequency,[17] this results in the aforementioned phase lag, $\phi_{interacting}$. If the cantilever experiences a repulsive field gradient then the frequency of maximum oscillation amplitude is increased, and the corresponding phase lag of the interacting cantilever, $\phi_{interacting}$ at the driving frequency drops below 90°. This results in the phase shift, $\Delta\phi$ becoming positive, with its magnitude corresponding to the degree of repulsion (contrast in phase images brightens for positive phase shifts), Figure 3.1b. Conversely an attractive force gradient reduces the frequency at which maximum oscillation amplitude occurs. Hence the interacting phase lag $\phi_{interacting}$

at the driving frequency rises above 90° and so the phase shift, $\Delta\phi$ becomes negative and decreases with increasing attractive force, (contrast in phase images brightens for positive phase shifts), Figure 3.1c. Table 3.1 summarises the effect of force gradients on cantilever phase shift. A more rigorous quantitative approach is reported in ref.18.

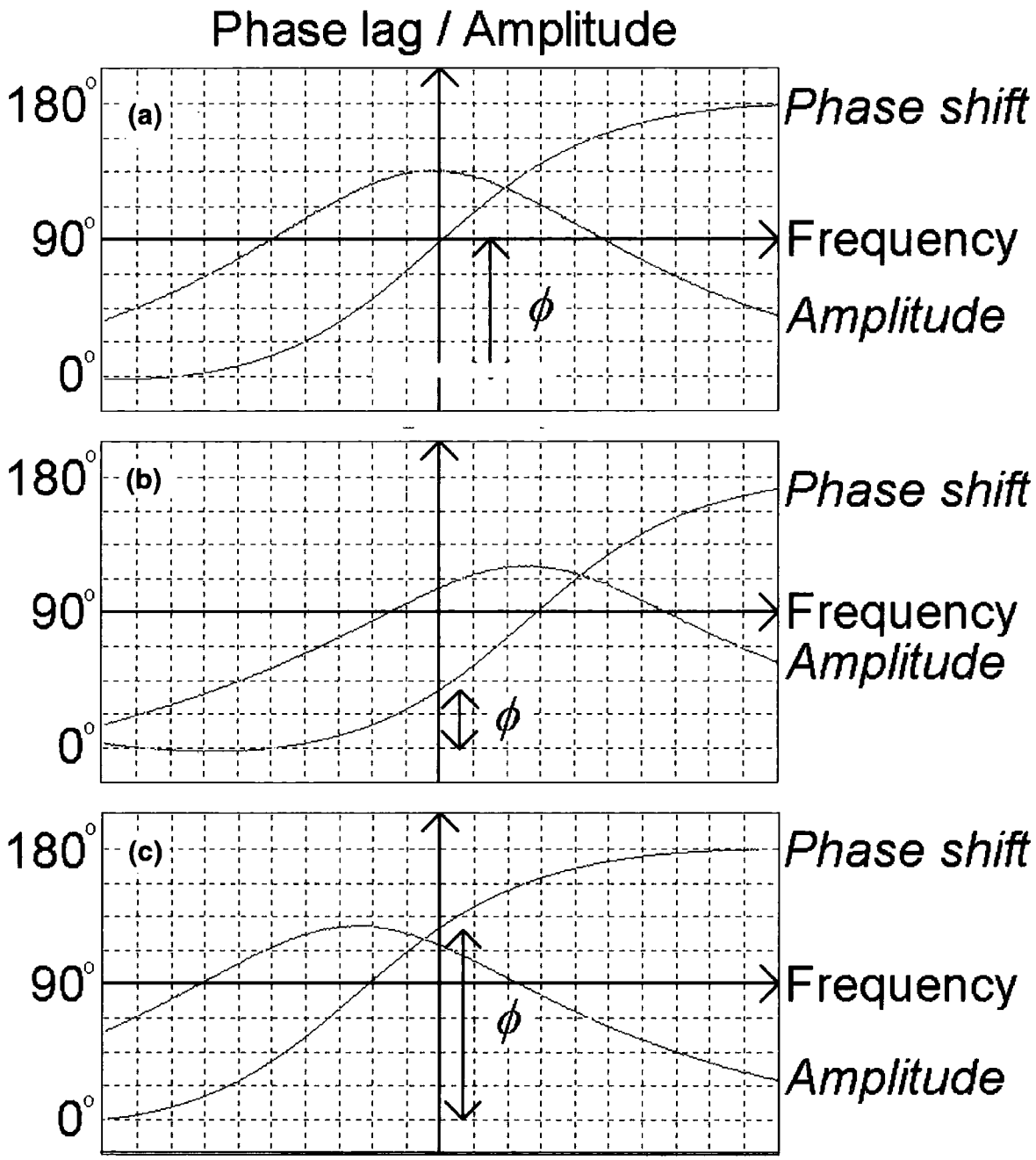

Figure 3.1 The effect of force gradients on the phase shift of a freely oscillating cantilever: (a) The phase lag of a freely vibrating cantilever at resonance, ϕ_{free} is 90°; (b) The phase lag of a vibrating cantilever exposed to a repulsive force, $\phi_{interacting}$ is less than 90°; and (c) The phase lag of a vibrating cantilever exposed to an attractive force, $\phi_{interacting}$ is greater than 90°.

Force Gradient	Resonance Frequency of Cantilever	Phase Shift, $\Delta\phi$	AFM Phase Image
Repulsive	Increases	Positive	Brighter
Attractive	Decreases	Negative	Darker

Table 3.1 Summary of the effect of force gradients on the phase shift of a freely oscillating cantilever.

3.2.2. Mapping Surface Charge Distributions with Lift-Mode EFM

Tapping-mode AFM phase images (where the tip is in intermittent contact with the surface) are dominated by the short-range forces above the sample surface, hence they provide information about mechanical properties such as elasticity,[19] adhesion,[20] and energy dissipation.[21] In the case of EFM, a lift-mode is employed, where the tip does not contact the surface. The tip is held at a constant height above the substrate during scanning, and so any changes in phase shift are due to long-range forces. The important long-range forces are considered to be Van der Waals and electrostatic. The latter are dominant for charged surfaces.[9]

Lift-mode phase shift depends upon the electrostatic interaction between the surface and tip voltage. The voltage at the surface is simply the surface potential, $V_{surface}$. Surface charge induces a mirror charge in the tip, $-V_{surface}$ in addition to the voltage applied to the tip from the external power supply, $V_{applied}$. So the total voltage on the tip is given by Equation 3.2.

$$V_{tip} = V_{applied} - V_{surface} \qquad \textbf{Equation 3.2}$$

The phase shift will depend on the sign and magnitude of V_{tip} and $V_{surface}$. When V_{tip} and $V_{surface}$ have the same sign, a repulsive force results, and so a bright phase shift occurs. Whereas when they have opposite polarity, the force is attractive and a dark phase shift results. The magnitude of the phase shift will depend on the product $V_{tip}.V_{surface}$, i.e. increasing V_{tip} for a given $V_{surface}$ will produce a greater phase shift. For instance, consider a positive surface charge,

$V_{surface}$. When a negative voltage, $V_{applied}$ is applied to the tip, V_{tip} will also be negative, and so a dark, attractive phase shift will occur. The image will darken as increasingly negative voltages are applied. If a positive voltage, $V_{applied}$ smaller than $V_{surface}$ is applied to the tip, V_{tip} remains negative and the phase shift will still be dark. As $V_{applied}$ increases the image will brighten. When $V_{applied}$ = $V_{surface}$, there will be no phase shift attributable to electrostatic forces since V_{tip} = 0 V. A further increase in $V_{applied}$ will produce bright, repulsive phase contrast in the image as V_{tip} becomes more positive, Figure 3.2a. The converse argument applies to a negatively charged surface, Figure 3.2b.

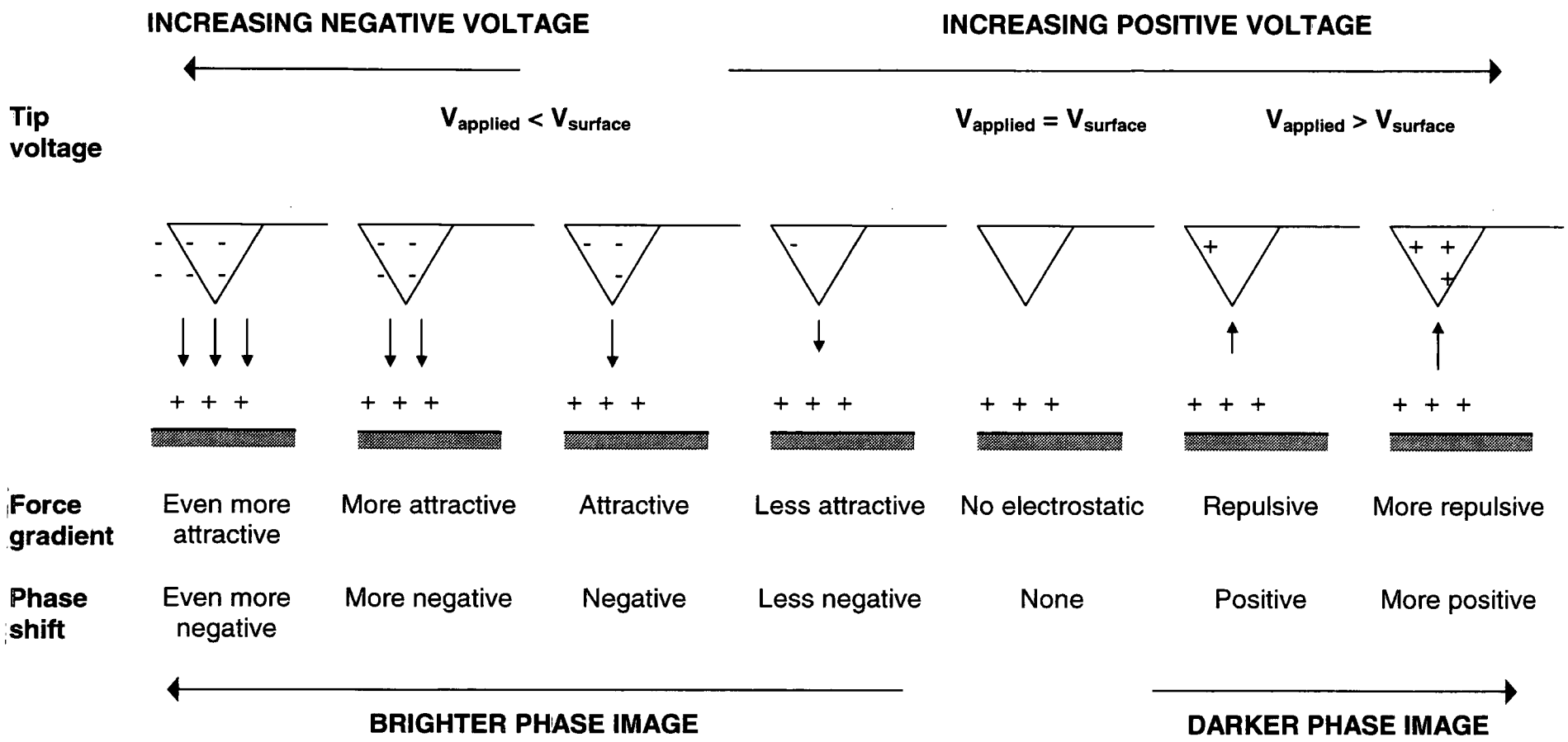

Figure 3.2a Schematic of the forces present between the EFM tip and a region of positive surface charge as a function of applied tip voltage.

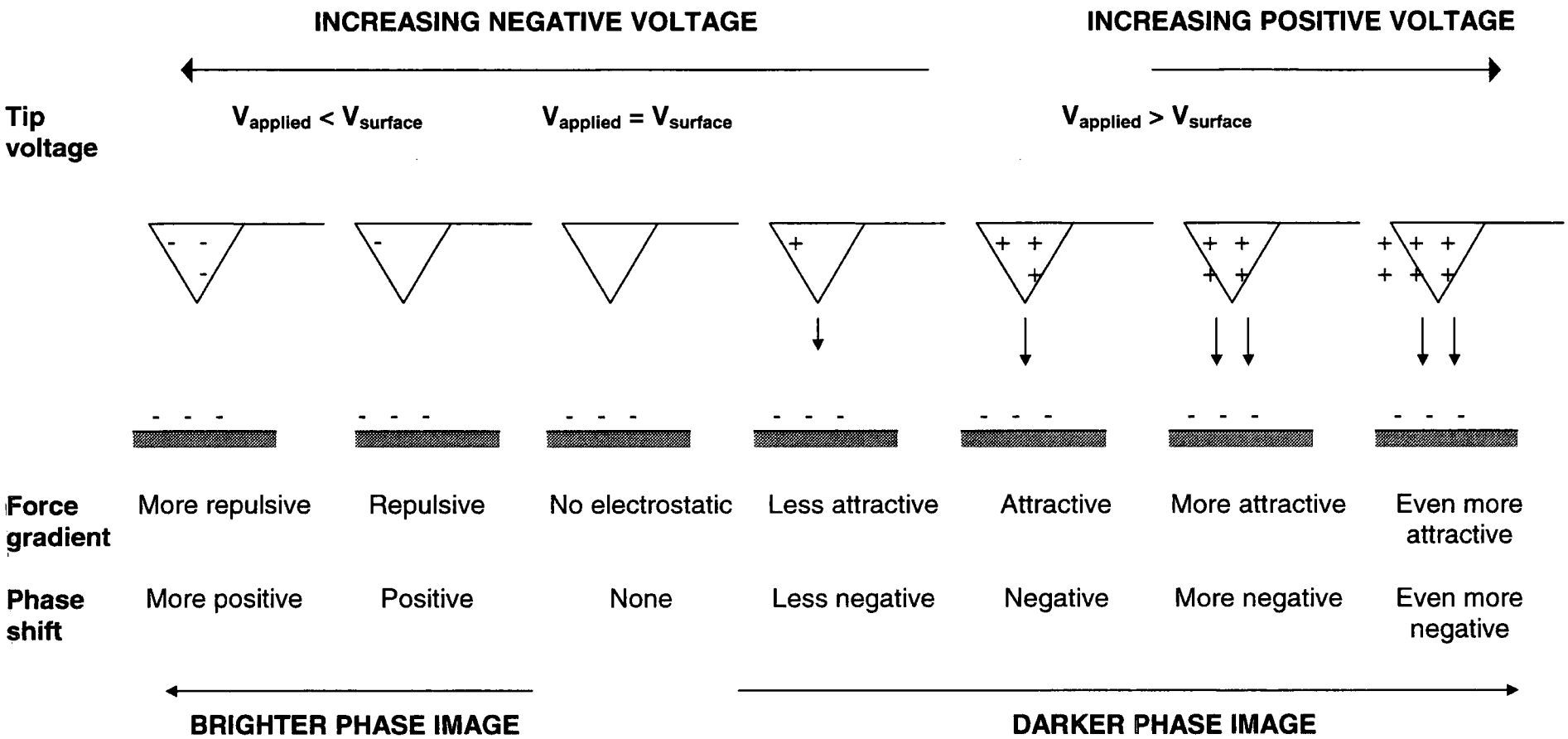

Figure 3.2b Schematic of the forces present between the EFM tip and a region of negative surface charge as a function of applied tip voltage.

Thus both the polarity and the magnitude of surface charge can be determined by comparing EFM lift-mode phase images recorded with different applied tip voltages. A region that darkens as applied voltage decreases from positive to negative is positively charged, with its magnitude equal to the positive voltage at which the phase image contrast is neither bright nor dark. A region that brightens as applied voltage decreases from positive to negative is negatively charged, with its magnitude given by the negative voltage corresponding to a neutral phase shift. Uncharged regions are expected to display no change in their EFM lift-mode phase contrast with varying applied voltage, Table 3.2. Uniformly charged surfaces should also give no variation in phase contrast, instead the phase shift of the entire image is altered (however this will appear as a neutral relative phase shift due to the arbitrary absolute phase shift value set by the microscope).

Surface Charge	**Lift-mode phase image contrast** **Positive applied voltage → Negative applied voltage**
Positive	Bright ⟶ Dark
Negative	Dark ⟶ Bright
None	Neutral ⟶ Neutral

Table 3.2 The effect of applied voltage on EFM lift-mode phase image contrast.

3.3. Experimental

Atomic force micrographs were recorded using a Nanoscope III microscope (Digital Instruments) fitted with an extender electronics module and a signal access module. Cr sputter coated (~ 10 nm thickness on bottom-side) 125 μm long silicon tips were used (Olympus OMCL-AC160TS-W, force constant of ≈ 40 nN, resonance frequency ≈ 270 kHz after metallization). Tapping Mode height and phase images were recorded with the tip in intermittent contact with the surface. Non-contact lift-mode phase data was collected at a constant tip-sample height (the lift-height). Height data from the Tapping Mode scan lines was used as a template for the lift-mode scan lines. In all experiments the lift-height was sufficiently high to ensure non-contact imaging. This was checked

by ensuring the Tapping Mode phase scan lines did not coincide the with lift-mode phase scan lines.

A standard set of Tapping Mode parameters was chosen to ensure consistent imaging. These conditions were a set-point : free amplitude ratio of 0.5 (set-point amplitude = 50 nm; free amplitude = 100 nm), a scan rate of 1.1 Hz, and a lift-height of 30 nm. In order to allow both charge deposition and imaging, it was necessary to apply a d.c. voltage to the AFM tip during lift-mode scan lines. The Nanoscope controller provides an internal low voltage signal (±12 V "Analogue 2") that is only turned on during lift-mode scan lines for this purpose. However, ±12 V is insufficient to allow charge deposition. To allow high tip voltages, the internal low voltage signal (accessed via the signal access module) was used to gate an external high voltage d.c. power supply (±180 V). The high voltage gated signal is applied to the tip through the "Analogue 2" input of the signal access module. As a result, no voltage was applied to the tip during the Tapping Mode height and phase scan lines.

Capacitor grade polypropylene (ICI) was used as the polymer substrate, this had been cleaned by ultrasonication in isopropanol (Fisher, 99.99 %) for 30 s. Each experiment comprised two stages: localised charging of the polymer surface using the AFM tip, followed by EFM lift-mode analysis. Charging was performed by scanning a 1 μm x 1 μm square region on the polymer surface with a high voltage applied to the tip. Characterisation entailed recording 10 μm x 10 μm images centred on this 1 μm x 1 μm square. In the latter case, the applied tip voltage was chosen to be sufficiently low so as not to distort the deposited surface charge distribution (between +40 and -40 V).

Two types of charging experiment were performed. First of all, EFM imaging parameters were explored for a single charging experiment. Here, the deposited charge distribution was imaged using several tip voltages. Subsequently, different discharge conditions were investigated. A corresponding set of EFM images were then collected for each fixed tip voltage (-20 V for positive charge and +20 V for negative charge), so as to allow a comparison to be made between changing discharge parameters.

3.4. Results

3.4.1. Localised Positive Charge Deposition

Scanning a small region of the polymer surface with a high positive voltage applied to the tip (+180 V) produced no contrast in the subsequent Tapping Mode AFM height or phase images, Figure 3.3a and b. However positive charge deposition was clearly evident in the EFM lift-mode images, Figure 3.3c-f. A bright square extending beyond the region exposed to the discharge is discernible in the +35 V image, Figure 3.3c. Reducing the imaging voltage to +20 V decreased the size of the bright patch, Figure 3.3d. At +12 V the bright patch is replaced by a similarly sized dark region, Figure 3.3e. The size of this dark square increased when the tip voltage decreased to -20 V, Figure 3.3f.

The precise magnitude of the applied discharge voltage employed during charge deposition was also found to influence the EFM lift-mode contrast, Figure 3.4. No localised EFM phase contrast was seen in the lift-mode image corresponding to the applied +80 V tip voltage scan, Figure 3.4a. At +100 V, a dark patch was evident within the scanned region, Figure 3.4b. A further increase in discharge voltage produced an expansion in the size and darkness of the charged area, Figures 3.4c-f.

The tip height above the surface during discharge exposure was another important parameter. A discharge lift-height of 30 nm yielded a faint dark localised region in the corresponding EFM lift-mode image, Figure 3.5a. However by reducing the discharge lift-height to 12 nm, a prominent large region of dark contrast was subsequently identified, Figure 3.5b.

Finally, increasing the scan speed during operation of the discharge from 1.1 Hz to 3.0 Hz (discharge voltage = +100 V, lift-height = 30 nm) reduced the size of the dark region seen afterwards in the lift-mode EFM image, Figure 3.6. This was taken as being indicative of less charge deposition.

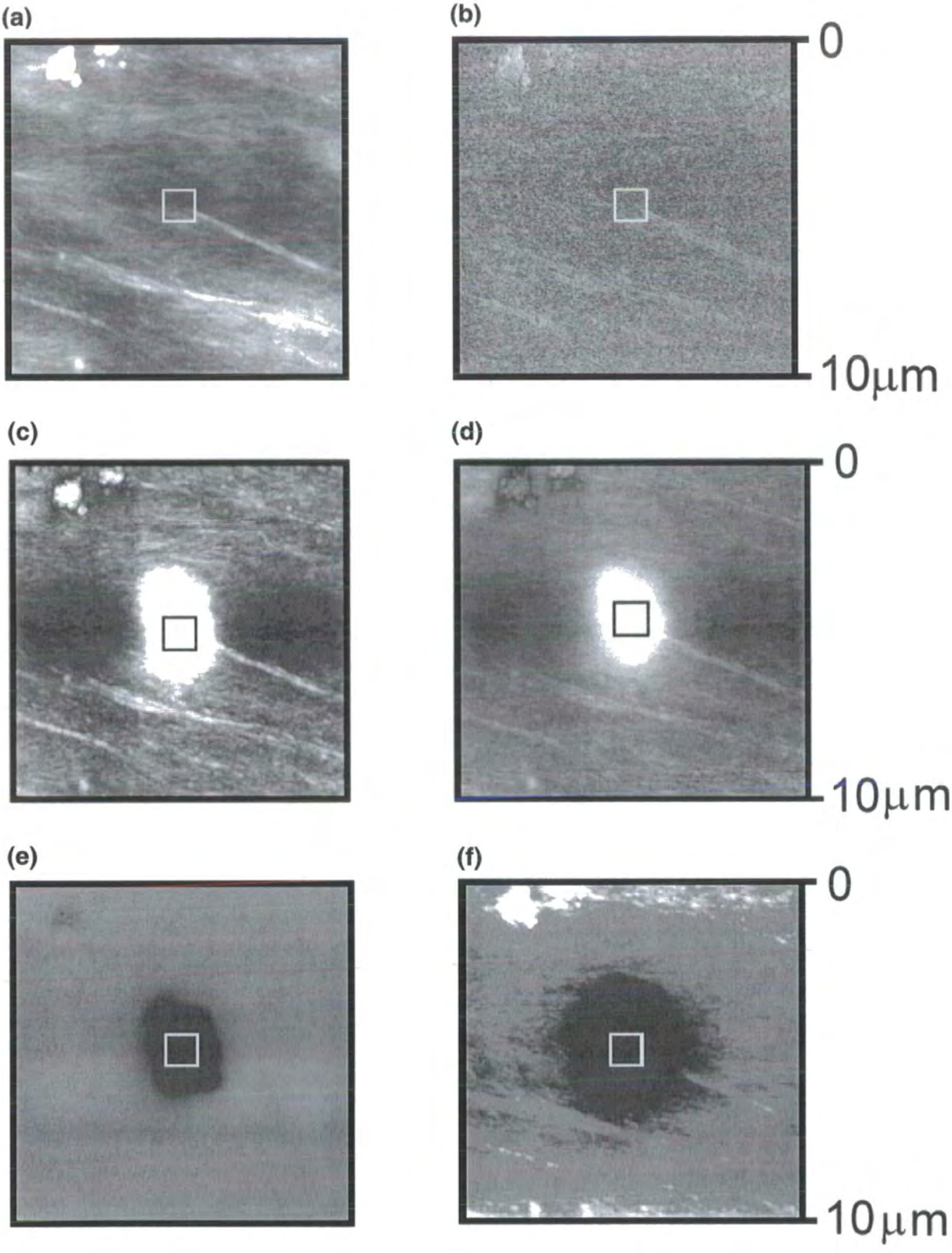

Figure 3.3 10 μm x 10 μm micrographs of polypropylene. The region marked with a square was previously exposed to a high positive lift-mode bias (+180 V): (a) Tapping Mode height image; (b) Tapping Mode phase image; (c-f) Lift-mode phase images recorded at +35 V, +20 V, +12 V and -20 V respectively.

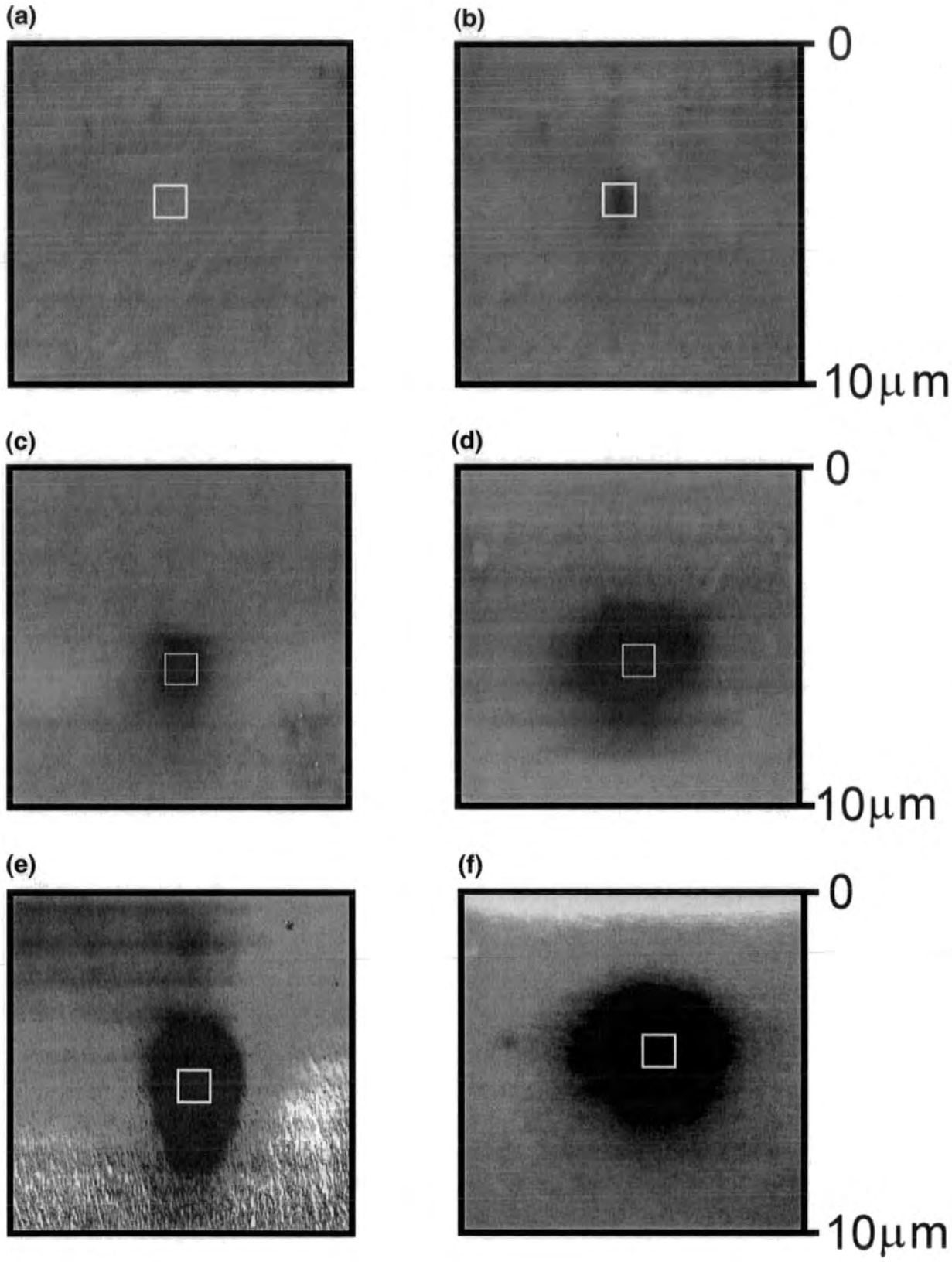

Figure 3.4 10 μm x 10 μm lift mode images of polypropylene recorded with -20 V applied to the tip: (a-f) the region marked with a square was previously exposed to lift mode bias of +80 V, +100 V, +120 V, +140 V +160 V and +180 V respectively (Lift-height = 30 nm; Scan speed = 1.1 Hz).

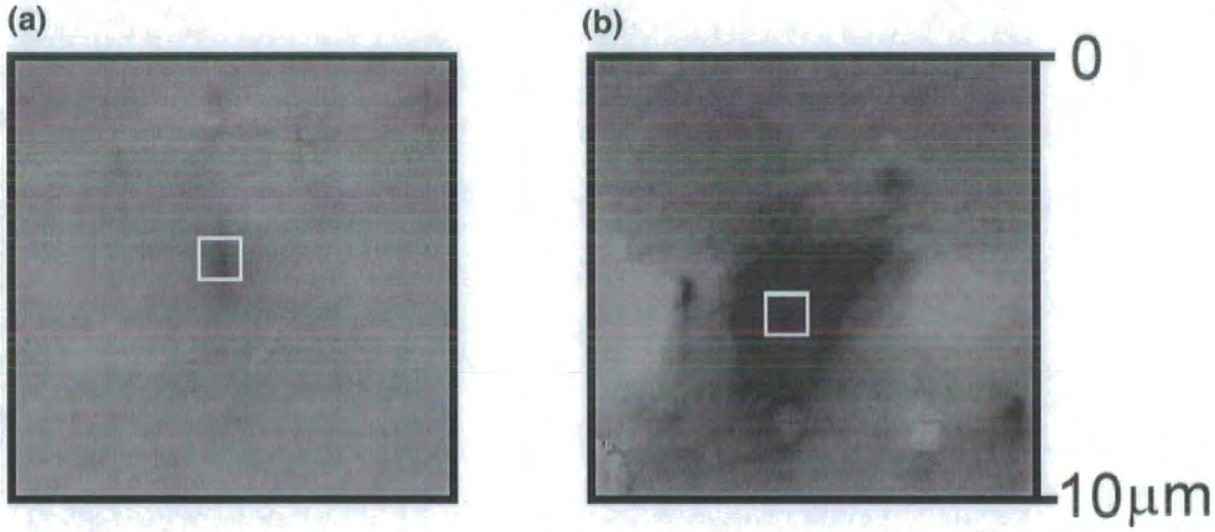

Figure 3.5 10 μm x 10 μm micrographs of polypropylene recorded with -20 V applied to the tip. The region marked with a square was previously exposed to a +100 V lift-mode bias (Scan speed = 1.1 Hz): (a) Lift-height during charge deposition = 30 nm; and (b) Lift height during charge deposition = 12 nm.

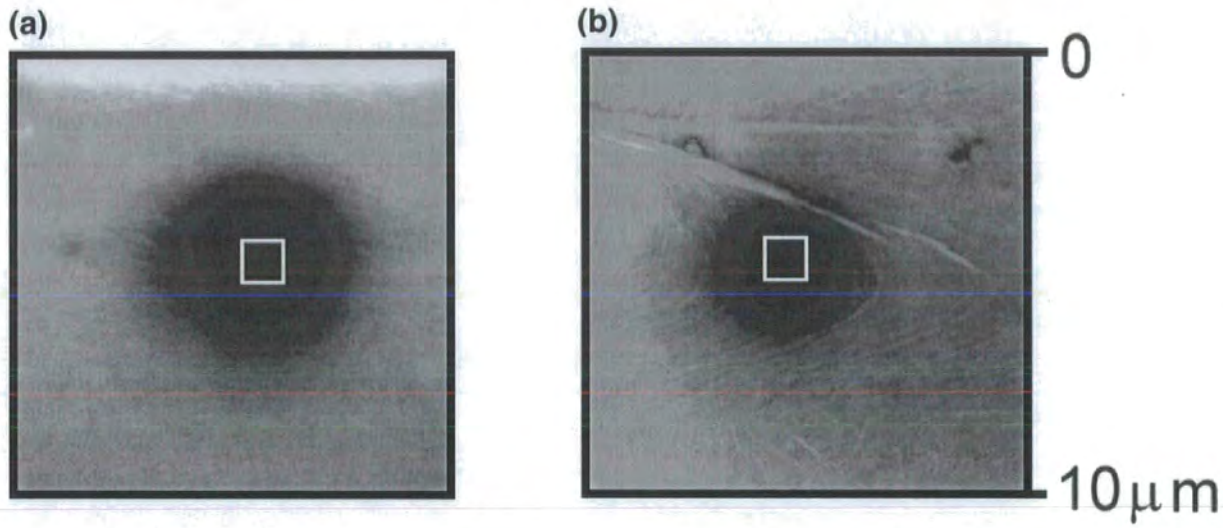

Figure 3.6 10 μm x 10 μm micrographs of polypropylene recorded with -20 V applied to the tip. The region marked with a square was previously exposed to a +160 V lift-mode bias (Scan speed = 1.1 Hz): (a) Scan speed while charging = 1 Hz; and (b) Scan speed while charging = 3 Hz.

3.4.2. Localised Negative Charge Deposition

Application of a high negative voltage to the tip during localised scanning produced corresponding contrast in the EFM lift-mode image; whereas, the Tapping Mode AFM images remained unaffected, Figure 3.7. With +20 V EFM lift-mode imaging voltage, a dark patch was seen, Figure 3.7c. Decreasing this voltage to -12 V caused the dark region to decrease in size, Figure 3.7d. At -17 V this patch became bright. A further reduction in EFM imaging voltage

increased the size of the bright patch, Figure 3.7e-f. This is consistent with a negatively charged surface, Table 3.2.

Once again, varying the discharge voltage altered the EFM lift-mode images acquired at a fixed imaging voltage, Figure 3.8. A discharge voltage of -40 V was insufficient to induce EFM lift-mode contrast, Figure 3.8a. However at -50 V a small dark region of contrast was generated, Figure 3.8b. Lowering the discharge voltage further, produced increased contrast over a larger area, Figure 3.8c and d.

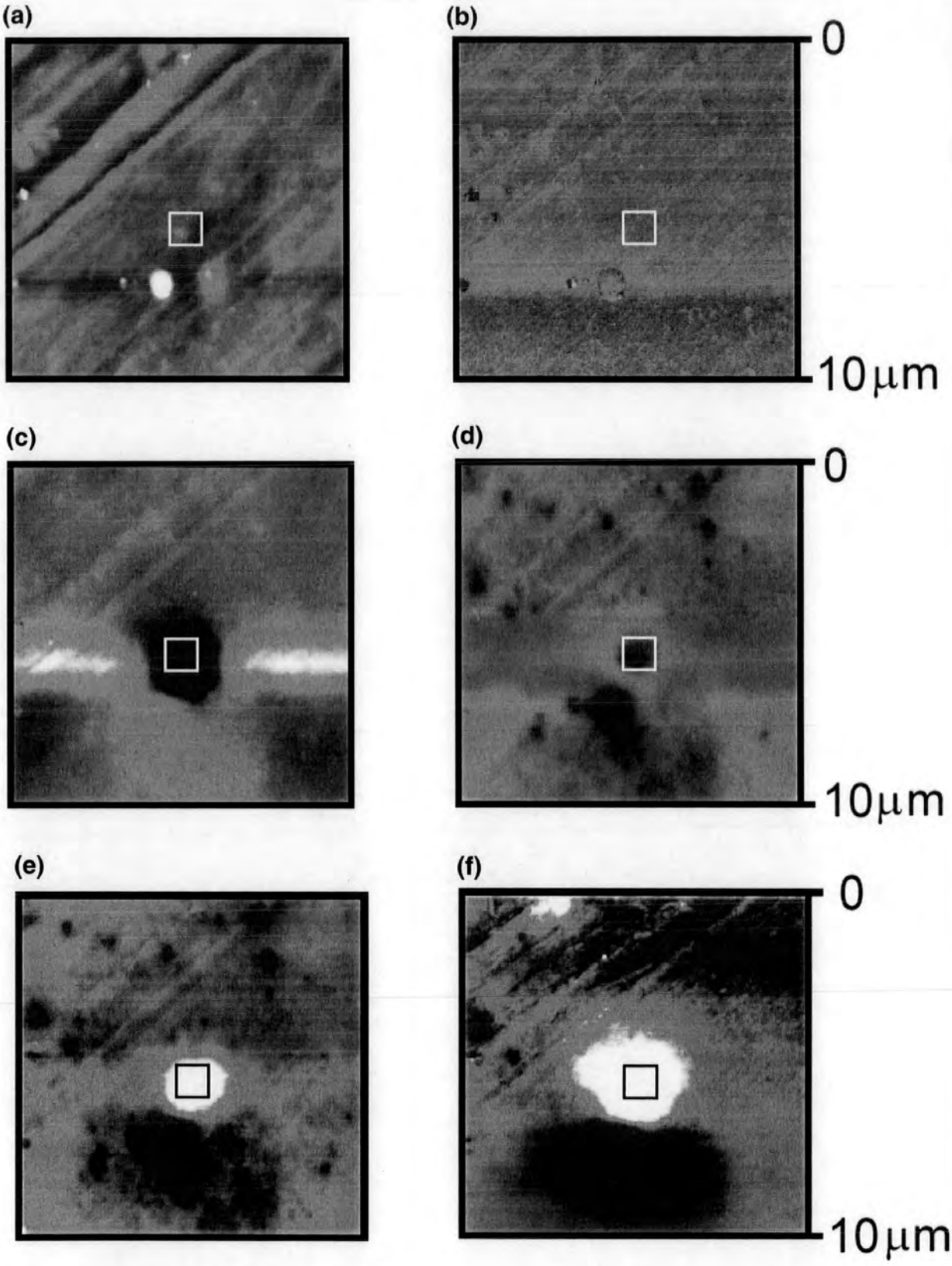

Figure 3.7 10 μm x 10 μm micrographs of polypropylene. The region marked with a square was previously exposed to a high negative lift-mode bias (-180 V): (a) Tapping Mode height image; (b) Tapping Mode phase image; (c-f) Lift-mode phase images recorded at +20 V, -12 V, -17 V and -20 V respectively.

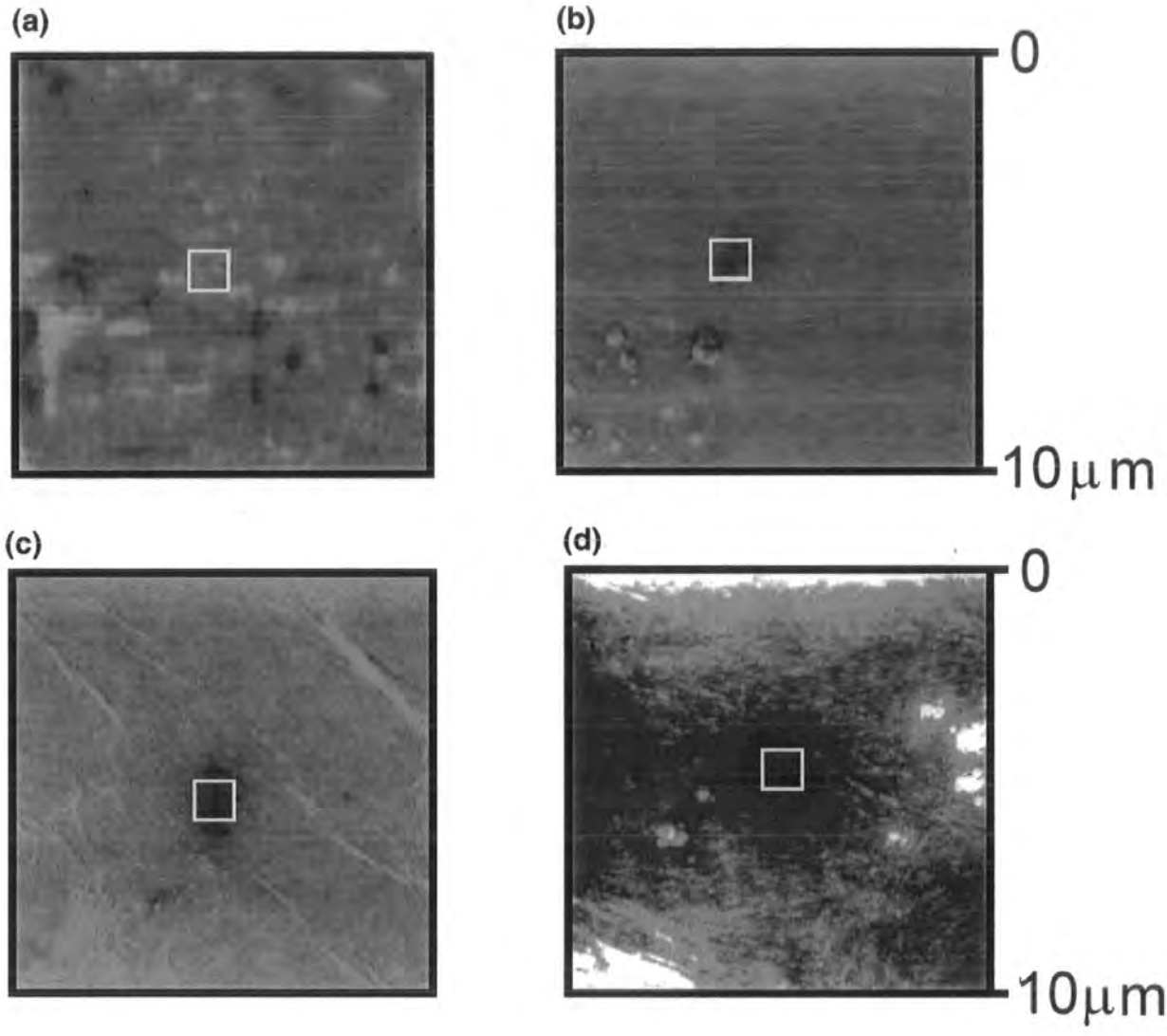

Figure 3.8 10 μm x 10 μm lift mode images of polypropylene recorded with +20 V applied to the tip: (a-d) the region marked with a square was previously exposed to lift mode bias of -40 V, -50 V, -60 V and -80 V respectively (Lift-height = 30 nm; Scan speed = 1.1 Hz).

3.5. Discussion

Conventional large scale corona discharge treatment has been reported to cause oxidation of polypropylene film surfaces,[22] together with changes in morphology.[23] In the current series of experiments, no evidence for topographic changes was found in the Tapping Mode height image, Figure 3.3a, nor chemical differences in the associated phase image, Figure 3.3b. Imaging SIMS (as in Section 2.2.2, ~1 ppm sensitivity to O), has also been used to characterise the positively and negatively charged samples (data not shown). No chemical modification was detected on either sample.

For the positive discharge modified polypropylene surfaces, systematically varying the EFM imaging voltage indicates that a positively charged region is being deposited onto the surface, Figure 3.3c-f and Table 3.2. At high positive EFM imaging voltages, the tip experiences repulsion from the positively charged surface; producing a bright lift-mode phase shift, Figure 3.3c and d. As the magnitude of the positive imaging voltage falls below the positive voltage at the surface, the negative mirror charge induced in the tip is no longer compensated. This leads to the tip acquiring an overall negative charge, which means it is attracted towards the positive surface charge, to give dark EFM phase contrast, Figure 3.3e. Contrast reversal occurs between +20 V and +12 V, indicating that the deposited surface voltage lies between these values. The positively charged region's polarity is confirmed by EFM imaging using a negative tip voltage, where the attractive force between tip and sample now becomes sufficiently large to produce a prominent dark localised EFM phase shift.

Deposition of positive charge onto the polymer surface using the EFM tip corresponds to a positive corona discharge being formed around the microscope tip.[24] Although the voltage applied to the tip is much smaller than the voltages associated with macroscopic corona discharges (a few kV[24]), the extreme curvature at the tip (~ 13 nm[25]) produces sufficient field strengths to ionise the surrounding air.[26] Accumulation of positive charge at the surface stems from positive ions (mainly hydrated H^+) drifting from the ionised region towards the polymer surface across the potential difference between the tip and insulating polymer surface.[24]

It is apparent that positive charge deposition requires the tip voltage to exceed a threshold value (between +80 and +100 V), Figure 3.4a and b. Corona discharges are well known to exhibit a threshold voltage, determined by the availability of free electrons to cause ionisation.[24] As the tip voltage increases above this value, the EFM lift-mode phase shift at the centre of the charge patch darkens, indicating a higher degree of charging, Figure 3.4b-f. The area affected by the discharge also increases. This is again consistent with a corona discharge, since as the corona voltage rises, the current of positive species travelling towards the surface increases resulting in a faster rate of charge accumulation.[24]

When the tip-voltage used for discharge generation was maintained at a constant value, the extent of surface charging could be enhanced by moving the tip towards the polymer surface, Figure 3.5. This is consistent with the threshold voltage for corona discharge dropping at shorter tip-sample distances.[8]

Increasing the scan speed effectively reduced the amount of charge deposited per unit area for an otherwise equivalent set of parameters, Figure 3.6. This is because higher scan speeds correspond to each region being exposed to the tip discharge for a shorter time period, hence less charge injection occurs.

The increase in charge patch size with EFM imaging voltage magnitude seen in Figure 3.3c-f can be explained on the basis of EFM lift-mode phase shifts being more sensitive towards lower surface charge densities at higher imaging tip-voltage magnitude, due to a stronger electrostatic tip-sample interaction. This observation implies that the positive charge patch on the polymer surface does not have an abrupt boundary, and that actually some positive charge density extends beyond the 1 μm x 1 μm treated area, Figure 3.3c and d. A similar variation in lateral charge distribution has previously been observed using an electrometer for a macroscopically charged surface.[27]

The arguments outlined above for the positive discharge are also applicable to the negative discharge experiments. Varying the EFM imaging lift-mode voltage produced an opposite trend in the corresponding images, Figures 3.3c-f and 3.7c-f. This is consistent with negative charge deposition. In this case, charge transfer will mainly result from CO_3^- ions drifting across the electric field towards the surface. A surface voltage of between -12 V and -17 V, was inferred from the point at which EFM lift-mode contrast reverses, Figure 3.7d and f. This potential has a similar magnitude to that resulting from positive discharge. Again, the charged region extends beyond the region that had been directly exposed to the discharge.

The threshold voltage for negative charge deposition was found to lie between -40 V and -50 V, Figure 3.8a and b. This is considerably lower in magnitude compared to the positive threshold voltage for equivalent conditions (between +80 V and +100 V). A similar effect has been observed on larger scales, where

the onset of a negative discharge for a high curvature tip (radius of curvature < 0.05 mm) occurs at a lower voltage than the equivalent positive discharge.[28] Again the size of the charged region correlates to the magnitude of the discharge voltage, due to the corresponding changes in the negative corona current, Figure 3.8b-d.

3.6. Conclusions

Localised charge deposition onto polymer surfaces can be achieved by scanning an atomic force microscope tip floating at high voltage. The polarity of the deposited charge region corresponds to the sign of the applied voltage. Whilst the scan parameters govern the amount of charge deposited. No accompanying morphological changes were detectable in the Tapping Mode AFM height images. Furthermore, Tapping Mode phase images and imaging SIMS spectra show that there is no associated chemical modification.

3.7. References

[1] Yamazaki, K.; Shingagawa, T.; Watanabe, T.; Takahira, T. *Jpn. Kokai Tokkyo Koho* 19881110, 1988.

[2] Y., K. Kitamura; Sawaguchi, T. E. U. S. Patent 19,720,104, 1972.

[3] Ando, K.; Ogawa, K. I., Y.; Okumura, Y. *Jpn. Kokai Tokkyo Koho* 19900312, 1990.

[4] Bruneel, J. L.; Micheron, F. *Congr. Int. Electrost* **1977**, Paper No. 38.

[5] Takamatsu, T.; Okada, K. K., F. *Jpn. Kokai Tokkyo Koho* 19850925, 1985.

[6] Barrett, R. C.; Quate, C. F. *J. Appl. Phys.* **1991**, *70*, 2725.

[7] Sessler, G. M.; West, J. E. *Phot. Sci. Eng.* **1974**, *18*, 162.

[8] Schönenberger, C. *Phys. Rev. B.* **1992**, *45*, 45.

[9] Stern, J. E.; Terris, B. D.; Mamin, H. J.; Rugar, D. *Appl. Phys. Lett.* **1988**, *53*, 2717.

[10] Nelson, M. W.; Schroeder, P. G.; Schlaf, R.; Parkinson, B. A. *Electrochemical Solid State Lett.* **1999**, *2*, 475.

[11] Nelson, M. W.; Schroeder, P. G.; Schlaf, R.; Parkinson, B. A.; Almgren, C. W.; Erikson, A. N. *Appl. Phys. Lett.* **1999**, *74*, 1421.

[12] Digital Instruments Application Notes. http://www.di.com/Appnotes/spot/spotmain/html (accessed May 2000).

[13] Karageorgiev, P.; Stiller, B.; Prescher, D.; Dietzel, B.; Schulz, B.; Brehmer, L. *Langmuir* **2000**, *16*, 5515.

[14] Magonov, S. N.; Elings, V. B.; Whangbo, M. H. *Surf. Sci.* **1997**, *375*, L385.

[15] Whangbo, M.-H.; Bar, G.; Brandsch, R. *Surf. Sci.* **1998**, *411*, L749.

[16] Whelan, P. M.; Hodgson, M. J. *Essential Principles of Physics*; John Murray: London, 1978.

[17] Martin, Y.; Williams, C. C.; Wickramasinghe, H. K. *J. Appl. Phys.* **1987**, *61*, 4423.

[18] Garcia, R.; Paulo, A. S. *Phys. Rev. B.* **1999**, *60*, 4961.

[19] Tamayo, J.; Garcia, R. *Appl. Phys. Letts.* **1997**, *71*, 2395.

[20] Noy, A.; Sanders, C. H.; Vezenov, D. V.; Wong, S. S.; Lieber, C. M. *Langmuir* **1998**, *14*, 1508.

[21] Tamayo, J.; Garcia, R. *Appl. Phys. Lett.* **1998**, *73*, 2926.

[22] Sarlaboux, J.; Mayoux, C. *J. Phys. D: Appl. Phys.* **1979**, *12*, L13.

[23] Leclerq, B.; Sotton, M.; Baszkin, A.; Ter-Minassian-Saraga, L. *Polymer* **1977**, *18*, 675.

[24] Giacometti, J. A.; Oliveria Jr., O. O. *IEEE Trans. Elect. Insul.* **1992**, *27*, 924.

[25] Ramirez-Aguilar, K. A.; Rowlen, K. L. *Langmuir* **1998**, *14*, 2562.

[26] Tipler, P. A. *Physics for Scientists and Engineers*; Worth: New York, 1991.

[27] Baum, E. A.; Lewis, T. J.; Toomer, R. *J. Phys. D: Appl. Phys.* **1977**, *10*, 487.

[28] Loeb, L. B. *Electrical Coronas*; University of California Press: Berkeley, 1965; p 326.

CHAPTER 4

CHARGED FLUOROCHEMICAL DOPED POLYPROPYLENE FILM SURFACES

4.1. Introduction

This chapter considers the charging behaviour of the fluorochemical doped polypropylene film surfaces, that were the subject of Chapter 2. Section 4.2 describes how electric force microscopy (EFM) is used in conjunction with a home-built scanning electrometer to map the charge distribution across corona charged fluorochemical doped surfaces. Section 4.3 probes surface charging properties using the localised EFM charging technique described in Chapter 3.

4.2. Mapping Charge on Fluorochemical Doped Polypropylene Film Surfaces

4.2.1. Introduction

Charged polymer surfaces have many technological uses; these include: electrostatic filter media,[1] device manufacture (such as microphones),[2] microbe resistant packaging,[3] optical display devices,[4] and biomedical applications.[5] Therefore, the identification and mapping of charge is of significant importance. Several powerful methods have been developed for measuring charge variation with depth,[6] however the visualisation of charge distributions at polymer surfaces is relatively unexplored. An indirect method developed in the past has utilised photoionised dye particles to stain charged polypropylene surfaces,[7] whereby the staining was then correlated to the lateral charge distribution using optical microscopy. In this case, the size of the dye particles placed a limit on the attainable spatial resolution (~ 2 μm). More recently, it has been shown that scanning probe microscopies are capable of mapping surface charge with greater accuracy.[8-12] In particular, EFM can provide lateral resolution down to below 30 nm,[8] and even single charge carriers have been identified by this technique.[9]

Very few EFM studies have examined polymer surfaces. One example has been poly(tetra-fluoroethylene-co-hexafluoropropylene) (FEP) film surfaces patterned with poly(amino-propyl) siloxane (APS).[8] Localised force plots were used to show that FEP regions contained negative charge, whilst the APS regions were neutral. However, this approach suffered from the drawback that

only very small regions of the surface could be examined (since a force plot needed to be acquired for each point above the surface). In this section, it is shown that larger areas of charged heterogeneous polymer surfaces can be examined using height, phase, and electric force AFM. A two-component polymer system comprising fluorochemical domains embedded in a polyolefin matrix has been chosen because of the different charging attributes of the constituents under the influence of a corona discharge.

4.2.2. Experimental

A melt blown isotactic polypropylene film (medium molecular weight "Fina 3860" grade) containing 1% bis-perfluorinated additive, Structure 2.1 was used. An additive-free polyolefin film was also prepared to act as a reference substrate. The films were charged by a positive corona discharge (constant current conditions: $I \approx 0.2$ mA). Subsequent annealing studies aimed at examining charge dissipation were performed in a temperature controlled oven.

EFM imaging with variable tip-voltage was carried out as described in Section 3.3. The cross-sections presented in Figure 4.8 were prepared by disabling the microscope's slow scan axis, and capturing successive line scans whilst the tip voltage was varied. Details of EFM theory and image interpretation are described in Section 3.2.

To allow large scale imaging, the surface potential distribution was also mapped using a electrostatic probe (Isoprobe electrostatic voltmeter model 244, Monroe electronics - New York; 0.1 % error) and a home-built motorised x-y sample manipulation stage, Figure 4.1. A PC was used to control sample x-y position and for data accumulation. The PC-electrometer interface was programmed using LabView software (version 5.1, National Instruments). Surface potential measurements were recorded every 400 μm covering a 20 mm × 20 mm area of the sample surface. Probe-sample spacing was fixed at ~1 mm, and the probe's voltage response was calibrated to a metal plate of known voltage prior to scanning. The spatial resolution of the probe head was 500 μm.

(a)

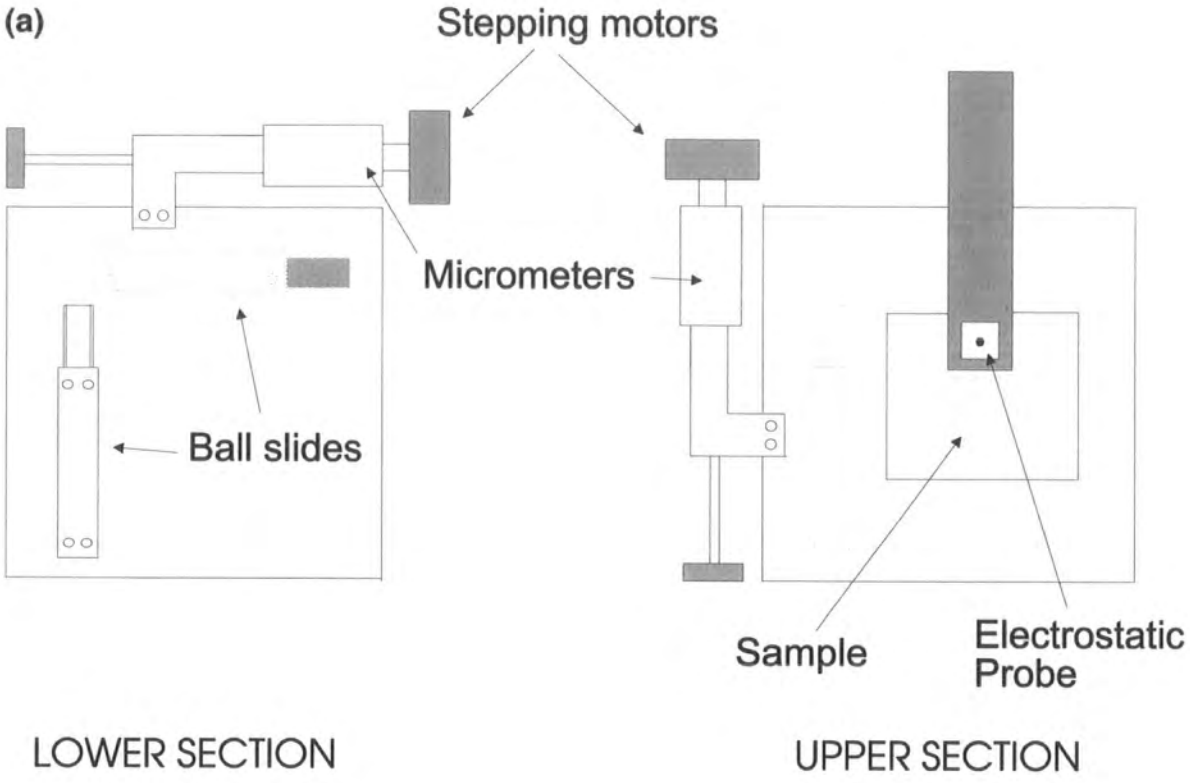

(b)

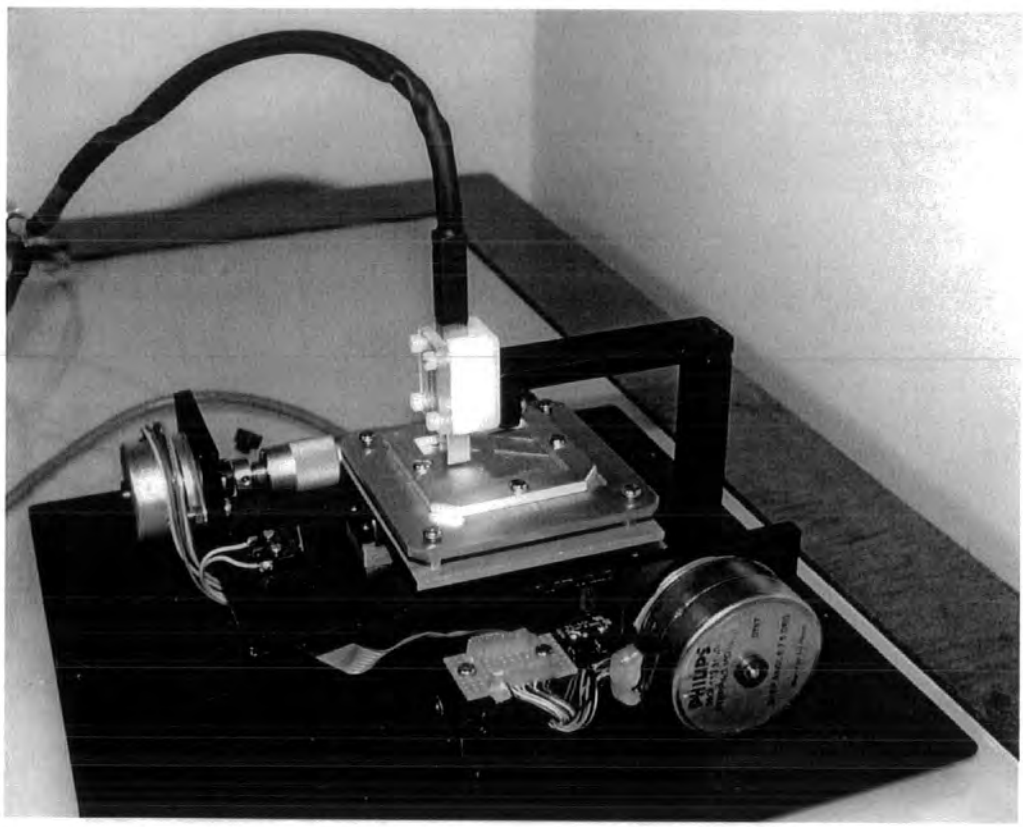

Figure 4.1 The scanning electrometer: (a) Schematic: shaded regions are attached to the base plate; and (b) Photograph.

4.2.3. Results

4.2.3.1. Uncharged Films

Large scale electrostatic probe analysis of both uncharged samples reveals a low level of negative surface potential, Table 4.1, Figures 4.2a and 4.3a. It is thought that this residual surface potential will have accumulated during sample manufacture and handling through tribocharging. Tapping-mode AFM height images of the two uncharged films depict spherulitic morphology, Figures 4.4a and 4.5a. The phase image of the pure film solely depicts crystalline morphology, Figure 4.4b, whereas fluorochemical domains are visible as bright contrast at the surface of the doped sample, Figure 4.5b. Uncharged pure and fluorochemical doped polypropylene films displayed no phase contrast in the EFM lift mode attributable to the presence of localised surface charge, Figures 4.4c and d, Figures 4.5c and d.

Sample	Mean uncharged surface voltage / V	Mean corona charged surface voltage / V	Mean corona charged, then annealed surface voltage / V
Pure	-41	+246	+82
Doped	-16	+367	-27

Table 4.1 Surface potential statistics.

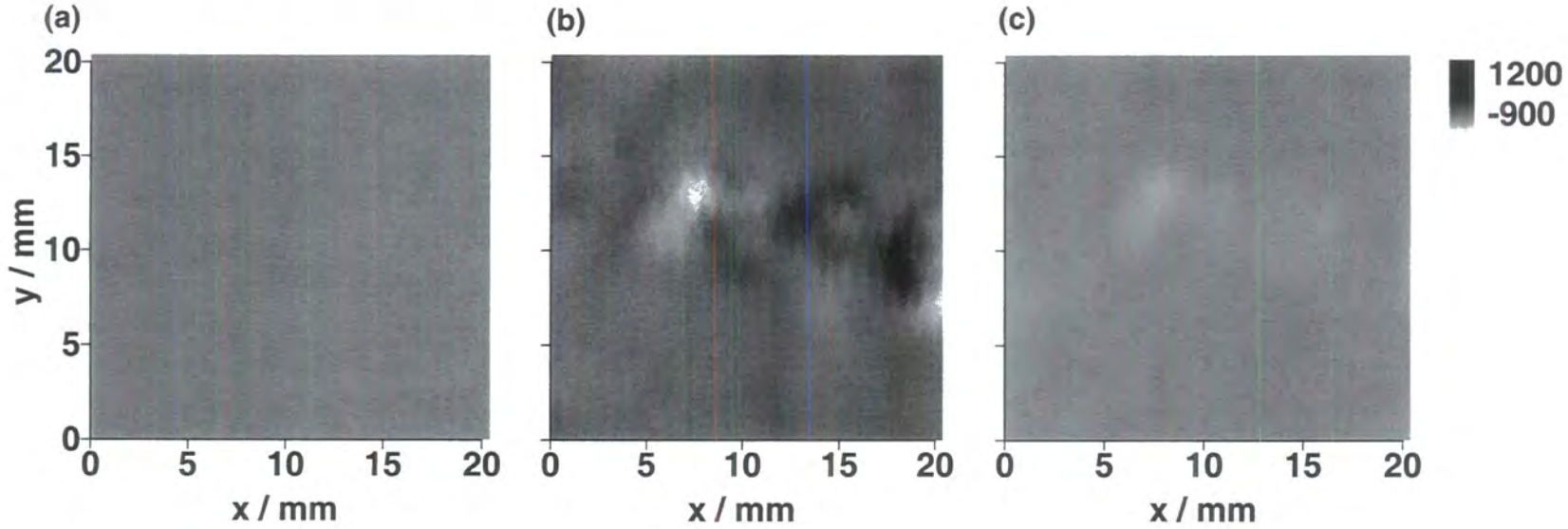

Figure 4.2 Electrometer image of pure polypropylene film: (a) uncharged; (b) charged; and (c) charged following annealing at 130°C.

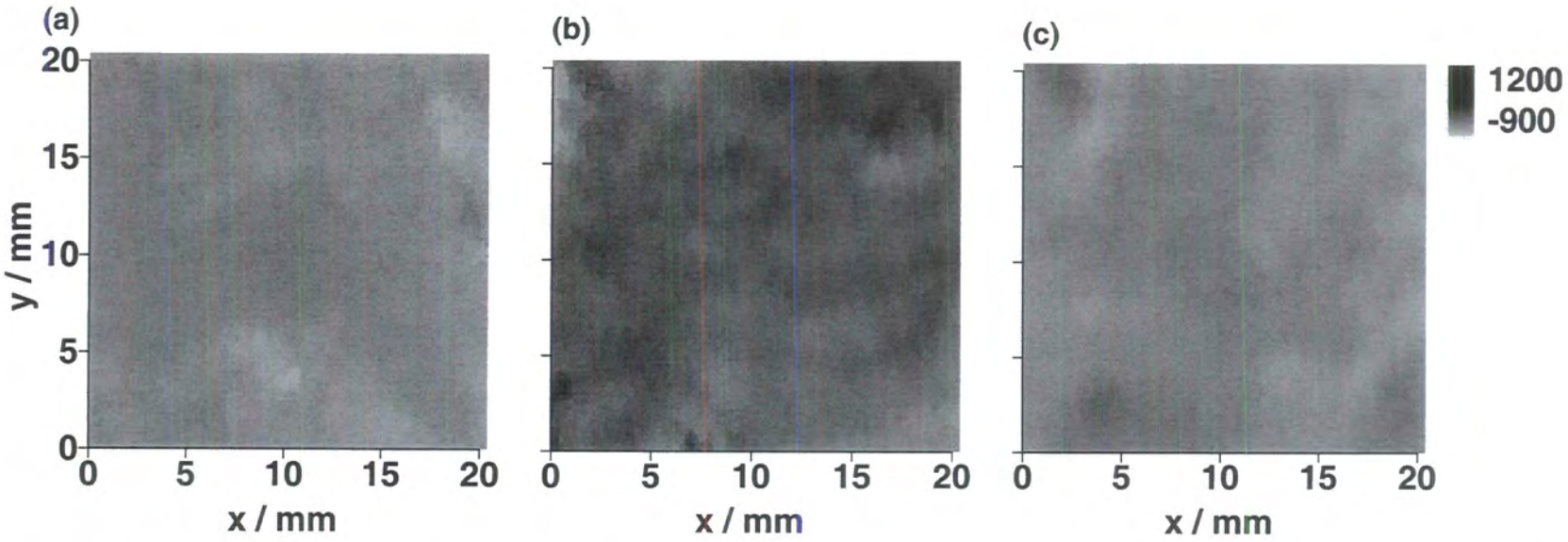

Figure 4.3 Electrometer image of fluorochemical doped polypropylene film: (a) uncharged; (b) charged; and (c) charged following annealing at 130°C.

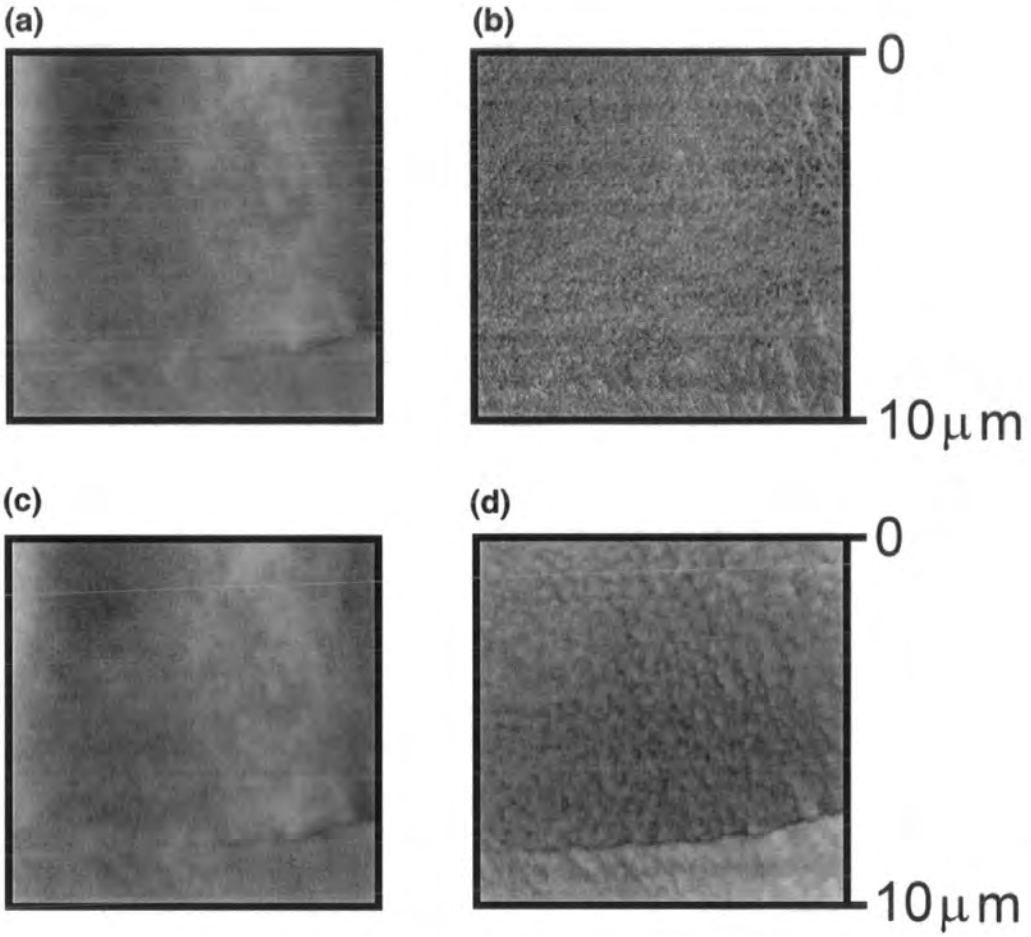

Figure 4.4 10 μm × 10 μm AFM micrographs of polypropylene film: (a) height image; (b) Tapping mode phase image; (c-d) EFM lift-mode phase images recorded at: +40 V and -40 V respectively.

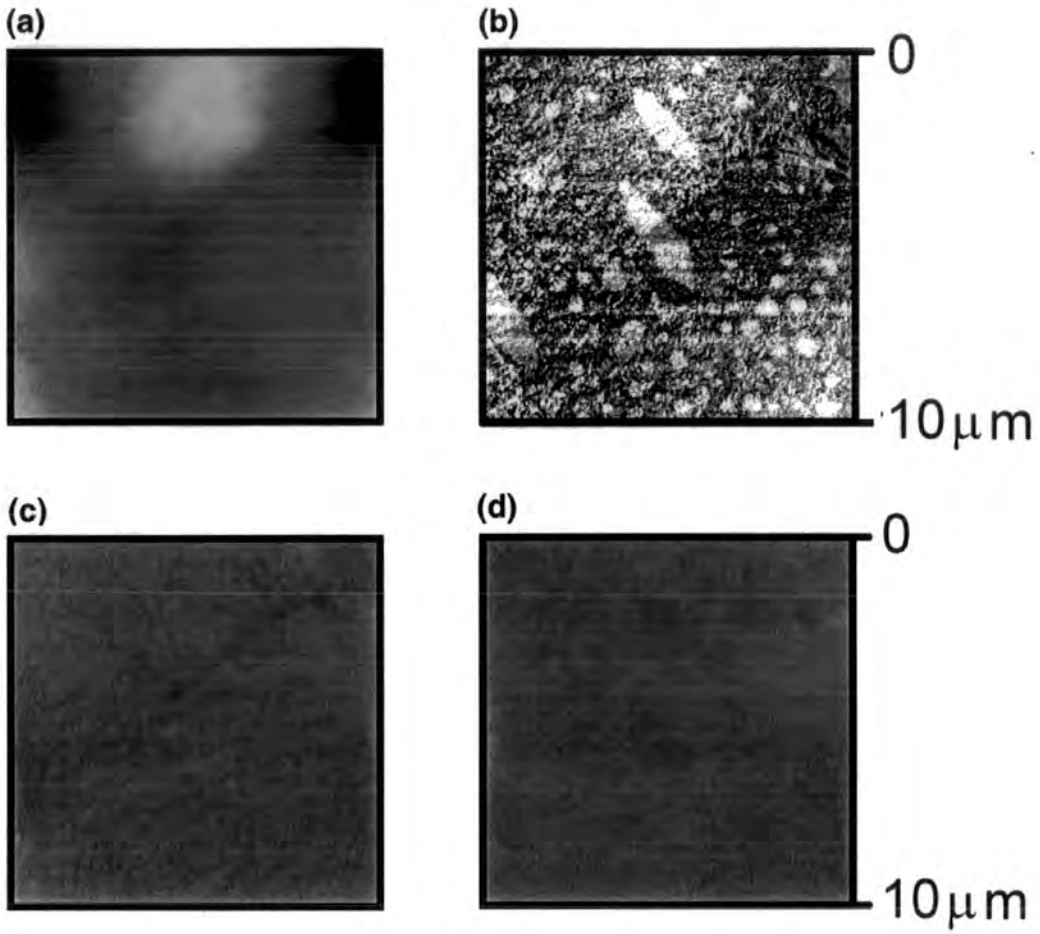

Figure 4.5 10 μm × 10 μm AFM micrographs of fluorochemical doped polypropylene film: (a) height image; (b) Tapping mode phase image; (c-d) EFM lift-mode phase images recorded at +40 V and -40 V respectively.

4.2.3.2. Charged Films

Positive corona charging was found to impart a positive potential to both the pure and fluorochemical doped polymer surfaces, Table 4.1. The presence of fluorochemical gave rise to a greater build-up of positive charge at the surface (+367 V) compared to the pure polypropylene sample (+ 246 V). However, the spatial distribution of charge was non-uniform, with both types of surface exhibiting some regions of negative charge, Figure 4.2b and 4.3b. This is consistent with the previous observation that corona discharge produces non-uniform surface charge distributions.[15]

Tapping-mode AFM height and phase images of charged pure polypropylene film showed the same features as the uncharged equivalent, Figure 4.6a and b. EFM lift-mode phase images displayed contrast depicting surface morphology, and a localised feature centred on the spherulite nuclei, Figure 4.6c and d. Changing the tip voltage from +40 V to -40 V inverted the EFM lift mode contrast at the spherulite centres from bright to dark, which indicates that they are positively charged.

Tapping-mode AFM height and phase micrographs of charged fluorochemical doped film also match those of the uncharged equivalents, Figure 4.7a and b. The corresponding EFM lift-mode phase images displayed contrast variation corresponding to regions of the fluorochemical additive, Figure 4.7c and d. With +40 V applied to the tip, locations enriched in fluorochemical produced bright EFM lift-mode phase contrast, Figure 4.7c. Reversing the tip voltage to -40 V inverted the EFM lift-mode phase contrast corresponding to the fluorochemical domains, Figure 4.7d. The magnitude of EFM lift-mode phase shift above a fluorochemical domain varied smoothly with changing tip-voltage, Figure 4.8. The line scans also show that the high phase shift corresponding to the location of a fluorochemical patch does not have a corresponding feature in the height scan, Figures 4.8b and 4.8a respectively. At +20 V applied tip voltage, the EFM lift-mode profile displays high phase shift at the location of the fluorochemical, Figure 4.8c, switching the tip voltage to -20 V removes any localised contrast, Figure 4.8d; while reducing the tip voltage further produces increasingly negative phase shifts, Figure 4.8e-g. All of these observations are consistent

with positively charged fluorochemical domains at the polypropylene film surface, Table 3.2.

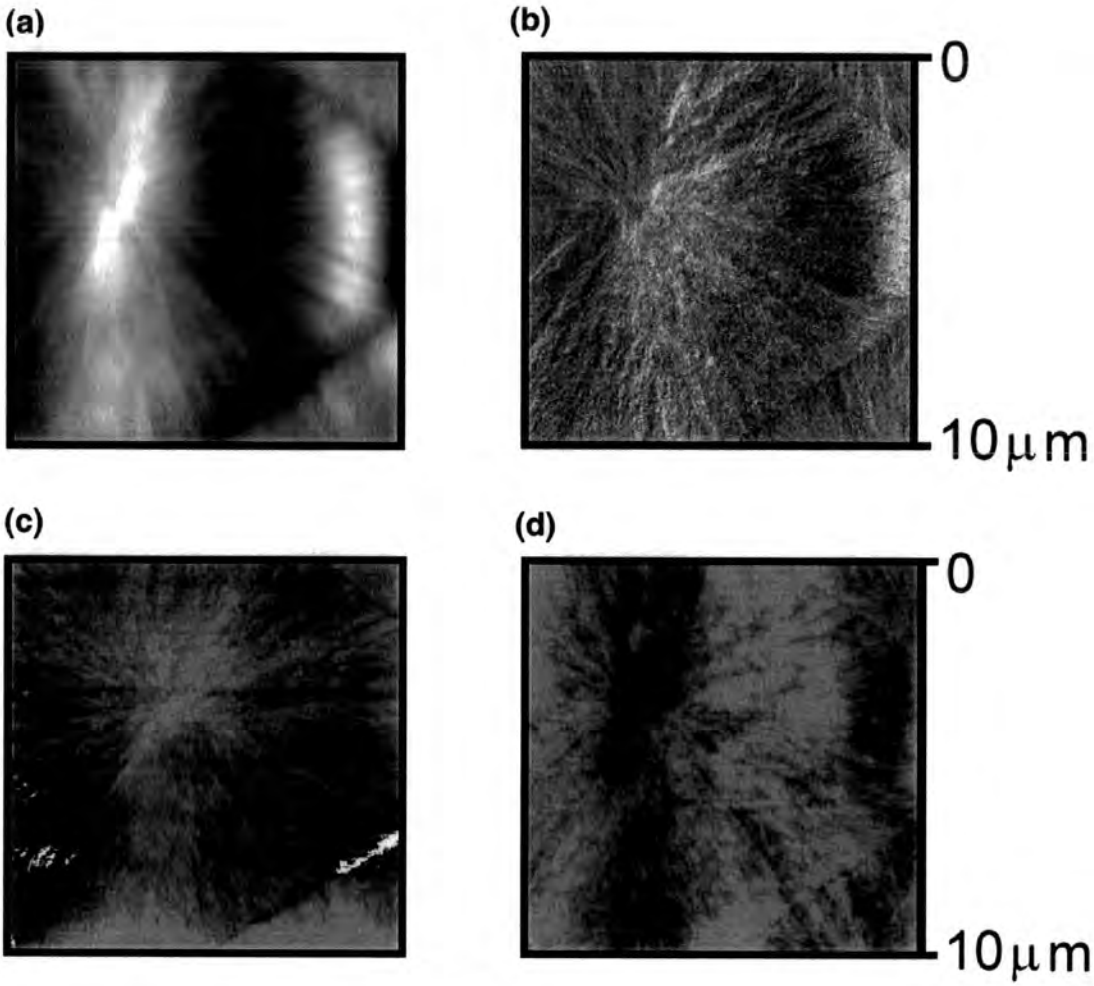

Figure 4.6 10 μm × 10 μm AFM micrographs of charged polypropylene film: (a) height image; (b) Tapping mode phase image; (c-d) EFM lift-mode phase images recorded at: +40 V and -40 V respectively.

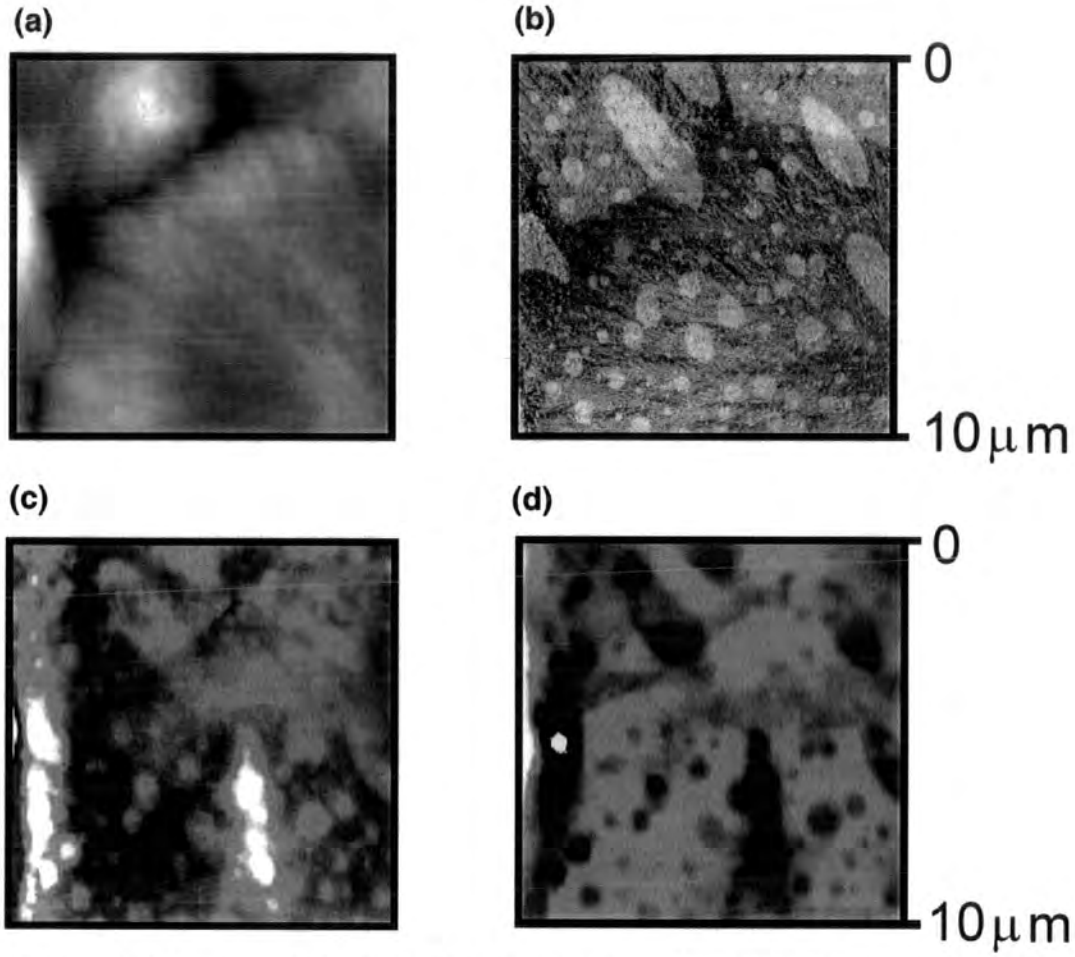

Figure 4.7 10 μm × 10 μm AFM micrographs of charged fluorochemical doped polypropylene film: (a) height image; (b) Tapping Mode phase image; (c-d) EFM lift-mode phase images recorded at +40 V and -40 V respectively.

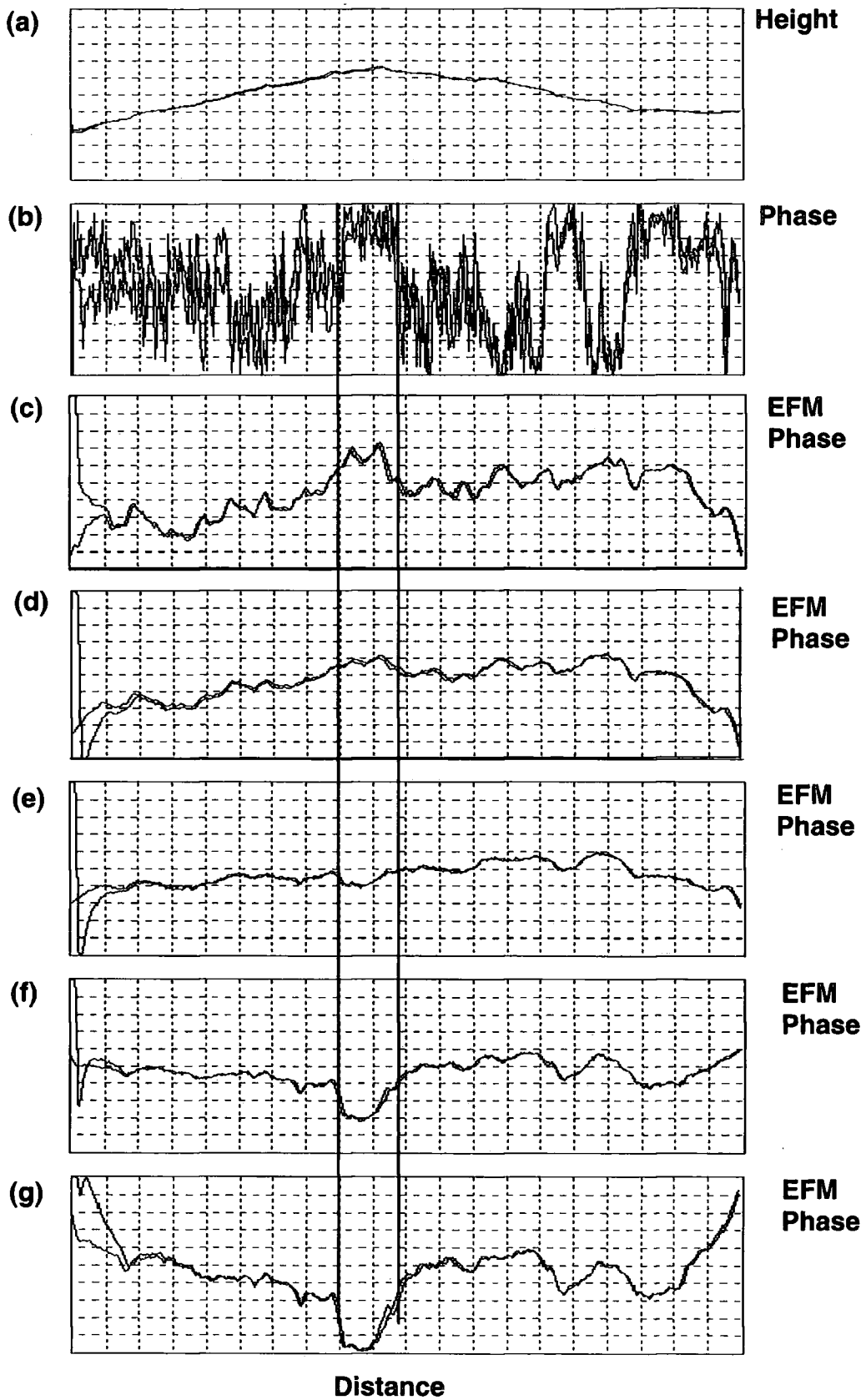

Figure 4.8 10 μm line scans of charged fluorochemical doped polypropylene: (a) Height; (b) Tapping-mode phase; (c-g) EFM Lift-mode phase images recorded at +20V, -20V, -40V, -60V, -80 V respectively. The location of a fluorochemical domain is indicated by vertical lines.

4.2.3.3. Effect of Annealing on Spatial Charge Distribution

Tapping Mode height, phase and electrical force AFM micrographs of charged fluorochemical doped polypropylene films which had been annealed at 60 °C for 1 minute showed no changes, Figure 4.9. However, increasing the annealing temperature to 100 °C (1 minute exposure) altered the EFM lift-mode phase contrast associated with the fluorochemical domains, Figure 4.10. Whilst the appearance of the domains themselves remains unchanged in the corresponding Tapping Mode phase images, Figure 4.10b, the EFM lift-mode phase contrast of the fluorochemical domains had decreased in magnitude at the higher temperature, Figure 4.10c and d. Changing the polarity of the tip voltage again inverted the EFM lift-mode image contrast, indicating the presence of positive charge on the fluorochemical domains.

Annealing at 130 °C for 1 minute produced changes in both Tapping Mode and EFM lift-mode phase images, Figure 4.11. Tapping Mode AFM phase images were indicative of the fluorochemical surface coverage increasing, Figure 4.11b. EFM lift-mode phase contrast no longer matched the location of the fluorochemical domains, and the polarity of the applied tip voltage had little effect on the EFM lift-mode phase image contrast, Figure 4.11c and d.

Regions of the charged samples previously analysed using the surface potential probe, Figures 4.2b and 4.3b, were re-imaged following annealing at 130 °C for 1 minute. Both samples show thermally stimulated surface potential decay, Table 4.1. Although the amount of surface charge has been reduced by annealing, the distribution of charge across the surface remains the same (i.e the most positive and negative regions of the surface are located in the same position both before and after annealing), Figures 4.2b and c, Figures 4.3b and c. This suggests that large scale charge features do not laterally migrate to cancel each other out, rather they discharge via migration into the bulk.

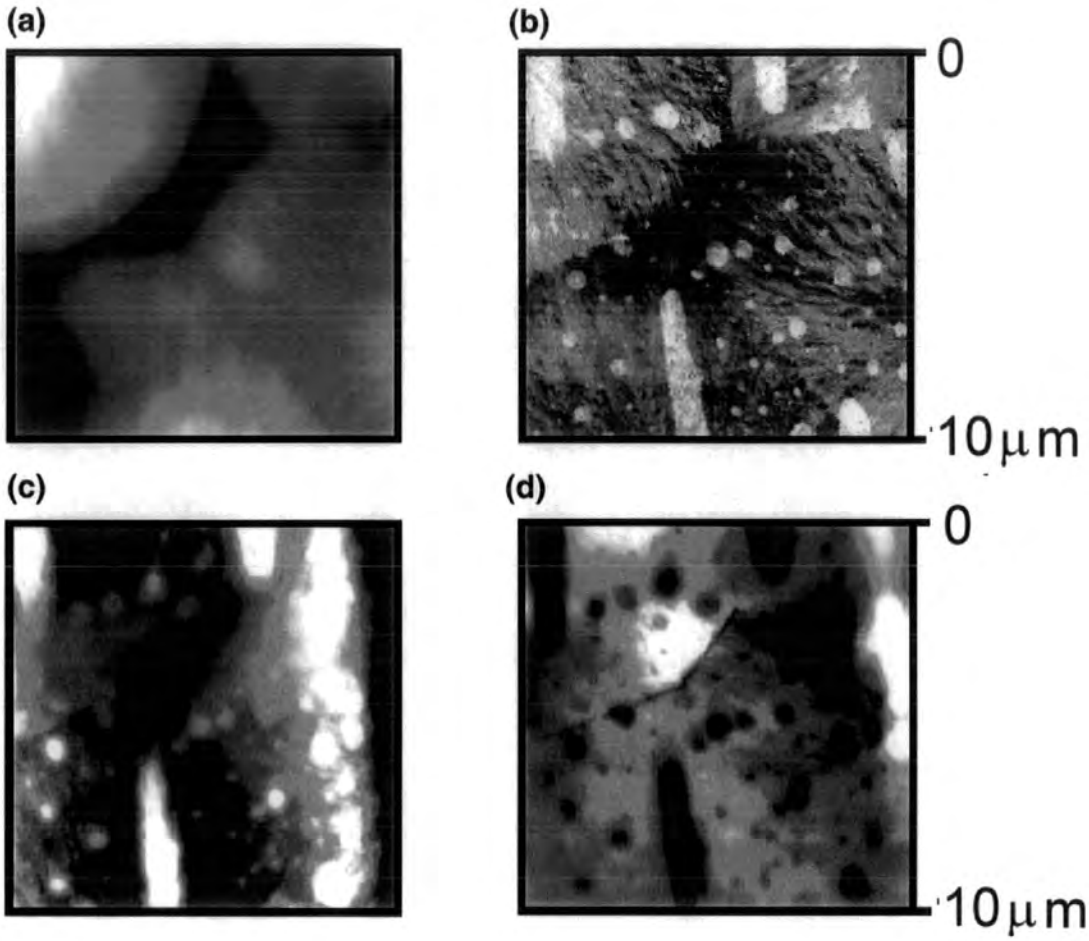

Figure 4.9 10 μm × 10 μm AFM micrographs of charged fluorochemical doped polypropylene after annealing at 60 °C for 1 minute: (a) height image; (b) Tapping Mode phase image; (c-d) EFM lift-mode phase images recorded at +40 V and -40 V respectively.

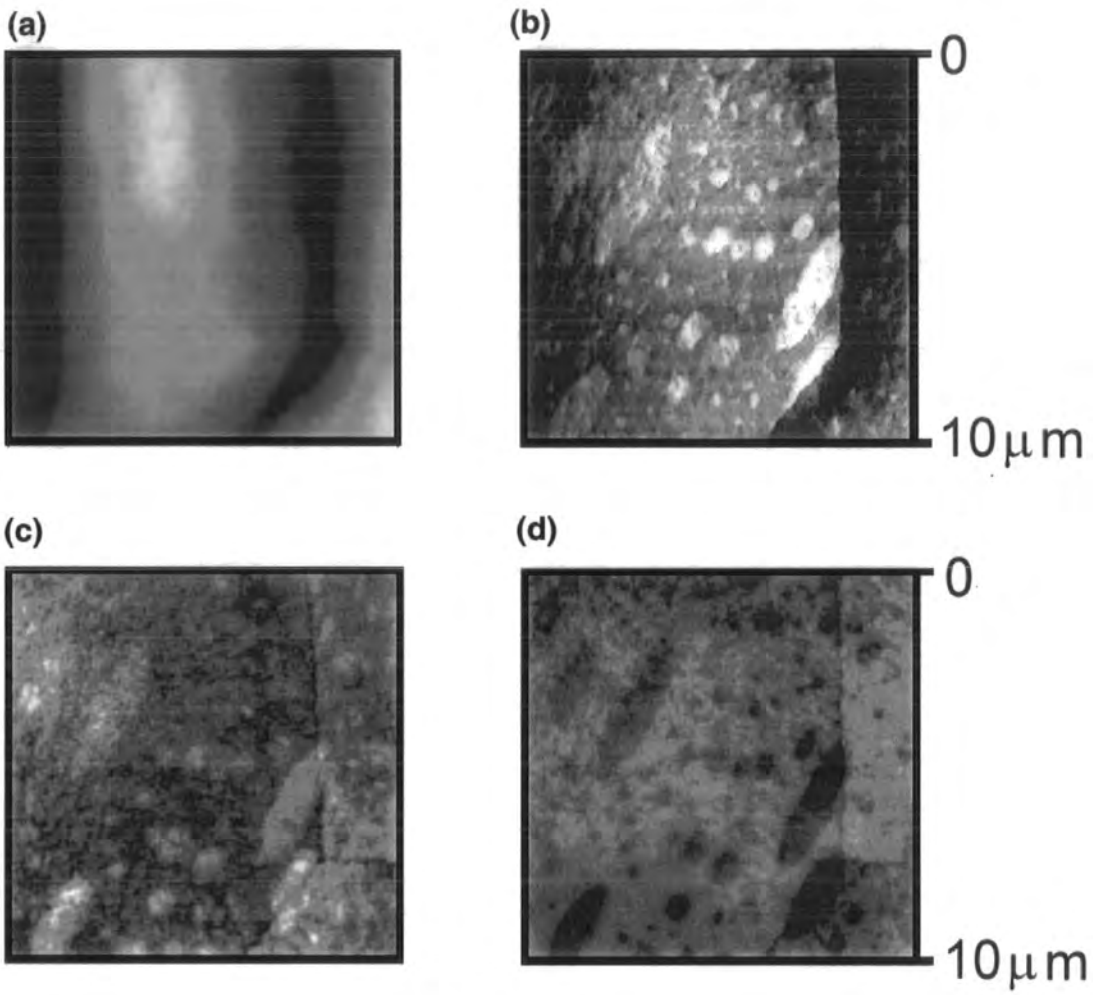

Figure 4.10 10 μm × 10 μm AFM micrographs of charged fluorochemical doped polypropylene after annealing at 100 °C for 1 minute: (a) height image; (b) Tapping Mode phase image; (c-d) EFM lift-mode phase images recorded at +40 V and -40 V respectively.

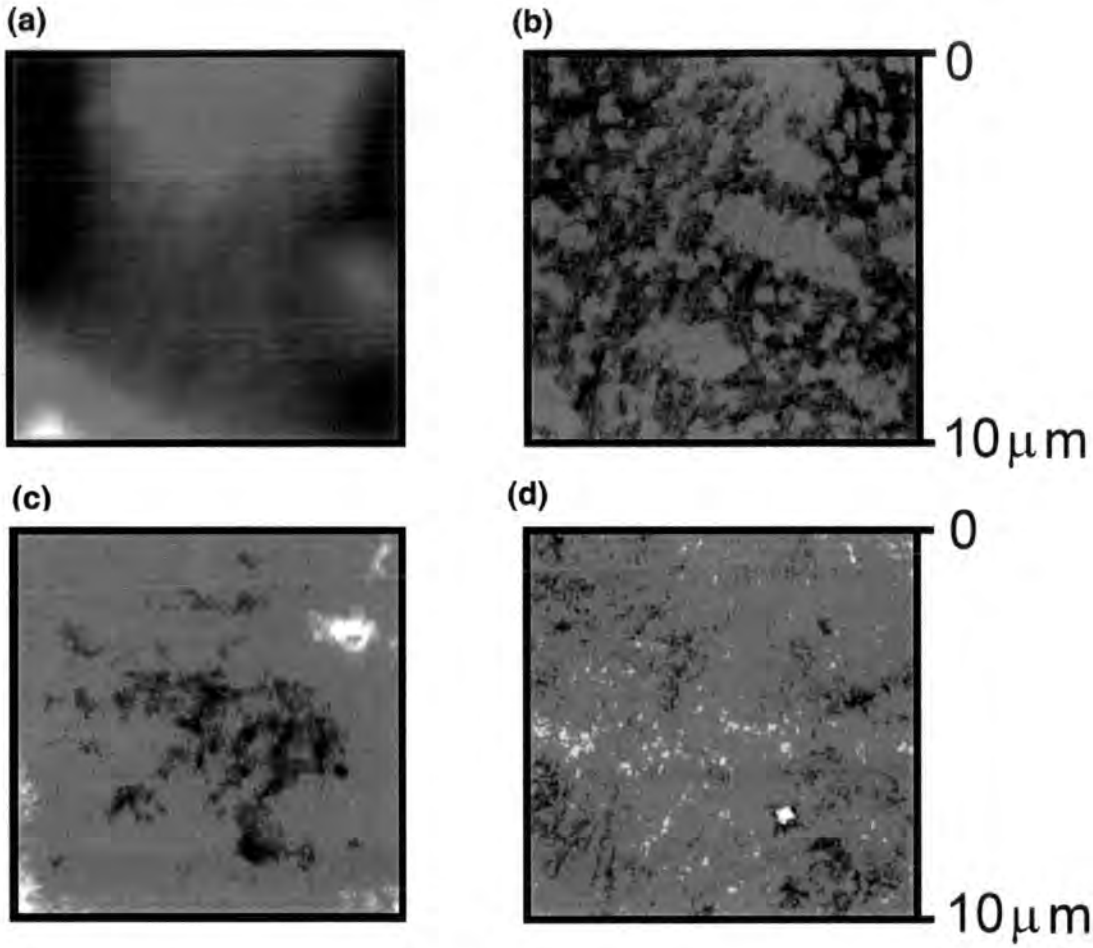

Figure 4.11 10 μm × 10 μm AFM micrographs of charged fluorochemical doped polypropylene after annealing at 130 °C for 1 minute: (a) height image; (b) Tapping Mode phase image; (c-d) EFM lift-mode phase images recorded at +40 V and -40 V respectively.

4.2.3.4. ADDENDUM: Poling of Fluorochemical Domains During Low Temperature Annealing

This section reports on an interesting spatial charge distribution effect observed for another of the fluorochemical doped polypropylene films considered in Chapter 2. A film comprising 1% bis-perfluorinated additive mixed with isotactic polypropylene (low molecular weight "Exxon 3505" grade) was charged as described in Section 4.2.2, then annealed at 60 °C for 1 minute. EFM was used to characterise the surface charge distribution.

The Tapping Mode AFM height image of the charged doped film following annealing depicts spherulitic morphology, while the phase image locates the fluorochemical domains as bright contrast, Figure 4.12a and b respectively. Film

morphology and the distribution of fluorochemical are the same as that previously observed for the equivalent uncharged film before annealing, Figure 2.3b. Lift-mode EFM phase images recorded at + 40 V show striking contrast corresponding to the location of fluorochemical at the surface, Figure 4.12c. Each fluorochemical domain is split into two parts, with one region giving dark contrast and the other bright contrast. Furthermore, the orientation of the contrasting segments is common to each of the fluorochemical patches. The effect of changing the tip voltage from + 40 to - 40 V is to reverse the contrast of both parts of the fluorochemical domains, Figure 4.13. The right hand regions of the fluorochemical domains change from bright to dark lift-mode contrast, indicating positive charge, conversely the left hand side regions are negatively charged. Therefore it can be concluded that the charged, annealed doped polypropylene surface possess orientated dipoles spatially confined to the regions enriched in fluorochemical additive.

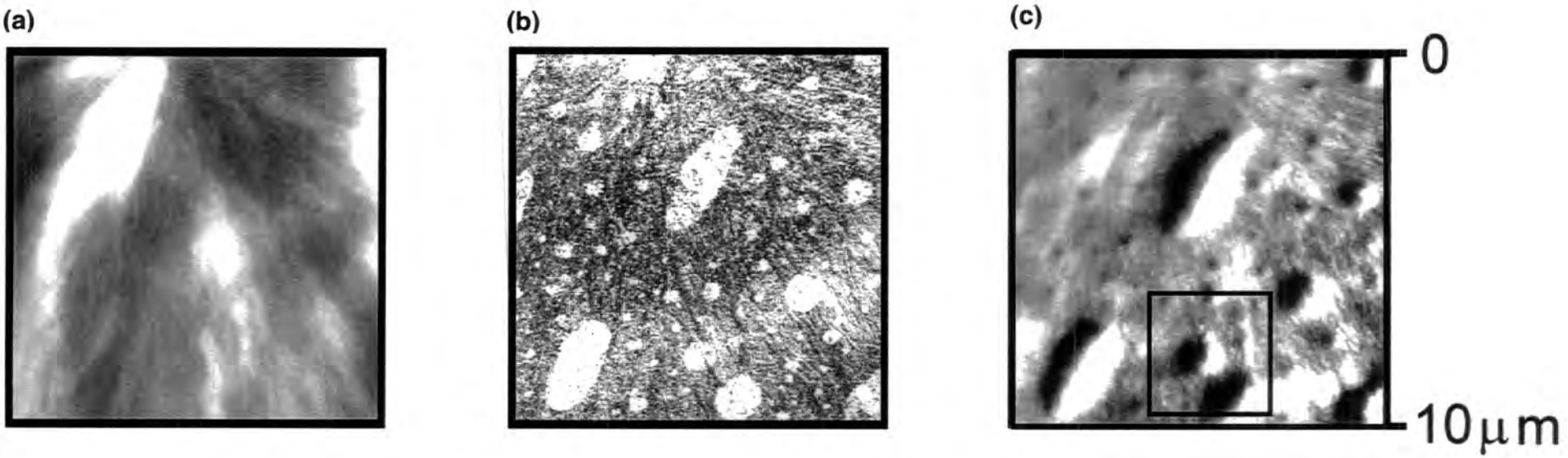

Figure 4.12 10 μm × 10 μm AFM micrographs of charged fluorochemical doped polypropylene (Exxon 3505) after annealing at 60 °C for 1 minute: (a) height image; (b) Tapping Mode phase image; and (c) EFM lift-mode phase images recorded at +40 V.

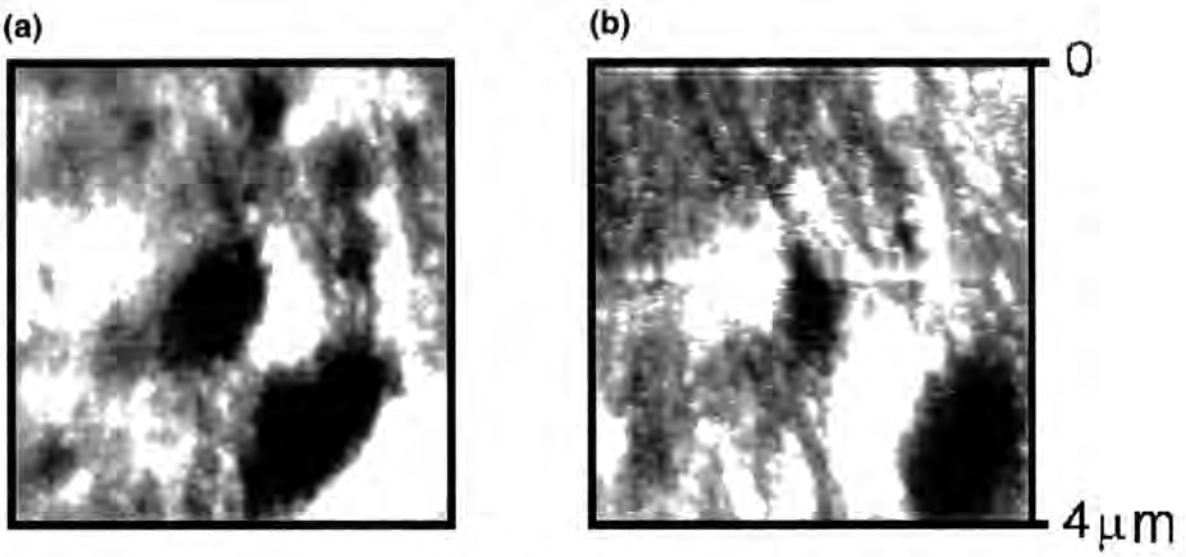

Figure 4.13: 4 μm × 4 μm lift-mode phase images of charged fluorochemical doped polypropylene after annealing at 60 °C for 1 minute, recorded in the box marked on Figure 4.11c: (a) + 40 V tip voltage (b) - 40 V tip voltage.

4.2.4. Discussion

Although polypropylene is often used as an electret material, polymers containing fluorine (such as poly(tetrafluoroethylene) - PTFE) tend to exhibit better charge storage properties.[13] Indeed, in this study it has been observed that the presence of fluorochemical at the surface enhances the average surface potential acquired following positive corona discharge. This improvement in charge longevity can be attributed to the high surface hydrophobicity[14] and exceptionally low electrical conductivity of fluorinated materials.[15] Furthermore, the differences in charging characteristics between polyolefin and fluorinated chains suggest that a charged polypropylene surface containing regions of fluorochemical will display a corresponding spatial variation in charge distribution.

EFM lift-mode phase images of charged pure polypropylene show contrast reflecting sample topography (due to the increased electric field gradient at highly curved regions of a uniformly charged body combined with Van der Waals forces[16]), Figure 2.6. This is consistent with a previous study where it was shown that charged dye particles adhere to the surface of oppositely charged polypropylene spherulites.[7] Closer inspection reveals concentration of

charge at the spherulite centres. The effect of tip voltage on the EFM lift-mode contrast for these regions suggests that they are positively charged with respect to the surrounding surface. A plausible explanation for this charge build-up could be that spherulites often nucleate around impurities in the polymer melt, and such impurities are known to act as localised charge traps.[15]

In the case of the charged fluorochemical doped polypropylene film, EFM lift-mode phase images indicate that the additive domains possess a different level of charge at the surface compared to the surrounding polypropylene regions. A positive applied tip voltage results in the EFM lift-mode phase shift becoming more repulsive for the fluorochemical regions compared to the tip-polypropylene interactions. Negative voltages cause the tip to experience a more attractive field gradient when it is above fluorochemical regions compared to the polypropylene. These observations are consistent with the fluorochemical domains being positively charged with respect to the surrounding polypropylene matrix, Table 3.2.

The polarity acquired by fluorinated species at surfaces relative to polyolefin media has only previously been studied during tribocharging experiments. In this case, fluorinated polymers were reported to acquire negative charge relative to polypropylene upon contact.[17] A study of poly(tetrafluoroethylene-co-hexafluoropropylene) (FEP) patterned with poly(amino-propyl-siloxane) (APS) also found the FEP regions to be negatively charged.[8] This latter conclusion is only of limited relevance since APS does not possess electret properties and was reported to be uncharged. The current study differs in that the mechanism of charging is corona discharge. In this case it appears that the mainly positive deposited charge resides preferentially on the fluorochemical domains.

The subsequent annealing studies of the positively charged fluorochemical doped polypropylene (medium molecular weight "Fina 3860" grade) films have shown that the entire surface becomes uniformly charged over the micron scale at high temperatures, Figures 2.9 - 2.11. This is consistent with the electrical properties of polymers being temperature dependent. For example, the conductivity of polymer electrets increases with temperature, due to trapped charge being unloaded via thermally activated processes.[15] An important

parameter is the discharge temperature, this is defined as the temperature at which all trapped surface charge disappears.[15] Polypropylene has a discharge temperature of 155 °C, and gives peaks at ~70 °C and ~130 °C in open circuit thermally stimulated current (TSC) measurements.[6] These peaks correspond to de-trapping of charges near the surface and in the bulk respectively. PTFE can be taken as an analogue for the segregated perfluorinated arms of the fluorochemical additive at the surface, this is reported to have a higher discharge temperature of 230 °C, with no loss of charge occurring below 100 °C.[13]

The observed charge decay with annealing for the charged fluorochemical doped polypropylene films is consistent with these observations. As well as the actual loss of charge density from the surface, lateral migration of surface charge to reduce the field gradient resulting from the differential charging between the fluorochemical domains and the surrounding polypropylene matrix may be a contributing factor. This energetically favourable charge redistribution will become more likely at higher temperatures, due to better charge transport. It should also be noted that elevated temperatures will encourage the migration of the lower surface energy fluorochemical molecules towards the air-solid interface, Section 2.3. This will have the effect of disrupting the existing charged fluorochemical domains, and placing additional uncharged additive molecules at the surface.

On this basis, the observed annealing behaviour of the charged fluorochemical doped polypropylene films can be accounted for as follows: at 60 °C insufficient thermal excitation is available for charge to de-trap in either polypropylene or the fluorochemical. This low conductivity also prevents lateral charge migration. At 100 °C the surface charge residing on polypropylene is released, but charge is retained on the more stable fluorinated domains. In this case, lateral charge migration between neighbouring fluorochemical and polypropylene domains accounts for the partial loss of the localised charge domains. At the highest temperature of 130°C, the combination of increased surface segregation, lateral charge migration and loss of surface charge density from the fluorinated regions gives rise to a uniform surface charge distribution. Although this produces the removal of the small scale charge heterogeneity attributable to differences in

chemical composition across the surface, the large scale surface potential variation introduced as a result of the corona discharge process remains.

Annealing to 60 °C did not change the spatial charge distribution of the medium molecular weight doped polypropylene, whereas equivalent treatment of the low molecular weight sample produced orientated dipoles localised on the fluorochemical domains. A dipole arrangement could be produced by the presence of an electric field gradient across the surface. This gradient would drive positive and negative charge carriers to laterally migrate in opposite directions during annealing. If the field gradient was constant over the 10 μm x 10 μm area examined by EFM then all carriers would migrate in the same direction, explaining the dipole's common orientation. Highly charged domains on other regions of the polymer surface could produce such an electric field. The observation that the lateral charge migration was bounded by the edges of the fluorochemical domains is consistent with the segregated perfluorinated arms of the additive molecule having better charge retaining properties than the surrounding polypropylene.

4.3. Localised Charging Properties of Fluorochemical Doped Polypropylene Film Surfaces by EFM

4.3.1. Introduction

The variation of surface potential across positively corona charged fluorochemical doped surfaces have been studied on millimeter and micrometer scales using a scanning electrometer and EFM respectively, Section 4.2. Although such surfaces are found to be predominantly positively charged, variations in large scale surface potential (sign and magnitude) exist, Figures 4.2 and 4.3. However EFM consistently indicates that fluorochemical enriched domains acquire positive charge relative to the surrounding polypropylene. This presents a familiar problem for scanning force microscopy methods: how to ensure the minute sampling area is representative of the entire surface. Usually this is addressed by recording and comparing scans from several different regions of the surface. However, this approach does not allow comparison

between the overall polarity of a given region and its small scale charge distribution.

A solution is provided by using a scanning EFM tip to deposit controlled levels of charge with high spatial precision, and subsequently image the resulting charge distribution as described in Chapter 3. This allows the unambiguous identification of the relative charging behaviour of polypropylene and fluorochemical regions when exposed to positive and negative discharges.

4.3.2. Experimental

Uncharged bis-perfluorinated additive doped (1% by weight) polypropylene (medium molecular weight "Fina 3860" grade) films were used. Lift-mode EFM charge deposition and imaging were performed as described in Section 3.3. Optimum discharge conditions were found to be: set-point : free amplitude ratio of 0.5; a scan rate of 0.5 Hz and a lift height of 30 nm.

Each experiment consisted of two stages: localised surface charging, followed by imaging the modified region. Charging was performed by scanning a 5 μm x 5 μm square of polymer with a high voltage (± 140 V) applied to the tip. Subsequently images centred on this square were recorded.

4.3.3. Results

While the fluorochemical enriched regions (bright tapping-mode phase contrast) outside the 5 μm x 5 μm square exposed to negative discharge are undistinguished in lift mode images, those within produce dark lift-mode contrast relative to the surrounding polypropylene, Figure 4.14. However, the lift-mode contrast of the pure polypropylene regions is not altered by negative discharge. With positive tip voltage (+20 V) dark lift-mode contrast signifies negative surface charge, Table 3.2. Hence it appears that negative EFM discharge deposits negative charge selectively onto the fluorochemical domains, without effecting the surrounding polypropylene.

However, localised positive discharge produces a change in the lift-mode contrast of both the surrounding polypropylene and the fluorochemical patches,

Figure 4.15. With the tip voltage now at - 20 V, positive surface charge causes the lift-mode image to darken. Polypropylene regions within the modified region darken, but to a lesser extent than the fluorochemical domains. Therefore, in the case of positive discharge both polypropylene and fluorochemical regions acquire positive charge, however more potential resides on the fluorochemical.

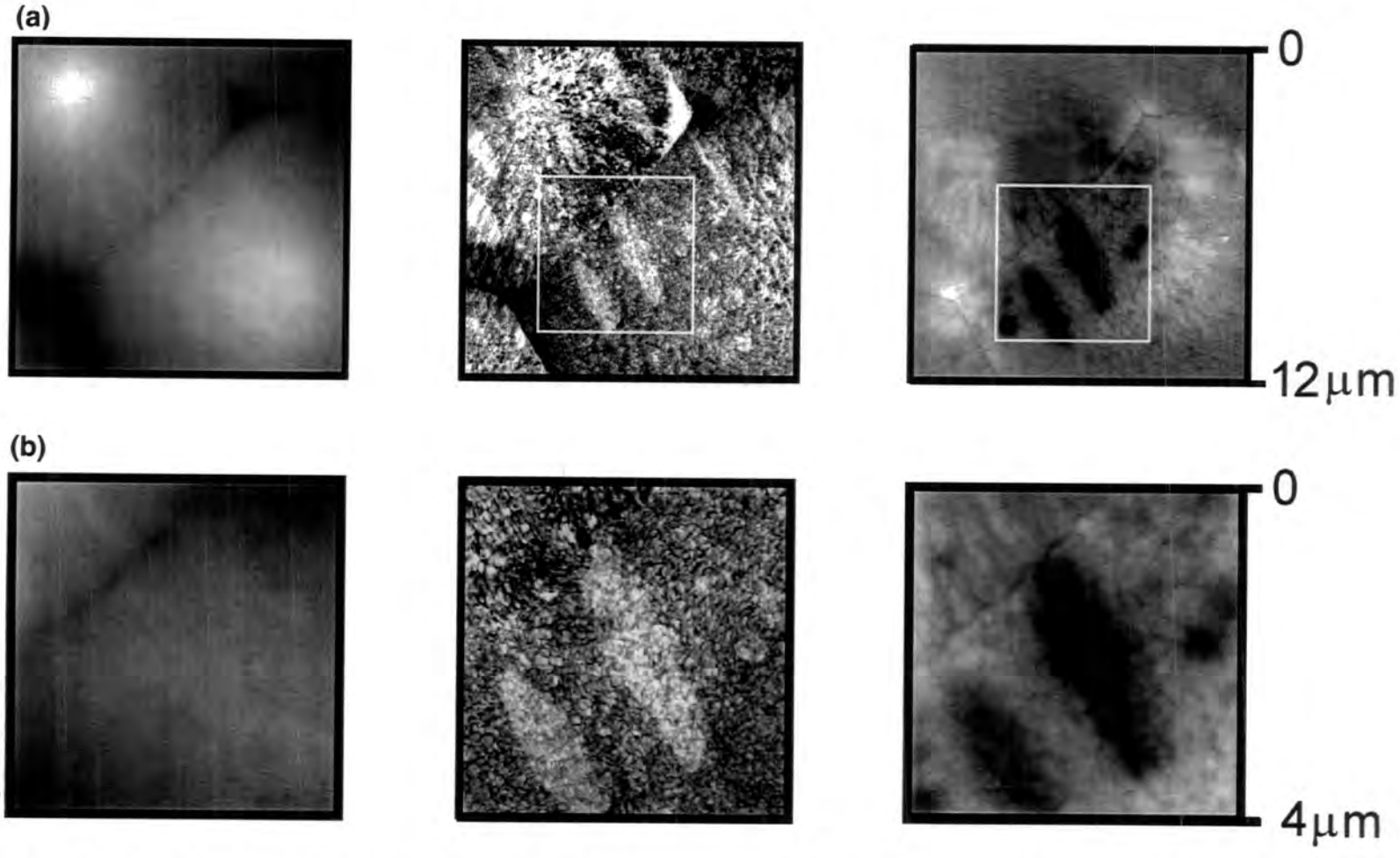

Figure 4.14 EFM micrographs of fluorochemical doped polypropylene (LHS: height; middle: Tapping mode phase; RHS: lift-mode phase recorded with + 20 V imaging voltage): (a) 12 μm × 12 μm image, the region within the square has been exposed to - 140 V discharge voltage; (b) 4 μm × 4 μm image recorded in the square marked on (a).

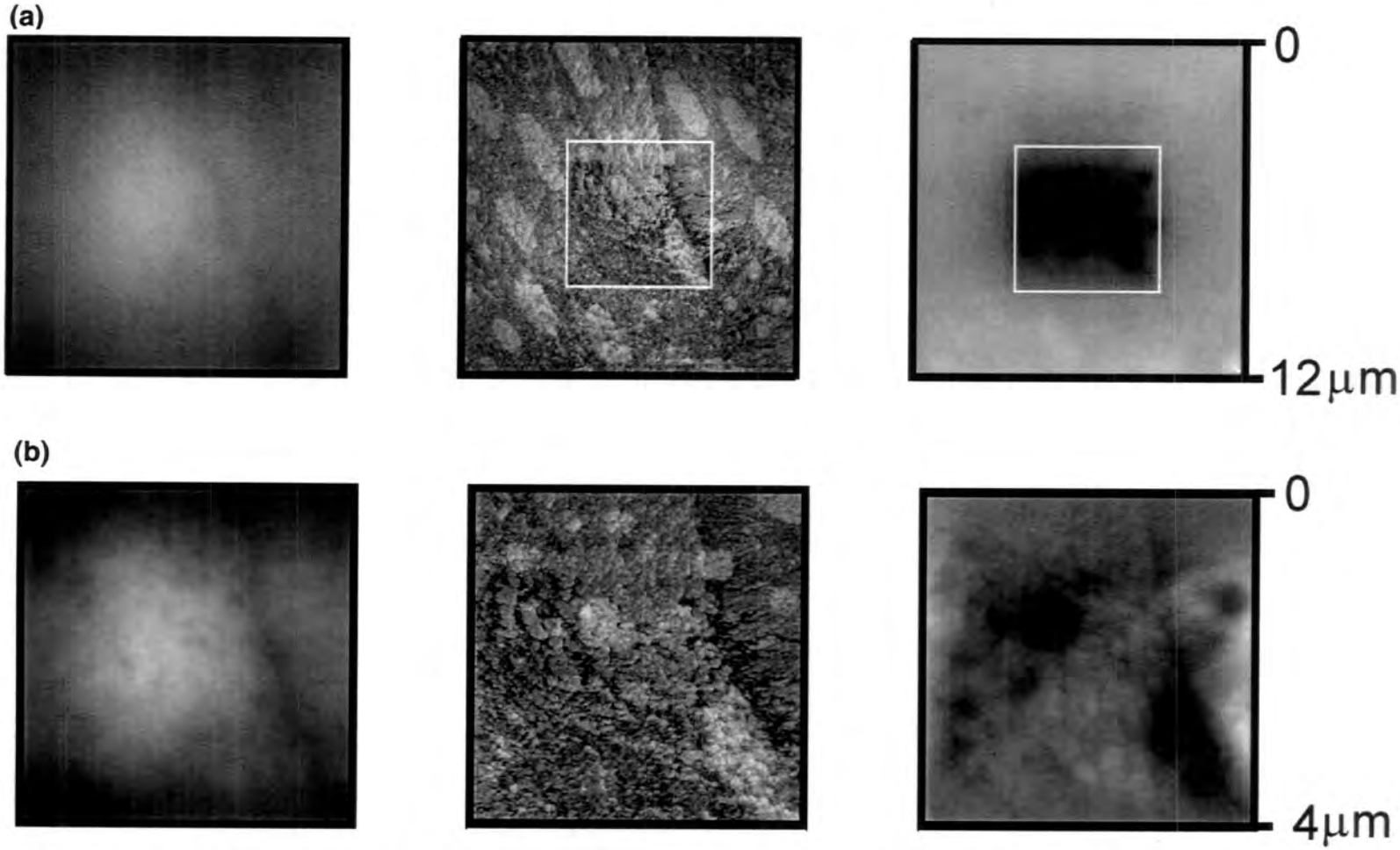

Figure 4.15 EFM micrographs of fluorochemical doped polypropylene (LHS: Height; middle: Tapping mode phase; RHS: lift-mode phase recorded with - 20 V imaging voltage): (a) 12 μm × 12 μm image, the region within the square has been exposed to + 140 V discharge voltage; (b) 4 μm × 4 μm image recorded in the square marked on (a).

4.3.4. Discussion

Fluorochemical enriched regions accumulate both positive and negative charge more readily than the surrounding polypropylene matrix. This is consistent with prior studies of the charging characteristics of fluorinated material compared to polyolefins, Section 4.2.4. The polypropylene surface is observed to accumulate positive charge, but is not effected by the negative discharge. It has previously been found that the stability of negative charge injected into polypropylene is higher than that of positive charge.[18] This has been attributed to negative charge carriers being trapped deeper in the bulk of the polymer. Positive carriers, which stay at the surface, can be more easily neutralised by surface recombination. This explains why EFM detects positive charge on the polypropylene surface, while the negative charge injected into the bulk produces no contrast.

In should be noted that in the localised charging performed in Chapter 3, both positive and negative charge is observed on the polypropylene film surface, presumably this reflects the different polypropylene substrate used for this work.

4.4. Conclusions

Electric force microscopy can be used to map charged fluorochemical domains embedded in polypropylene film surfaces. EFM images show that positive corona charging leads to the fluorochemical regions acquiring a positive charge relative to the surrounding polypropylene matrix. Subsequent annealing causes a redistribution of charge at the surface.

Furthermore, localised charge deposition from a scanning EFM tip onto fluorochemical doped polypropylene surfaces proves that fluorochemical domains accumulate both negative and positive charge preferentially to the polypropylene surrounds.

4.5. References

[1] Yamazaki, K.; Shingagawa, T.; Watanabe, T.; Takahira, T. (Misui Petrochemical Industries, Ltd., Japan; Nitta Industries Corp.) *Jpn. Kokai Tokkyo Koho* 19881110, 1988.

[2] Kodera. Y.; Kitamura, T.; Sawaguchi, E. (Sony Corp.) U.S. Patent 19720104, 1972.

[3] Ando, K.; Ogawa, K.; Ii, Y.; Okumura, Y. (Toray Industries, Inc., Japan) *Jpn. Kokai Tokkyo Koho* 19900312, 1990.

[4] Bruneel, J. L.; Micheron, F. *Congr. Int. Electrost.* **1977**, Paper No. 38.

[5] Takamatsu, T.; Okada, K.; Kagawa, F. (Institute of Physical and Chemical Research, Japan; Mitsubishi Petrochemical Co., Ltd.) *Jpn. Kokai Tokkyo Koho* 19850925, 1985.

[6] Kressmann, R.; Sessler, G. M.; Günther, P. *IEEE Trans. Elect. Insul.* **1996**, *3*, 607.

[7] Ikezaki, K.; Yagishita, A.; Yamanouchi, H.; Ikezaki, K. *Jpn. J. Appl. Phys.* **1999**, *38*, 2053.

[8] Leng, Y.; Wiliams, C. C. *Colloids Surf., A* **1994**, *93*, 335.

[9] Schönenberger, C.; Alvarado, S. F. *Phys. Rev. Lett.* **1990**, *65*, 3162.

[10] Stern, J. E.; Terris, B. D.; Mamin, H. J.; Rugar, D. *Appl. Phys. Lett.* **1988**, *53*, 2717.

[11] Karpov, I.; Belcher, R. W.; Linn, J. H. *Appl. Surf. Sci.* **1998**,*125*, 332.

[12] Nelson, M. W.; Schroeder, P. G.; Schlaf, R.; Parkinson, B. A. *Electrochemical and Solid-State Letters* **1999**, *2*, 475.

[13] Creswell, R. A.; Perlman, M. M.; Kabayama, M. In *Dielectric Properties of Polymers*; Karasz, F. E., Ed.; Plenum Press: New York, 1962, p 295.

[14] Domanský, K.; Leng, Y.; Williams, C. C.; Janata, J.; Petelenz, D. *Appl. Phys. Lett.* **1993**, *63*, 1513.

[15] Hilczer, B; Malecki, J. *Electrets*; Elsevier: New York, 1986.

[16] Tipler, P. A. *Physics for Scientists and Engineers*; Worth: New York,1991.

[17] Charlson, E. M.; Charlson, E. J.; Burkett, S.; Yasuda, H. K. *IEEE Trans. Elect. Insul.* **1992**, *27*, 1144.

[18] Keller, J. M.; Datt, S. C. *Phys. Stat. Sol.* **1985**, *91*, 205.

CHAPTER 5

LOCALISED ELECTROSTATIC ATTACHMENT OF POLYMER SPHERES TO SOLID SURFACES USING EFM

5.1. Introduction

The interaction of particulate matter with charged surfaces is of technological importance for processes such as xerography,[1,2] electrostatic aerosol filtration[3] and membrane filtration.[4] AFM has recently emerged as a useful tool in the characterisation of such systems. For example, experiments have been performed with individual particles attached to a AFM cantilever in order to probe the electrostatic interaction of colloids with membrane pores.[4] The adhesion of toner particles to charged surfaces has also been investigated.[5]

Electrostatic fields can control the attachment of colloidal particles to surfaces during the formation of the mono- and multilayers of current interest in materials science.[6,7] As an example, the attachment of negatively charged gold nano-particles to a positive surface produces a closely packed conducting layer.[6] Such layers are usually assembled in solutions, where the electrostatic interactions are between ionic surface groups. This chapter investigates an alternative approach, namely the use of charged polymer surfaces to attract and trap particles from dry aerosols. The advantage of this strategy is that it can be combined with the localised EFM charging method described in Chapter 3, to achieve spatially controlled particle localisation. This approach offers high spatial definition and does not require the vacuum apparatus necessary for the deposition of localised charge using electron beams.[8]

Section 5.3.1 investigates the deposition of polystyrene spheres onto a localised charge patch. Electric force micrographs are recorded to provide an insight into the mechanism of particle capture on the sub-micron scale. Section 5.3.2 explores the attachment of chemically modified polystyrene beads to charged surfaces. Strategies for the functionalisation of amine bead surfaces with metallic gold coatings are also investigated, with the goal of developing a new method for localised surface metallization. Colloidal gold particles have been shown to attach to surfaces with amine functionality.[6] In addition, the plasma reduction of gold (III) chloride on a nitrogen containing surface is known to produce gold surfaces.[9] Both methodologies are considered.

5.2. Experimental

EFM charge deposition was performed as described in Section 3.3. Details of EFM theory and image interpretation are found in Section 3.2.

XPS and optical microscopy characterisation were employed as described in Section 2.2.2. A theoretical sensitivity factor of 0.05 was used for the Au(4f) XPS analysis.[10]

Capacitor grade polypropylene film (ICI) served as the substrate in Section 5.3.1; and was also used for the localised bead deposition experiments in Section 5.3.2. This was cleaned by ultrasonication in propan-2-ol (Fisher, 99.99% purity) for 30 seconds. The substrates used for the large scale investigations in Section 5.3.2 were melt blown isotactic polypropylene films (Fina 3860 grade). Charged surfaces were prepared by corona discharge (constant current conditions: I ≈ 0.2 mA). Three types of particle have been investigated: pure polystyrene (Agar Scientific Ltd.), amine terminated polystyrene (Bangs Labs Inc.) and carboxyl terminated polystyrene (Bangs Lab Inc.), Table 5.1.

Bead Type	Mean diameter / μm	Nebulising concentration / ml^{-1}	Exposure time / min
Polystyrene	0.0091	8×10^{10}	90
Amine	0.66	4.3×10^{9}	30
Carboxyl	0.60	4.3×10^{9}	30

Table 5.1 Bead properties.

Surfaces were exposed to an aerosol generated by nebulizing an aqueous bead suspension in a dry N_2 air stream (BOC >99.99% purity), Figure 5.1. Bead concentrations, and exposure times are detailed in Table 5.1.

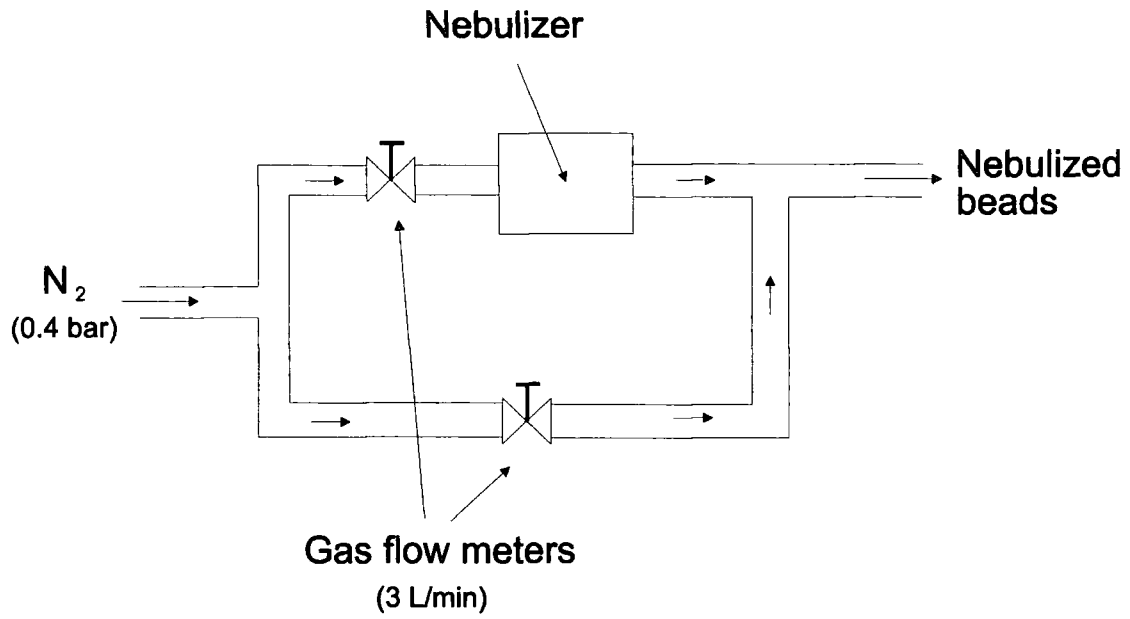

Figure 5.1 Schematic of the apparatus used to nebulize beads.

The EFM charging experiments consisted of three stages: firstly, localised charging was performed by scanning a 20 μm × 20 μm square of polymer while a high voltage was applied to the AFM tip (± 180 V); then the surface was exposed to a bead aerosol, and finally electric force or optical micrographs were recorded.

The initial attempt to functionalise amine beads was carried out by surface exposure to an aqueous suspension of colloidal gold (diameter = 250 nm, concentration = 1.2×10^{8} n /ml, Agar Ltd.) for 10 minutes. Following this the surfaces were washed with water (B. S. 3987 Grade 1). Gold functionalisation of the amine beads involved first exposing the surface to a gold (III) chloride (Aldrich 99% purity) solution (20 % w/v in methanol) for 10 minutes, then washing with pure methanol (Aldrich 99% purity). Dried samples were treated with a low pressure H_2 (BOC >99.99 % purity) plasma (Biorad Plasma Asher E2000 reactor: duration = 15 min; power = 20 W; chamber pressure = 0.4 mbar).

5.3. Results

5.3.1. Localised Attachment of Polystyrene Beads to Polypropylene Surfaces using EFM

5.3.1.1. Negative Surface Charge

A 20 μm × 20 μm negative charge square (dark contrast, Table 3.2) was deposited onto the polypropylene film surface using a highly biased negative tip voltage, Figure 5.2a. The Tapping Mode phase image also showed dark contrast in the charged region, due to increased tip-sample attraction. Following exposure to polystyrene beads, particulate material was observed to accumulate preferentially on the charged region, particularly at its edges, Figure 5.2b. The horizontal streaks in the Tapping Mode height and phase images can be attributed to particles adhering to and being perturbed by the AFM tip. Particles aggregated in clumps at the surface. However, rounded features with diameters of about 100 nm can be seen at the edges of the agglomerates, in good agreement with the known sphere diameters (91 nm), Figure 5.3a. Lift-mode images also identify the presence of polystyrene beads by the concentration of electric field gradients at the curved height surface features. Furthermore, EFM analysis indicates that the edges of the deposited charge patch remain negatively charged, (dark contrast) while the central regions display neutral contrast, corresponding to loss of charge. When imaged at higher resolutions, the region around the beads can be seen to give bright EFM lift-mode contrast with positive tip voltage, whereas with negative voltage this contrast reverses and becomes dark, Figure 5.3. This is consistent with regions surrounding the attached beads being positively charged relative to their surroundings, Table 3.2.

High resolution images taken outside the negatively charged region show low polystyrene sphere densities, Figure 5.4. These particles only show EFM lift-mode contrast due to their curvature; no associated electrostatic features are seen.

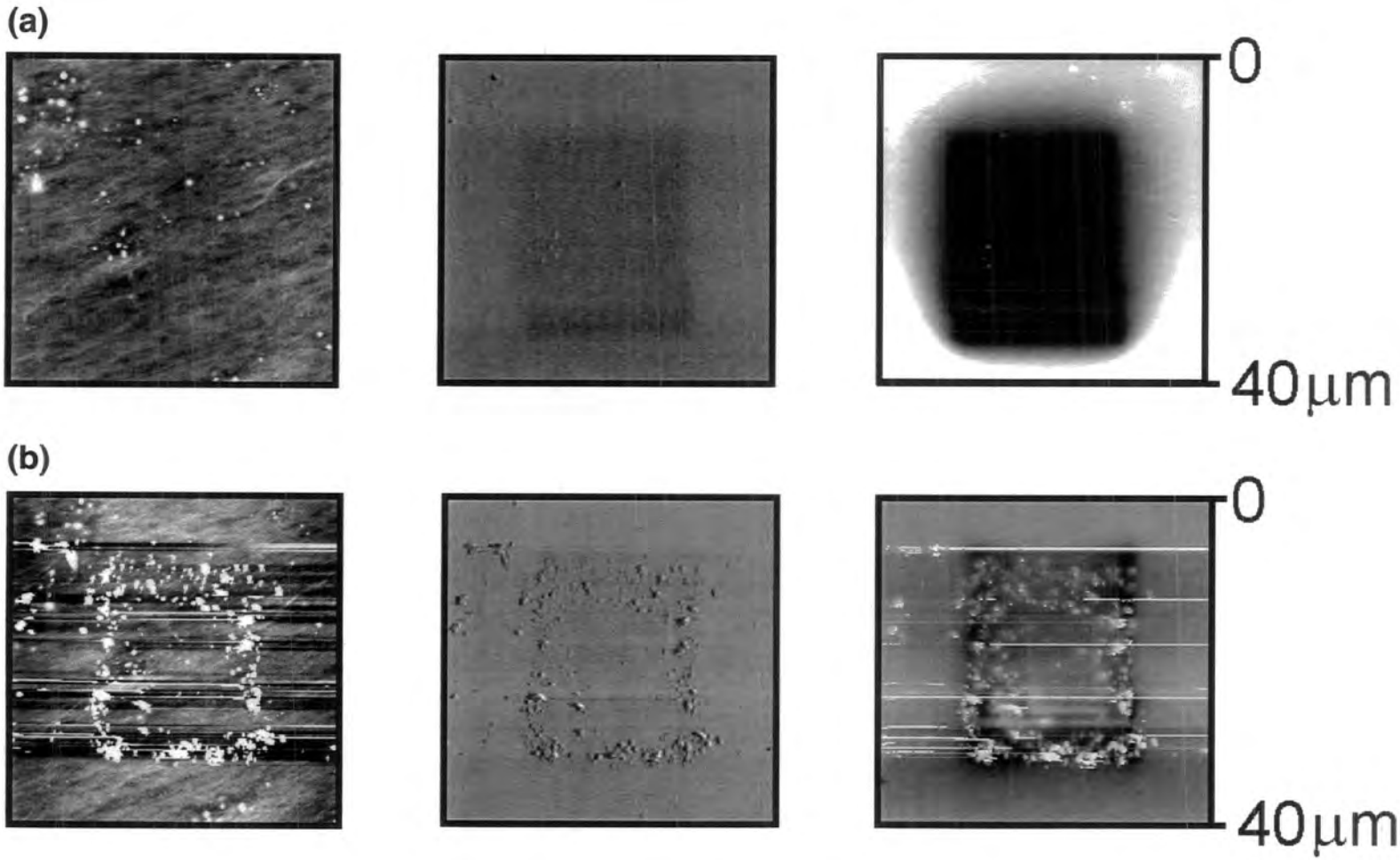

Figure 5.2 AFM micrographs of the polypropylene surface (LHS: height data; middle: phase data; RHS: EFM lift-mode data with + 20 V tip voltage): (a) The dark square region in the lift-mode image has been exposed to a -180 V lift-mode bias; and (b) same region as depicted in (a) after the entire surface has been exposed to a polystyrene bead aerosol.

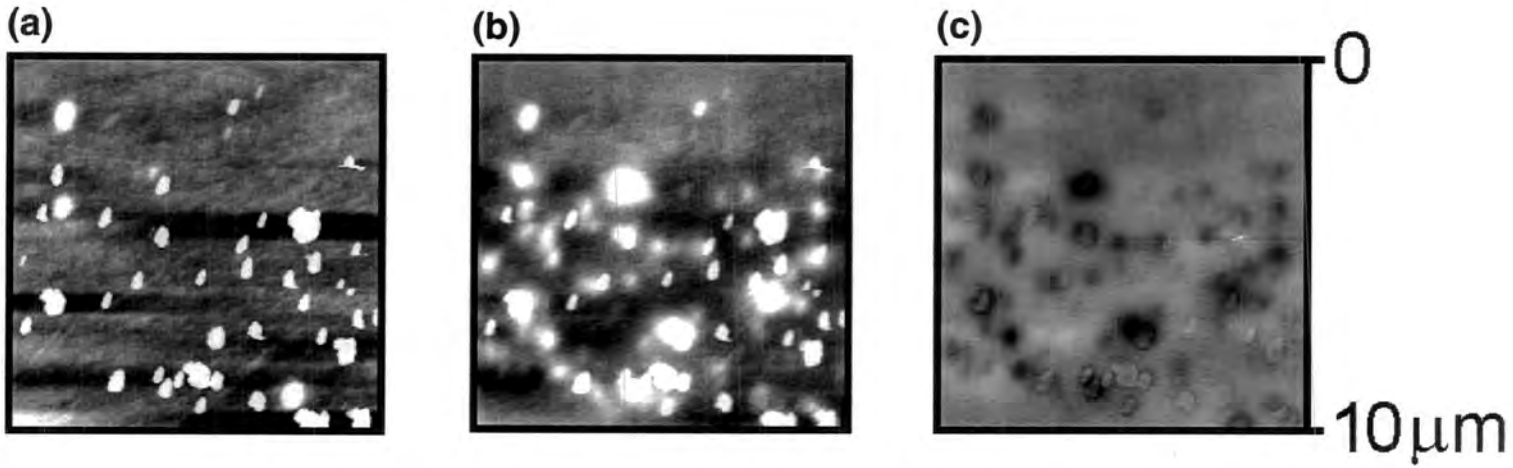

Figure 5.3 High resolution AFM micrographs of a region near the edge of the deposited negative charge patch, after bead deposition: (a) height image; (b) and (c) EFM lift-mode images recorded with + 20 V and - 20 V tip voltages respectively.

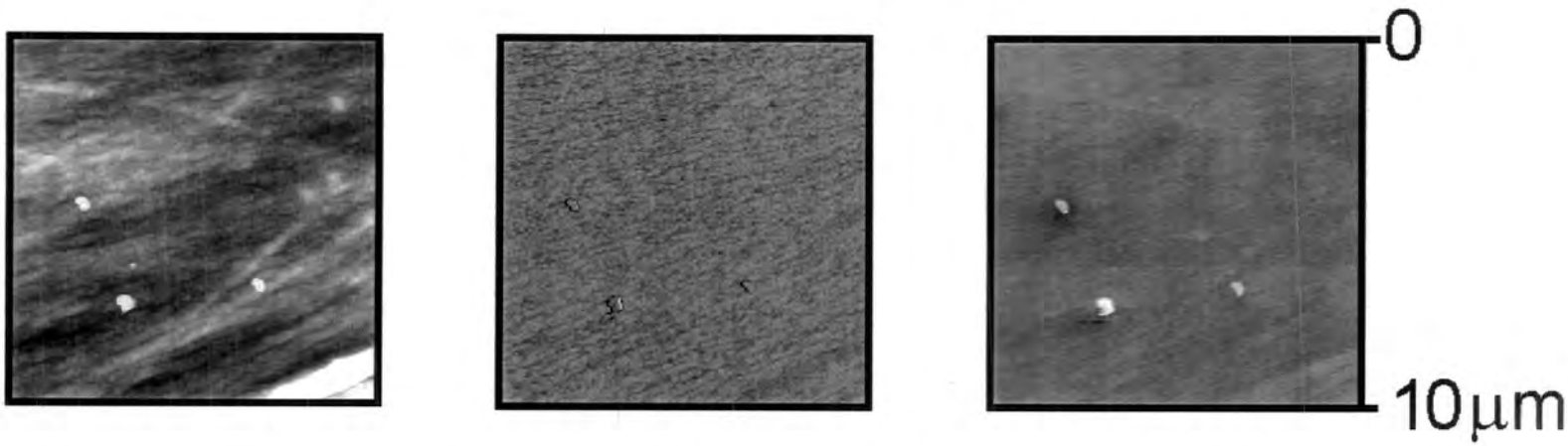

Figure 5.4 High resolution AFM micrographs of an uncharged region of the polypropylene surface following exposure to beads, (LHS: height data; middle: phase data; RHS: EFM lift-mode data recorded with + 20 V tip voltage).

5.3.1.2. Positive Surface Charge

Polystyrene spheres were also found to localise preferentially around the peripheries of a positively charged region, Figure 5.5. Furthermore, EFM lift-mode images recorded with positive applied tip voltage showed that positive charge was retained around the boundaries (dark contrast); whilst charge loss occurred in the central region. More horizontal streaking was apparent than for the case of beads attached to the negative surface. To prove that the tip was sweeping beads across the surface, two successive images were recorded. Figure 5.5a and b. Fewer beads could be seen in the second image, Figure 5.5b, compared to the first, Figure 5.5a.

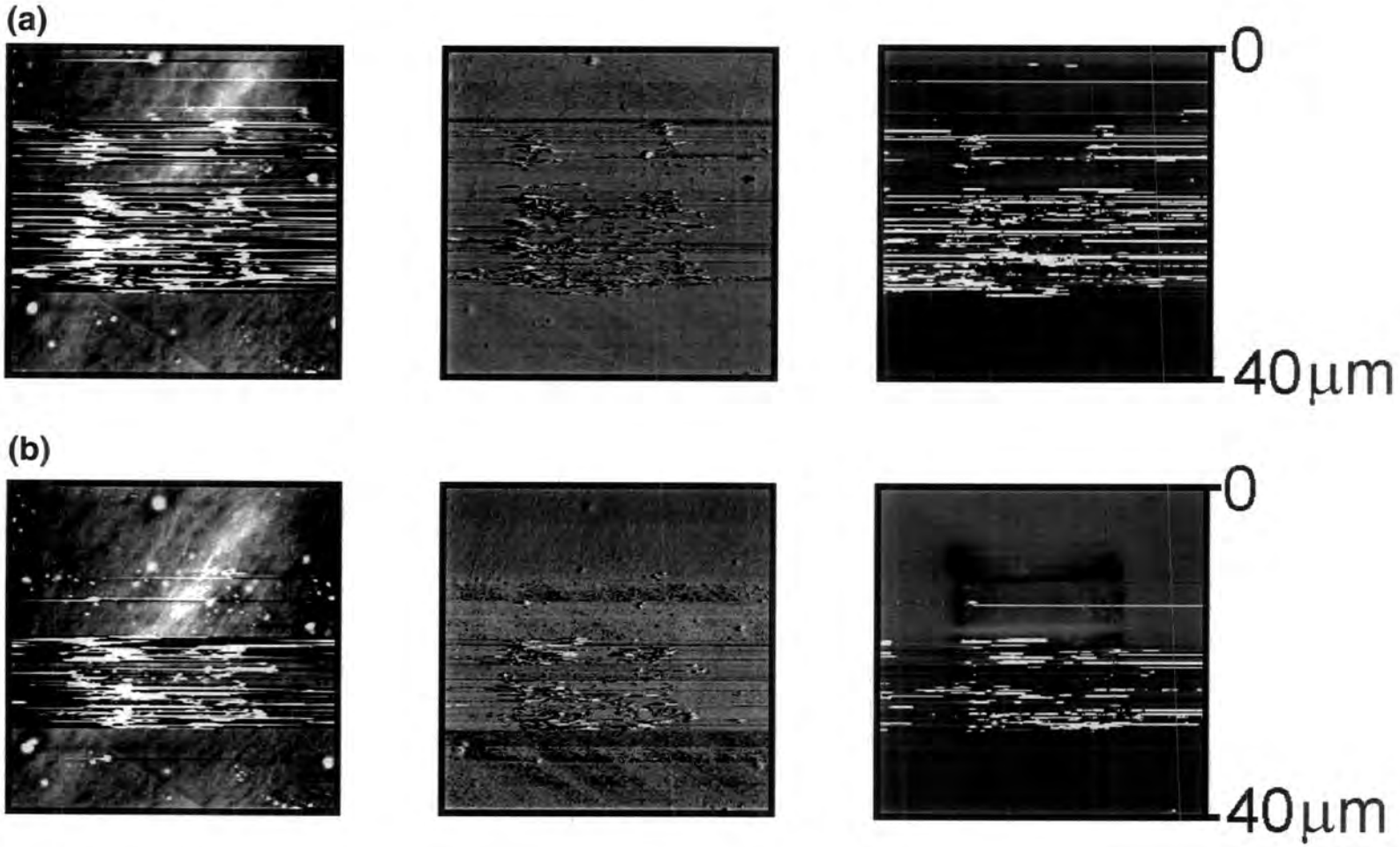

Figure 5.5 AFM micrographs of the polypropylene surface (LHS: height data; middle: phase data; RHS: EFM lift-mode data with - 20 V tip voltage). The hollow dark square visible in the lift-mode images has been exposed to + 180 V lift-mode bias, and the entire surface has subsequently been exposed to polystyrene beads: (a) first scan; (b) second scan.

5.3.2. Surface Attachment of Functionalised Beads

5.3.2.1. Attachment of Amine and Carboxyl Beads

Positively and negatively charged polymer films (with approximately ± 500 V surface potential as determined using the scanning electrometer described in Section 4.2.2) together with an uncharged reference sample were exposed to an aerosol of amine terminated beads and then examined by optical microscopy, Figure 5.6. A high density of mainly separate particles with the expected diameter are observed to attach to both the positively and negatively charged surfaces. No beads are visible on the uncharged surface. When this experiment is repeated using carboxyl terminated beads, the surface of the uncharged sample also shows no sign of bead attachment, Figure 5.7. However, both positively and negatively charged surfaces became covered with carboxyl material. Individual carboxyl beads cannot be discerned, instead larger clumps of aggregated material are visible.

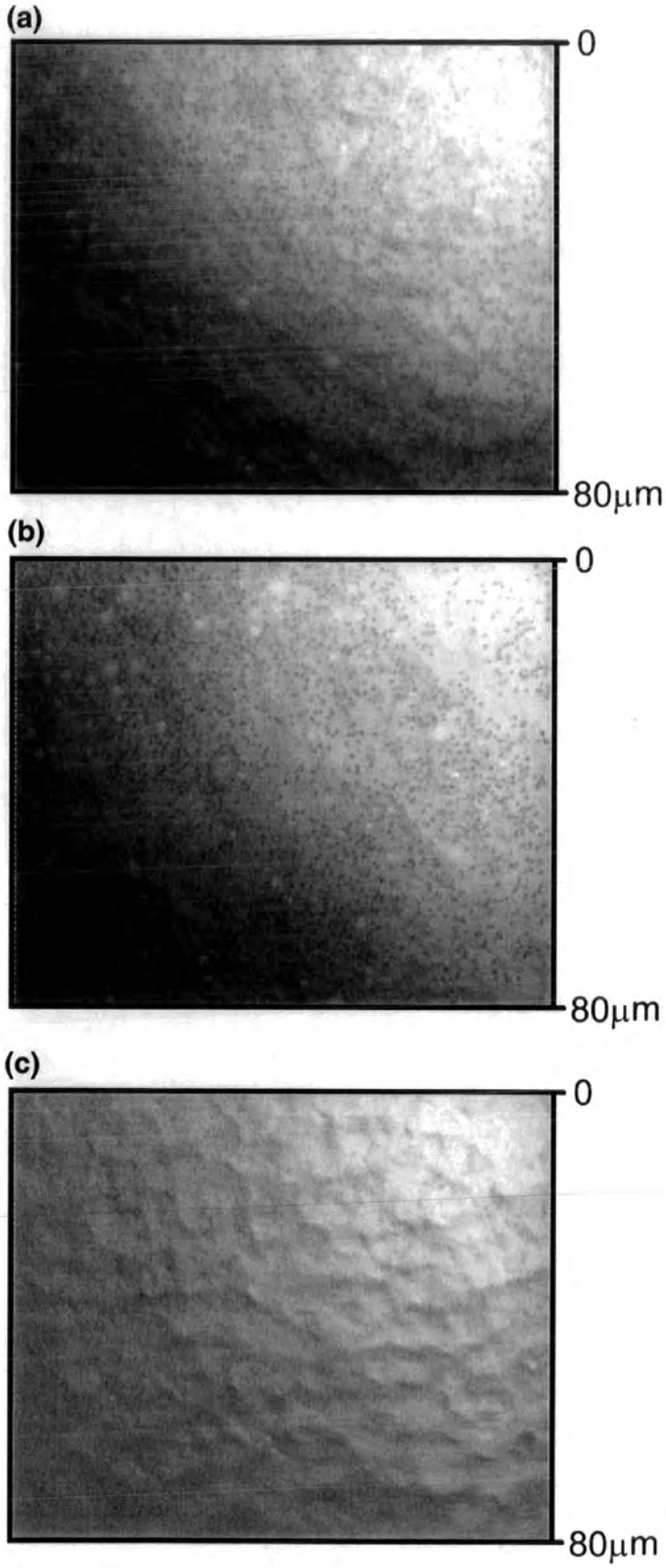

Figure 5.6 Optical micrographs of polypropylene following exposure to -NH_2 bead aerosol: (a) positively charged surface; (b) negatively charged surface; and (c) neutral.

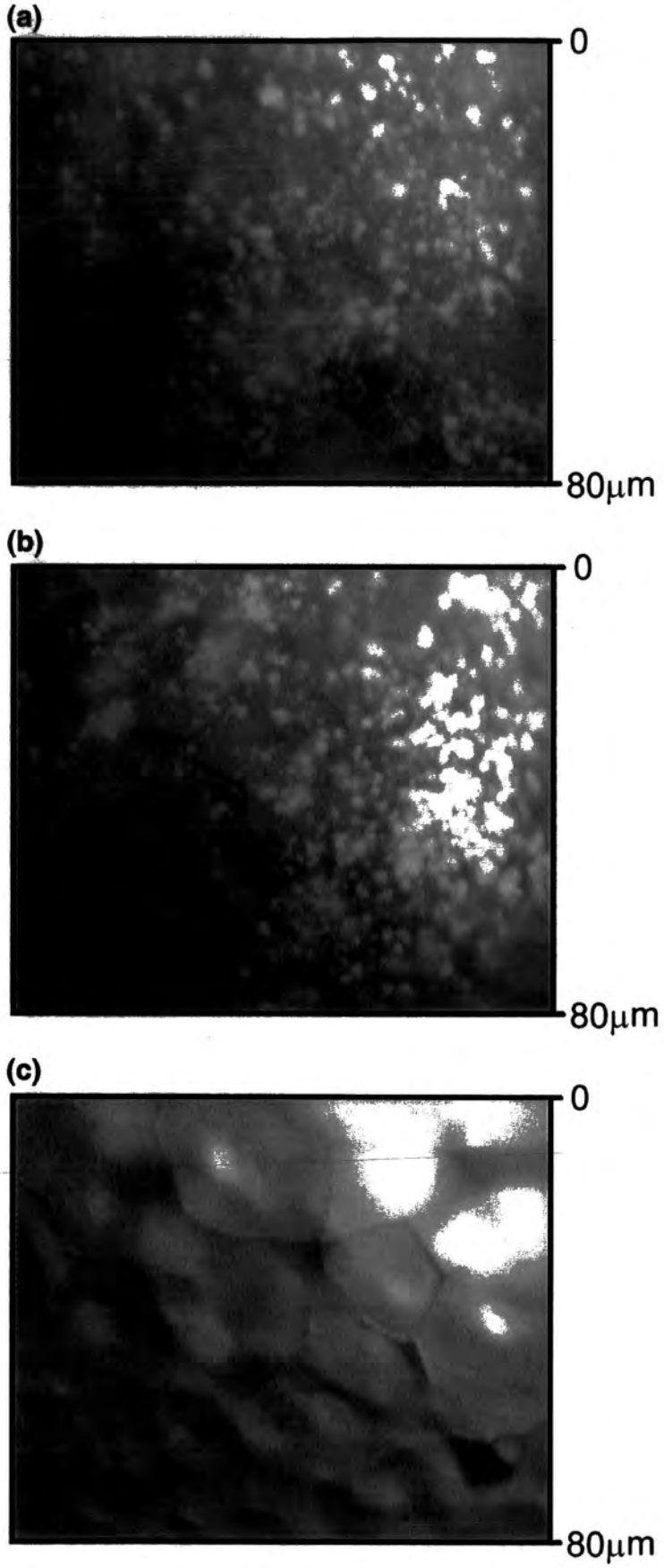

Figure 5.7 Optical micrographs of polypropylene following exposure to -COOH bead aerosol: (a) positively charged surface; (b) negatively charged surface; and (c) neutral.

5.3.2.2. Localised Attachment of Amine Terminated Beads

Amine beads were observed to develop the shape of both positive and negative localised charge patches, Figure 5.8. Bead attachment occurred uniformly over the entire charged region.

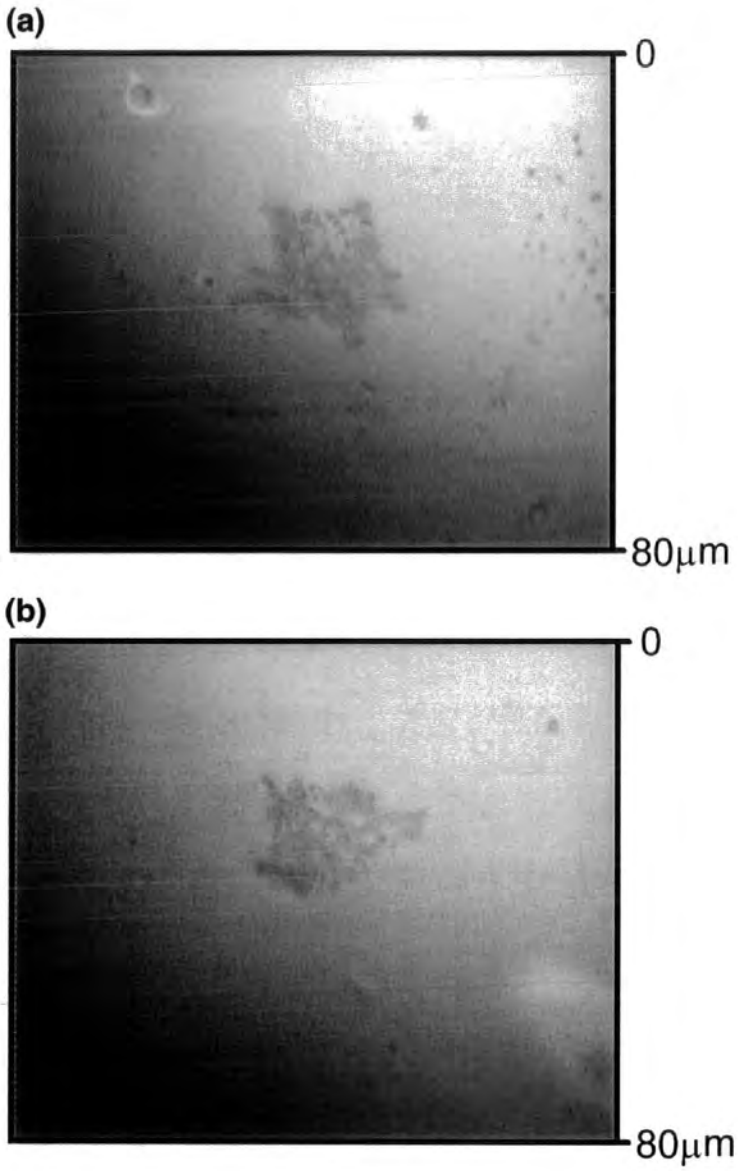

Figure 5.8 Optical micrographs of locally charged polypropylene surfaces following exposure to -NH_2 bead aerosol: (a) positive charging; and (b) negative charging.

5.3.2.3. Surface Functionalisation of Amine Terminated Beads

(a) Gold Colloid Exposure

XPS of the amine bead surfaces depicted in Figure 5.6 after exposure to colloidal gold showed no signals in the Au(4f) envelope, Table 5.2. Oxidation of the charged samples occurred due to modification by the corona charging process. Only trace N(1s) signals due to the amine functionality on the surface of the beads were detected.

(b) Gold (III) Chloride Treatment

XPS analysis of the uncharged polypropylene surface depicted in Figure 5.6c after treatment with gold (III) chloride indicated low levels of Au and Cl, Table 5.2. However both of the large scale charged surfaces (Figure 5.6a and b) had higher surface concentrations of Au and Cl. The Au(4f) spectral region contained peaks consistent with Au^{3+} incorporation ($Au(4f_{7/2})$ at ~87.6 eV; $Au(4f_{5/2})$ at ~91.5 eV), Figure 5.10.[11,12] More Au and Cl incorporation occurred on the positively charged surfaces than the negatively charged equivalents. Optical micrographs following the treatment depicted individual beads attached to the polypropylene substrate, Figure 5.9.

Positive, negative and uncharged polypropylene substrates were also exposed to gold (III) chloride, to ascertain if polymer surface charge was contributing to the observed Au and Cl concentrations. All three substrates gave lower Au and Cl concentrations than those covered with amine beads, Table 5.2. This indicates that most of the gold complexation is with the amine groups on the bead's surface rather than the underlying polypropylene.

Having established that a Au^{3+} complex was attached to the surface of the amine beads, low pressure H_2 plasma discharge was investigated as a method of reducing the Au^{3+} to Au^0. XPS elemental analysis of the plasma treated surfaces indicated a reduction in the amount of Cl relative to Au, Table 5.2. Such a reduction in Cl concentration has been reported to accompany Au^{3+} reduction.[9] Furthermore, the $Au(4f_{7/2})$ and $Au(4f_{5/2})$ XPS peaks shifted from ~87.6 eV and ~91.5 eV for the high oxidation state adduct to ~85.4 eV and ~88.9 eV after reduction respectively, Figure 5.10. Such shifts reflect the

reduction of gold (III) chloride to metallic gold.[13] Optical micrographs depicted beads remaining intact at the surface, Figure 5.11. The beads attached to the positively charged surface had higher gold concentrations than those localised on negative charge, Table 5.2.

A patch of beads localised using EFM charge deposition was also subject to the same gold (III) chloride treatment and subsequent plasma reduction. Optical images revealed that the beads remained in a localised square, Figure 5.12.

Surface Treatment	XPS Elemental Analysis[a]			
	C	Au	Cl	O
None + gold (III) chloride	96.5 (± 1.7)	0.3 (± 0.2)	1.6 (± 1.4)	1.6 (± 0.1)
Positive corona + gold (III) chloride	94.8 (± 0.7)	0.5 (± 0.2)	2.4 (± 1.5)	2.3 (± 1.0)
Negative corona + gold (III) chloride	95.4 (± 0.5)	0.2 (± 0.1)	1.2 (± 0.5)	3.3 (± 0.1)
NH_2 beads + Au colloid	98.2 (± 0.5)	0.0	-	1.8 (± 0.1)
Positive corona + NH_2 beads + Au colloid	97.0 (± 0.5)	0.0	-	3.0 (± 0.1)
Negative corona + NH_2 beads + Au colloid	96.5 (± 0.2)	0.0	-	3.5 (± 0.8)
NH_2 beads + gold (III) chloride	94.4 (± 1.0)	0.5 (± 0.3)	1.8 (± 1.7)	3.3 (± 1.0)
Positive corona + NH_2 beads + gold (III) chloride	73.0 (± 5.7)	4.0 (± 0.5)	16.2 (± 3.6)	6.8 (± 1.6)
Negative corona + NH_2 beads +gold (III) chloride	88.7 (± 0.3)	1.6 (± 0.4)	4.0 (± 1.3)	5.8 (± 0.6)
NH_2 beads + gold (III) chloride + H_2 plasma	95.7 (± 0.2)	0.4 (± 0.5)	1.0 (± 0.2)	2.9 (± 0.5)
Positive corona + NH_2 beads + gold (III) chloride + H_2 plasma	91.5 (± 0.7)	2.1 (± 0.1)	4.8 (± 1.0)	1.6 (± 0.5)
Negative corona + NH_2 beads + gold (III) chloride + H_2 plasma	94.4 (± 0.5)	0.6 (± 0.5)	1.4 (± 0.2)	3.7 (± 0.4)

Table 5.2 Chemical modification of NH_2 beads.

[a] Only trace levels of N were detected in the N(1s) envelope.

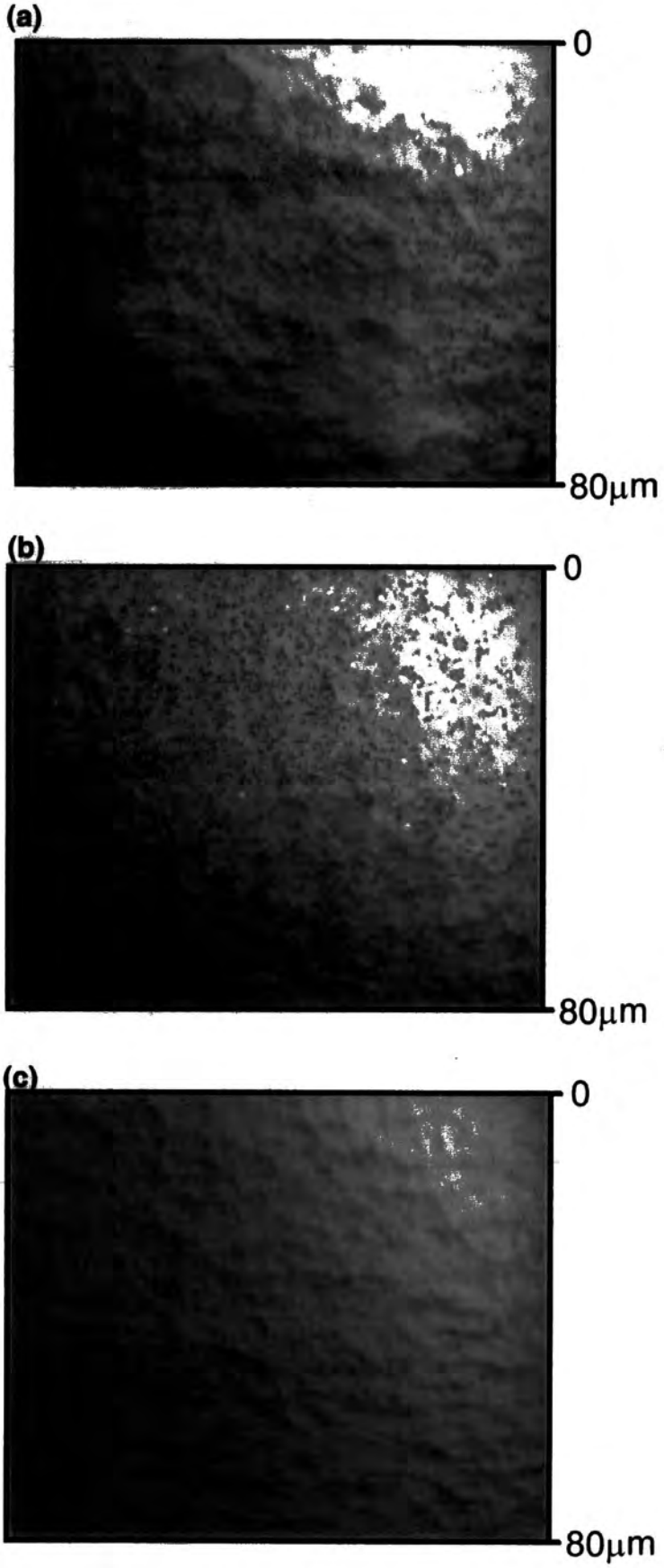

Figure 5.9 Optical micrographs of polypropylene following exposure to NH_2 bead aerosol, and gold (III) chloride solution: (a) positively charged; (b) negatively charged; and (c) neutral.

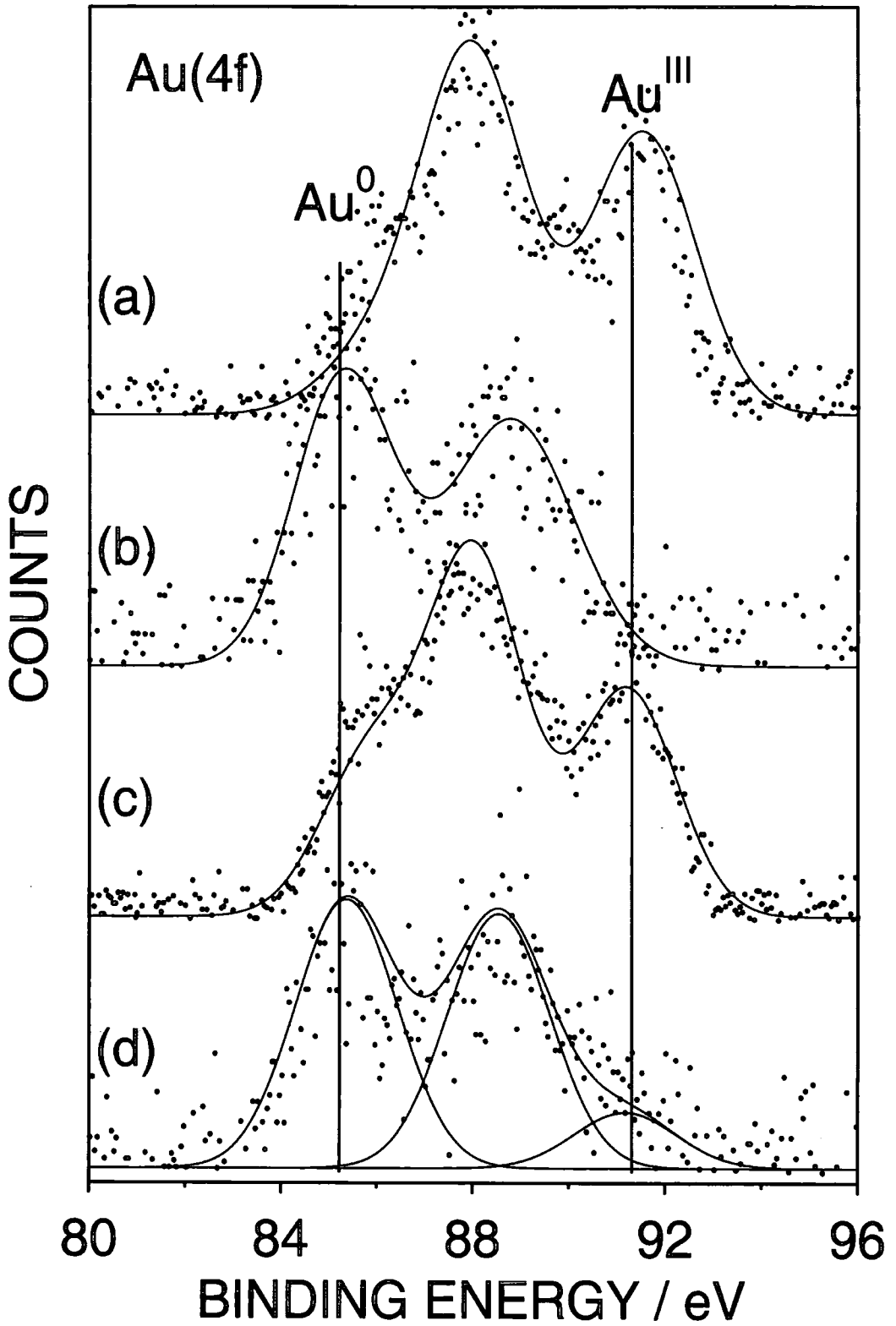

Figure 5.10 Au(4f) region of polypropylene after exposure to an -NH_2 bead aerosol and gold (III) chloride solution: (a) positively charged surface; (b) positively charged surface after H_2 reduction; (c) negative surface; and (d) negatively charged surface after H_2 reduction.

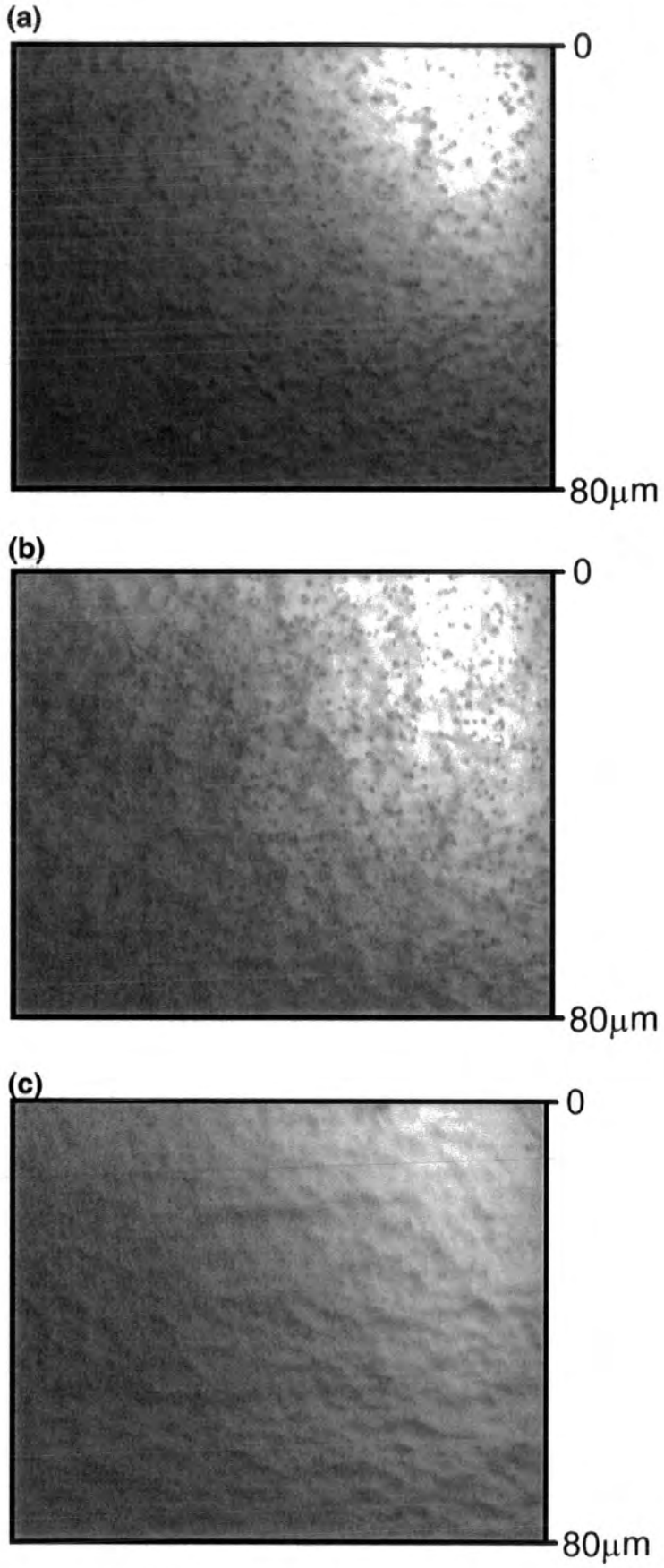

Figure 5.11 Optical micrographs of polypropylene following exposure to a -NH_2 bead aerosol, gold (III) chloride solution and H_2 plasma reduction: (a) positively charged; (b) negatively charged; and (c) neutral.

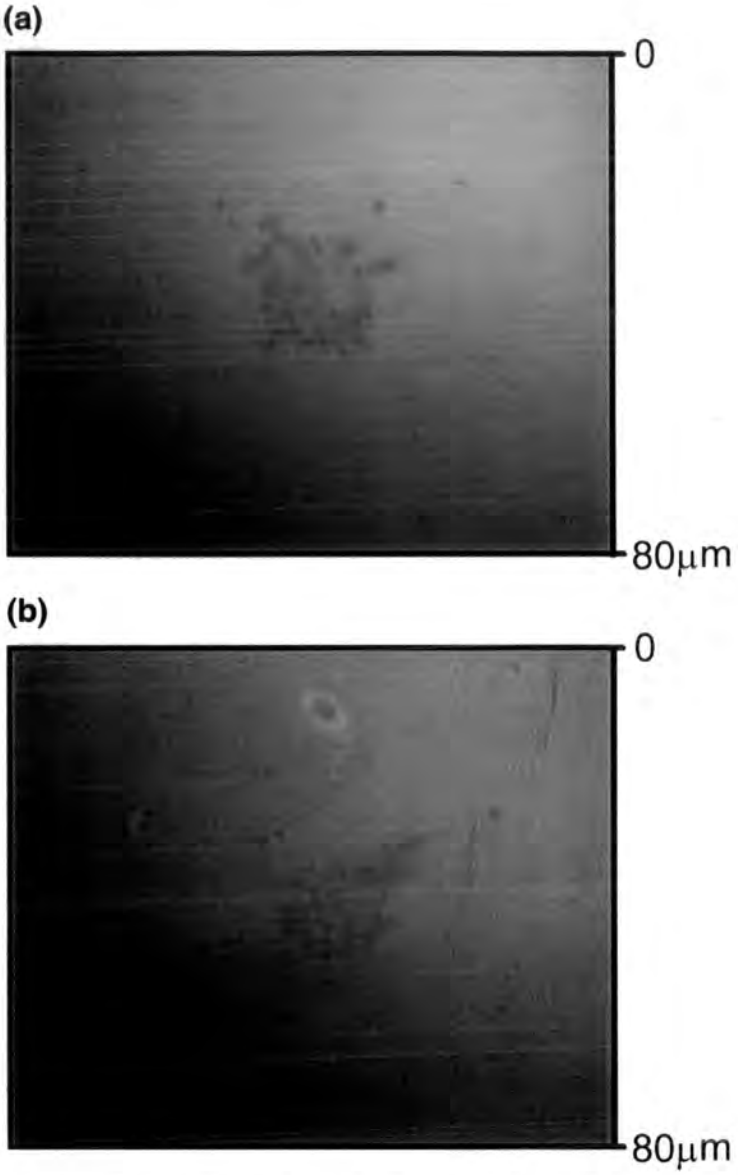

Figure 5.12 Optical micrographs of locally charged polypropylene following exposure to a -NH_2 bead aerosol, gold (III) chloride solution and H_2 plasma reduction: (a) positive charging; and (b) negative charging.

5.4. Discussion

5.4.1. Electrostatic Attachment of Polystyrene Beads

It is well known that charged surfaces readily capture sub-micron sized air-borne particulate matter.[14] In Section 5.3.1 it was demonstrated that polystyrene beads preferentially accumulate onto both negatively and positively charged patches, compared to the uncharged surroundings. As similar particle densities are observed for both the negative and positively charged patches, then the polystyrene aerosol must have no overall dominant polarity, i.e. there are equal

numbers of positively and negatively charged beads. Charged particles interact with surface charge distributions via Coulombic forces, whereas uncharged particles are acted on by induction forces.[3] Particles at the surface are seen to possess an opposite polarity charge to the underlying charged substrate. This may arise from particle charging during aerosol formation,[15] or be induced by the substrate's charge.

The observed accumulation of particles at the peripheries of charged squares rather than at their centres is an example of an "edge effect". This phenomena is well known in xerography.[1] Edge effects are usually attributed to the large electric field gradient at the boundary between charged and uncharged regions. In this work, the distribution of beads reflects the fact that charge only remains at the edges of the deposited square after bead deposition. The change in the charge distribution resulting from exposure to the beads suggests that the central region of the charge patch is less stable than the boundary regions. This can be explained by considering that the characteristics of discharge from an EFM tip are similar to those of corona discharge, Section 3.5. Furthermore, it has been previously reported that the region directly exposed to the corona loses charge more rapidly than the indirectly charged surrounding areas due to excitation by UV photons.[16] Therefore, it seems likely that the observed distribution of particles results from the greater field gradient at the edge of the deposited charge patches in combination with the reduced stability of their central regions.

The lateral mobility of particles attached to the negative charge patch is lower than those attached to an equivalently deposited positive region. This is consistent with the previous observation that negative charge is deposited from the EFM tip more readily than positive charge, Section 3.5 (negative breakdown voltage = -40 V to -50 V; positive breakdown voltage = +80 V to +100 V). The higher density of negative charge would allow stronger induced and Coulombic interactions with particles at the surface and so reduce lateral movement compared to the positively charged region.

5.4.2. Electrostatic Attachment of Functionalised Polystyrene Beads

Both carboxyl and amine terminated bead aerosols can be localised onto charged surfaces. Despite the ionisable nature of the surface functional groups, no selectivity between positive and negative surface charge was observed. This suggests that particle capture occurred as described for the polystyrene beads, Section 5.4.1. The electrostatic interaction between amine beads and the charge patches has been shown to be sufficient to withstand exposure to solvents and chemical reagents. The "edge effect" noted when polystyrene beads deposit onto localised charge patches is not evident for amine beads, Figures 5.2, 5.5 and 5.8. This could be a result of the larger size of the amine beads reducing their sensitivity to electric field gradients.

5.4.3. Localised Patterning of Amine Beads with Gold

No evidence of the attachment of gold colloidal particles to amine beads was found. This suggests that the density of amine groups at the surface is lower than the densely packed arrangement of ammonium groups that have previously been shown to allow attachment.[6]

The absorption of gold (III) chloride onto the surface of the amine terminated beads was observed. It has been previously suggested that the adduct of gold (III) chloride and a nitrogen containing surface produces a $[L_xAuCl_2]^+[AuCl_4]^-$ type ion (L represents the N containing ligand).[9] Results here suggest that the polarity of surface charge used to attach the amine beads is altering the amount of gold (III) chloride incorporation achievable. More co-ordination is observed for a positive substrate than a negative equivalent, whilst the concentrations of attached beads appear unaffected by the charge polarity. EFM of electrostatically localised uncoated polystyrene beads showed that the beads had acquired an induced surface charge. This induced charge might promote the formation of a Au^{+3} adduct on the surface of the amine beads attached to positive substrates.

Successful reduction of gold (III) chloride attached to the amine beads to metallic gold has been observed. The concentration of gold following reduction reflects the differences in the amount of gold (III) chloride complexed to the bead surfaces. Localised amine beads appear to be resilient to this process, suggesting a new method for localised surface metallization.

5.5. Conclusions

Localised charge deposition using a scanning EFM tip provides a method for electrostatic patterning of surfaces. EFM has been used to map the charge distribution of such patterned surfaces, and reveal the induced charges on the captured particles. Small aerosol beads are found to accumulate at the edges of the deposited charge, in a similar way to the "edge-effect" reported in xerography. This electrostatic patterning method can also be used attach beads possessing desired functional groups (amine and carboxyl). Here it is demonstrated that co-ordination of a localised patch of amine terminated beads to gold (III) chloride, followed by plasma reduction provides a route to spatially controlled surface metallization. Some evidence is found that induced charge in the attached beads alters the co-ordination process.

5.6. References

[1] Williams, E. M. *The Physics and Technology of Xerographic Processes*; Wiley: New York, 1984.

[2] Hays, D. A. *J. Adhesion* **1995**, *51*, 41.

[3] Hilczer, B.; Malecki, J. *Electrets*, Elsevier: New York, 1986; p 341.

[4] Mizes, H.; Ott, M.; Eklund, E.; Hays, D. *Colloids Surf., A* **2000**, *165*, 11.

[5] Bowen, W. R.; Hilai, N.; Jain, M.; Lovitt, R. W.; Sharif, A. O.; Wright, C. J. *Chem. Eng. Sci.* **1999**, *54*, 369.

[6] Yonezawa, T.; Onoue, S.; Kunitake, T. *Adv. Mater.* **1998**, *10*, 414.

[7] Serizawa, T.; Takeshita, H.; Akashi, M. *Langmuir* **1998**, *14*, 4088.

[8] Sessler, G. M.; West, J. E. *Phot. Sci. Eng.* **1974**, *18*, 162.

[9] Crowther, J. C. Plasma Metallization. Ph. D. Thesis, Durham University, 1997.

[10] Seah, M. P.; Anthony, M. T. *Surf. Inter. Anal.* **1984**, *6*, 230.

[11] Batista-Leal, M.; Lester, J. E.; Lucchesi, C. A. *J. Elect. Spec. Rel. Phenom.* **1977**, *11*, 333.

[12] Kosaku, K; Shigero, I *J. Phys. Chem.* **1974**, *78*, 107.

[13] Moulder, J. F.; Stickle, W. F.; Sobol, P. E.; Bomben, K. D. In *Handbook of X-ray Photoelectron Spectroscopy;* Chastain, J., Ed. Perkin Elmer Corporation: Minnesota, USA, 1992.

[14] Van Turnhout, J. *Proc. Int. Symposium on Electrets and Dielectrics*, Academia Brasileira de Ciencias: Rio de Janeiro, 1975, 87.

[15] Forsyth, B.; Liu, B. Y. H.; Romay, F. J. *Aerosol Sci. Tech.* **1998**, *28*, 489.

[16] Baum, E. A.; Lewis, T. J.; Toomer, R. *J. Phys. D: Appl. Phys.* **1977**, *10*, 487.

CHAPTER 6

CONCLUSIONS

6.1. Conclusions

Various surface science techniques were used to investigate the surface enrichment of fluorochemical doped polypropylene films. During annealing, the lateral distribution of additive at the surface was found to spread outwards from isolated circular domains and patches into a continuous layer, with a corresponding drop in surface energy. The speed and extent of surface enrichment for fluorochemical doped polypropylene films was found to increase with polymer molecular weight. While a comparison between polypropylene films containing mono- and bis- perfluorinated additive molecules proved that the mono- additive migrates to the surface much more readily.

Localised charge deposition onto polymer surfaces from a scanning EFM tip was then considered. As well as having importance in its own right, the ability to deposit patches of charge with known polarity provided reference samples to confirm the effect of varying tip voltage on EFM image contrast. A thorough investigation of the effect of scan parameters and tip voltage on the deposited charge patch suggested that the mechanism of charging was corona discharge. A surprising result was that charging occurred without chemically or morphologically altering the polymer surface.

Having established that it is possible to identify the polarity and level of surface charge using EFM, attention turned to mapping charged fluorochemical domains embedded in polypropylene film surfaces. To aid this work, a scanning electrometer probe was designed and built to allow larger scale imaging of the surface potential distribution. EFM images proved that positive corona charging leads to the fluorochemical regions acquiring a positive charge relative to the surrounding polypropylene matrix and that subsequent annealing causes a redistribution of charge at the surface. Localised charge deposition from a scanning EFM was also used to investigate the fluorochemical doped polypropylene surfaces. This method proved that fluorochemical domains accumulate both negative and positive charge preferentially to the polypropylene surrounds.

Localised charge deposition from an EFM tip was shown to provide a method for electrostatic patterning of surfaces. Small aerosol beads were found to accumulate at the edges of deposited charge patches in a similar way to the "edge-effect" reported in xerography. EFM revealed that captured beads acquired an opposite polarity charge to the substrate. This electrostatic patterning method was then used to attach beads possessing desired functional groups. It was demonstrated that co-ordination of gold (III) chloride to a localised patch of amine terminated beads, followed by plasma reduction provides a route to spatially controlled surface metallization. Some evidence was found that induced charge in the attached beads alters the co-ordination process.

In summary, the work in this thesis has achieved two aims:

- The study of the chemical and electrical surface properties of fluorochemical doped polypropylene.

- The development and exploitation of a method to deposit spatially controlled charge distributions on insulating surfaces.

APPENDIX

COLLOQUIA, SEMINARS, PRESENTATIONS AND LECTURE COURSES

UNIVERSITY OF DURHAM

BOARD OF STUDIES IN CHEMISTRY

COLLOQUIA AND SEMINARS FROM INVITED SPEAKERS

1997-1998

October 15	Dr R M Ormerod, Keele University , Studying catalysts in action.
October 22	Professor R J Puddephatt, University of Western Ontario. Organoplatinum chemistry and catalysis.
October 23	Professor M R Bryce, University of Durham. New Tetrathiafulvalene Derivatives in Molecular, Supramolecular and Macromolecular Chemistry: controlling the electronic properties of organic solids.
November 12	Dr J Frey, Department of Chemistry, Southampton University. Spectroscopy of liquid interfaces: from bio-organic chemistry to atmospheric chemistry.
November 25	Dr R Withnall, University of Greenwich. Illuminated molecules and manuscripts.
November 26	Professor R W Richards, University of Durham, Inaugural Lecture. A random walk in polymer science.
December 2	Dr C J Ludman, University of Durham. Explosions.
December 3	Professor A P Davis, Department. of Chemistry, Trinity College Dublin. Steroid-based frameworks for supramolecular chemistry.

1998-1999

October 7	Dr S Rimmer, Ctr Polymer, University of Lancaster. New Polymer Colloids.
October 21	Professor P Unwin, . Warwick University Dynamic Electrochemistry: Small is Beautiful.
October 27	Professor A Unsworth, University of Durham. What's a joint like this doing in a nice girl like you?
October 28	Professor J P S Badyal, University of Durham. Tailoring Solid Surfaces, Inaugural Lecture.
November 3	Dr C J Ludman, University of Durham. Bonfire night Lecture.
.November 17	Dr J McFarlane. Nothing but Sex and Sudden Death!
January 20	Dr A Jones, University of Edinburgh. Luminescence of Large Molecules: from Conducting Polymers to Coral Reefs.
January 27	Professor K Wade, Department of Chemistry, University of Durham. Foresight or Hindsight? Some Borane Lessons and Loose Ends.

1999-2000

January 19	Dr. P.R. Fielden, UMIST. Miniaturised Chemical Analysis (Lab-on-a-Chip): Functional or Merely Fashionable?
January 25	Professor B. Meijer. From Supramolecular Architecture Towards Functional Materials.
February 1	Professor R. Snaith. Egyptian Mummies - what, why, who & how!
February 2	Chick Wilson, ISIS, Rutherford Appleton Lab . Protons in motion? Neutron diffraction studies of hydrogen atoms in organic crystal structures.
February 15	Professor D. Phillips.

	A Little Light Relief.
February 23	Dr. N. Clarke, UMIST
	The Flow of Polymer Blends.
February 22	Professor G. Stuart.
	Brewing - Evolution from a Craft into a Technology.
March 1	Professor D. Tildsley, Unilever (Head of Research)
	Computer Simulation of Interfaces: Fact and Friction.

EXAMINED LECTURE COURSES:

Mass Spectrometry,	Dr. M. Jones
Electron Microscopy,	Dr. K. Durose
Experimental Design and Instrumentation,	Prof. J. P. Badyal

CONFERENCES ATTENDED:

April 1998: Atomic Force Microscopy, Manchester University.

September 1998: AFM and Polymers, Bristol.

August 1999: 1st International Conference on Scanning Probe Microscopy of Polymers, Santa Barbara, California.

PRESENTATIONS:

August 1999: "Surface Enrichment in Fluorochemical Doped Polypropylene", 3M Technical Forum, St. Paul, MN